APPLICATION OF LIQUID CHROMATOGRAPHY TANDEM MASS SPECTROMETRY FOR THE SEPARATION AND QUANTITATIVE ANALYSIS OF SPHINGOLIPIDS.

A Thesis
Presented to
The Academic Faculty

by

Jeremy C. Allegood

In Partial Fulfillment
of the Requirements for the Degree
Doctorate of Philosophy in the
School of Chemistry and Biochemistry

Georgia Institute of Technology
December 2011

APPLICATION OF LIQUID CHROMATOGRAPHY TANDEM MASS SPECTROMETRY FOR THE SEPARATION AND QUANTITATIVE ANALYSIS OF SPHINGOLIPIDS.

Approved by:

Dr. Alfred H. Merrill Jr., Advisor
School of Biology
Georgia Institute of Technology

Dr. Donald Doyle
School of Chemistry & Biochemistry
Georgia Institute of Technology

Dr. Cameron Sullards
School of Chemistry & Biochemistry
Georgia Institute of Technology

Dr. Raquel Lieberman
School of Chemistry and Biochemistry
Georgia Institute of Technology

Dr. Facundo Fernandez
School of Chemistry & Biochemistry
Georgia Institute of Technology

Dr. May Wang
College of Biomolecular Engineering
Georgia Institute of Technology

Date Approved: April 8th 2008

ACKNOWLEDGEMENTS

I wish to thank Dr. Walter Shaw, Avanti Polar Lipids Inc., without whose development of reliable internal standards, this research would not have been possible. I would also specifically like to thank Dr. Alfred H. Merrill Jr. and Dr. Cameron Sullards for their continued commitment to teaching me everything I know and for never giving up on me. I would also like to thank my wife for putting up with me through this process and the rest of my family for all their support.

TABLE OF CONTENTS

LIST OF TABLES

Page

LIST OF FIGURES

Page

LIST OF SYMBOLS AND ABBREVIATIONS

APn	Aminopentol
Cer	Ceramide
Cer1P	Ceramide 1-phosphate
ESI	Electrospray Ionization
FB1	Fumonisin B1
GalCer	Galactosylceramide
GlcCer	Glucosylceramide
HexCer	monohexosylceramide
LacCer	Lactosylceramide
LC-MS/MS	Liquid chromatography tandem mass spectrometry
MRM	Multiple reaction monitoring
QQQ	Triple Quadrupole
QTrap	Quadrupole linear-ion trap
Sa	Sphinganine
Sa1P	Sphinganine 1-phosphate
SL	Sphingolipid
SM	Sphingomyelin
So	Sphingosine
So1P	Sphingosine 1-phosphate

SUMMARY

Sphingolipids are a highly diverse category of compounds that serve not only as components of biologic structures but also as regulators of numerous cell functions. Because so many of the structural features of sphingolipids influence their biological activity, there is a need for comprehensive methods for quantitation of as many individual subspecies as possible. This dissertation describes methods that have been developed and validated for the extraction, liquid chromatographic separation, identification and quantitation of sphingolipids by electrospray ionization (ESI), tandem mass spectrometry (MS/MS) using an internal standard cocktail developed by the LIPID MAPS Consortium. The compounds that can be readily analyzed are sphingoid bases and sphingoid base 1-phosphates, as well as more complex species such as ceramides, ceramide 1-phosphates, sphingomyelins, and mono- and di-hexosylceramides. For broader utility, the methods have been optimized for two categories of tandem mass spectrometers, a triple quadrupole mass spectrometer and a quadrupole linear-ion trap mass spectrometer. With minor modifications, these methods can be applied to the analysis of isomers such as glucosylceramide and galactosylceramide, and with the availability of additional internal standards, more complex species such as sulfatides can also be quantified. Using these methods 46 species of these compounds have been quantified in RAW264.7 cells, a macrophage cell line.

Quantitation of individual sphingolipid metabolites is possible using liquid chromatography, tandem mass spectrometry, and stable isotope labeling with [^{13}C]palmitic acid can be used to differentiate between metabolites produced by *de novo* synthesis versus turnover. This approach is more accurate when one knows the isotope enrichment of the precursor pool (in

this case, [^{13}C]-palmitoyl-CoA); therefore this dissertation describes methods to analyze both the various isotopic forms of palmitoyl-CoA and sphingolipids through sphingomyelins and monohexosylceramides using two cell models, HEK293 cells and RAW264.7 cells treated with Kdo2-Lipid A. The analysis of the fatty acyl-CoA's followed a fragmentation mechanism involving a neutral loss of 507 Da (with the charge residing on the acyl-chain and thioester portion of the CoA). The sphingolipid analysis was simplified by the fragmentation of most of the metabolites (sphingoid bases and 1-phosphates, ceramides, and monohexosylceramides) to backbone product ions. For example the presence of the isotopic label in the long chain base, N-acyl linked fatty acid, or both was determined via, *m/z* 264 for [^{12}C]sphingosine (d18:1) and *m/z* 280 for [^{13}C]sphingosine (m+16, d18:1), versus the *m/z* of the isotopically labeled precursor, (m+16 versus m+32). For sphingomyelins, which poorly fragment to the individual backbone moieties, the isotope label can be determined by first treating the samples with phospholipase D to produce ceramide 1-phosphates that give the backbone fragments. Sphingolipid isotope metabolic precursor labeling experiments (SIMPLE) give a more accurate estimate of the amounts of sphingolipids made from de novo biosynthesis than is possible without isotopic labeling, or with use of stable isotopes without estimation of the specific activity of the precursor pool.

The alteration of these existing methods for application to collaborative projects is a required task for practical implementation. Several collaborative scenarios are explored and the alterations to standard methodologies are presented.

CHAPTER 1

Introduction

Sphingolipids (SL's) are a highly diverse category of compounds that serve not only as components of biologic structures but also as regulators of numerous cell functions. SL's are structural components of cellular membranes in all eukaryotes and some prokaryotes and viruses, and are characterized by the presence of a sphingoid base in the backbone of their structures. The term 'sphingosin' originated with Johann Thudicum, who used the term in reference to the sphinx-like properties of alkaloidal lipids isolated from brain extracts[1]. These enigmatic molecules have continued to fascinate and challenge the scientific community after the identification of well over a thousand unique SL species[2]. Recent advances in SL research have refined the perception of this class of lipid. Once regarded as just structural components of biological membranes, SL's are now known to play important roles in signal transduction,[3, 4] in addition to their structural functions. SL's are currently considered key bioactive molecules that modulate processes such as proliferation[3, 5], differentiation[6, 7], and apoptosis[8, 9]. Because of their involvement in many cellular processes, SL's have become the focus of researchers in other fields, such as atherosclerosis[10-12], angiogenesis[13-15], insulin resistance[16-19], inflammation[20-23], and stem cell research[24].

The capacity for *de novo* SL biosynthesis is prevalent in many cells and tissues. Cells display a loss of viability in the absence of exogenous sphingoid bases (if they are not produced *de novo*), downregulation of the *de novo* SL biosynthetic pathway by mutation,[25-27] or inhibition by myriocin[11, 28, 29] of serine palmitoyltransferase (SPT), the first enzyme in the biosynthetic pathway. *De novo* SL biosynthesis is widespread in cells

and tissues *in* vivo most likely due to the degredation of sphingoid bases in the mammalian intestine (although SL are present in most foods)[30, 31].

Selected SL's and a portion of their *de novo* biosynthetic and turnover pathways are shown in Figure 1.1, including free sphingoid bases (non-acylated, long-chain bases). Other species are N-acylated sphingoid bases, and still other species are more complex with a polar moiety at the 1-position. Long-chain sphingoid bases are variations of the basic structure: 2-amino-1,3-dihydroxyalkanes with (2S,3R) erythro stereochemistry. Sphingoid bases vary from linear 18 carbon alkyl chain containing no sites of unsaturation (d18:0), to as short as d14:0 and greater than d22:0, with possible unsaturations (most commonly Δ4) for d18:1, d18:2, etc. This increasing molecular diversity results from a series of biosynthetic enzymatic reactions. Cells exert fine-tuned control over SL metabolic flux and opposing outcomes in cellular state may hang in the balance: sphingosine and sphingosine-1-phosphate are interconverted by kinases and phosphatases [32, 33], and in general, the non-phosphorylated sphingoid base is pro-apoptotic[34] while the phosphorylated sphingoid base is anti-apoptotic (if produced by sphingosine kinase 1[35, 36] and apoptotic if produced by sphingosine kinase 2[37]). Studies of SL biology clearly require a high degree of specificity for quantitation of multiple molecular species in a single sample because of the structural similarity and interconversion of SL species. Thus, the ability to analytically distinguish these species is critical for the accurate determination of the amounts and metabolic flux. Development of state-of-the-art technologies for SL analysis, along with rigorous regard for qualitative and quantitative specificity, are thus required for investigation of intriguing areas, such as SL metabolism [38, 39], metabolic inhibition[40], and signaling[41-44].

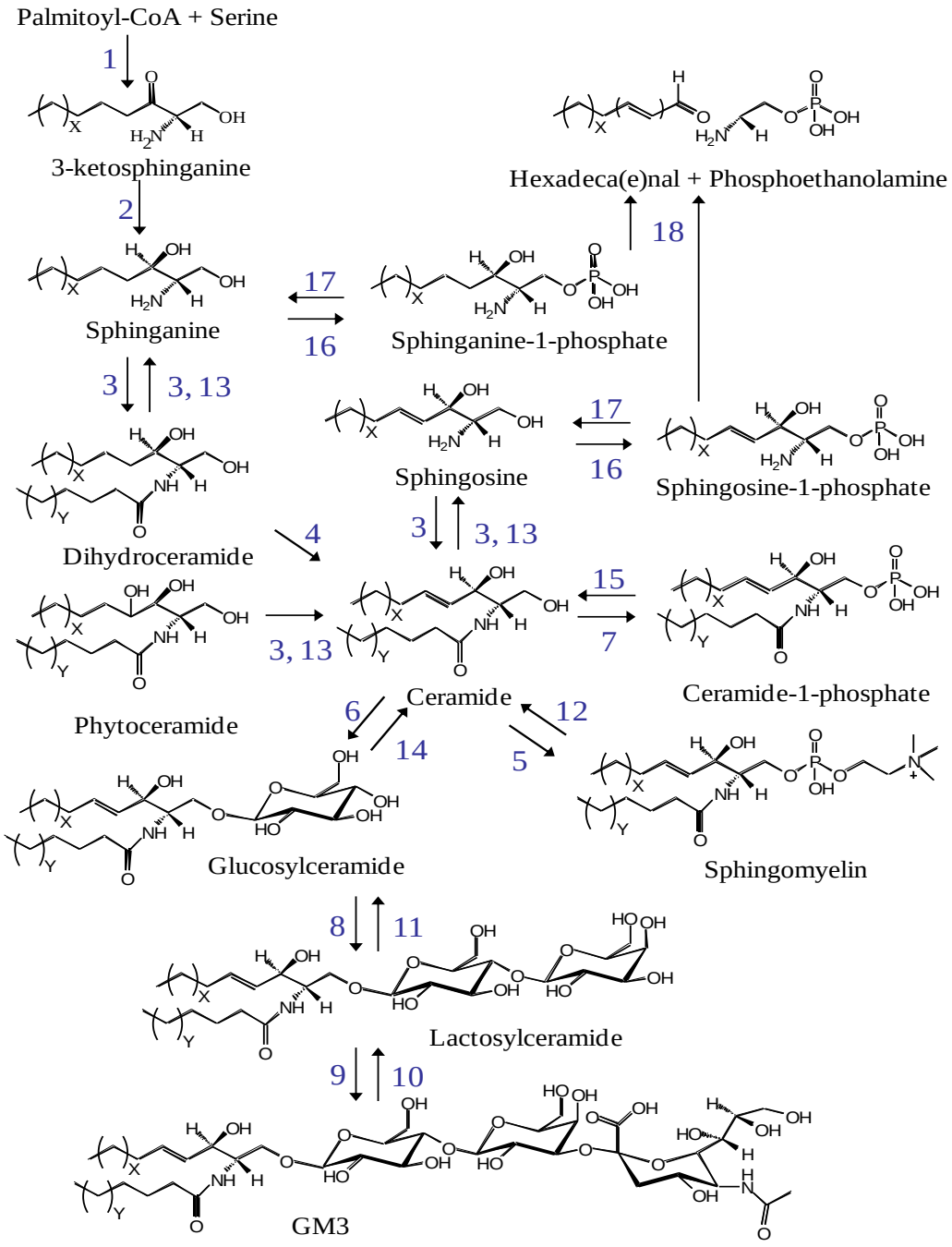

Figure 1.1 Partial sphingolipid metabolic pathway with structures of selected species and numerically designated enzymatic reactions. Enzymes in Figure 1 correspond to serine palmitoyltransferase – 1, 3-ketosphinganine reductase – 2, dihydroceramide synthases – 3, dihydroceramide desaturases – 4, sphingomyelin synthases – 5, glucosylceramide synthase - 6, ceramide kinase – 7, lactosylceramide synthase – 8, sialyltransferase 1 – 9, sialidase – 10, galactosidase – 11, sphingomyelinases (C-type) – 12, ceramidases – 13, β-glucoceramidase – 14, ceramide-1-phosphate phosphatase (putative) – 15, sphingosine / sphinganine kinases – 16, sphingosine-1-phosphate phosphatase – 17, and sphingosine-1-phosphate lyase – 18.

Sphingolipid Nomenclature

Sphingoid Bases

Sphingoid bases (also called long-chain bases) include 3-ketosphinganine, sphinganine, phytosphingosine (4-hydroxysphinganine), sphingodienes, and sphingosine (also called sphing-4-enine)[45]. The first product of *de novo* SL biosynthesis is 3-ketosphinganine, which is rapidly reduced to sphinganine by 3-keto-sphinganine reductase. In many mammalian cell types, phytosphingosine and sphingosine are the products of phytoceramide and ceramide de-N-acylation, respectively, not direct 4-hydroxylation and 4,5-*E*-desaturation of sphinganine. However, yeast cells and some mammalian cell types (i.e. intestinal epithelia [46]) directly synthesize 4-hydroxysphinganine. The number of carbon atoms in mammalian sphingoid bases is usually 18, but longer 20- and 22-carbon sphingoid bases have been detected in both human skin[47] and brain[48], and shorter sphingoid bases, 14 carbon atoms, are prevalent in the fruit fly *Drosophila memanogaster* [49]. A systematic sphingoid base nomenclature has been proposed [50] in which d and t designate the presence of two)di) or three (tri) hydroxyls, respectively, and the number of carbon atoms and desaturation(s) in the sphingoid base are expressed as x:y. A superscript indicates the first carbon atom of any double bond(s), thus, phytosphingosine is t18:0 and sphingosine (sphing-4-enine) is d18:1$^{\Delta 4}$ according to this system.

Metabolites of sphingoid bases include branched species (methyl group addition at n-1, n-2, and other positions), hydroxylated species at the 4- and 6-positions,1-phosphorylated species [37], mono-, di-, and tri-N-methyl species, and N-acyl (14 to 30 or more carbon atoms) species. Double bonds of the *E*-configuration (trans) at the Δ4-, Δ 8-

, and Δ 4,8-, and other positions of sphinganine are the product of direct sphingoid base desaturation in yeast, but in mammals, desaturation of N-acyl sphinganine (also called dihydroceramide) is the predominant source of sphingosine-based SL's [51]. Free long chain sphingoid bases (LCB's) are not typically abundant, for example, sub-micromolar concentrations have been detected in human glioma cells [52], however, sphingoid base phosphates are a significant component of blood platelet membranes [53]and HDL[54, 55]. Cleavage of sphingoid base phosphates at the carbon 2,3-position by sphingosine phosphate lyase eliminates the defining SL moiety, and remains the only known exit of SL from their metabolic pathway [56].

Dihydroceramide and Ceramide

The terms dihydroceramide and ceramide connote classes of N-acyl sphinganine and N-acyl sphingosine molecular species, respectively, where fatty acid alkyl chains of C16 to C24 [or greater than C30 in dermal tissues [57]] are amide linked to the amino group of the sphingoid base. This N-acyl chain variety derives from the acyl-CoA substrate specificity of six known human (dihydro)ceramide synthase isoforms [58, 59], for which the systematic names CerS1 to CerS6 have been proposed [60]. Dihydroceramide can be 4,5-*E*-desaturated to produce ceramide [61], or 4-hydroxylated by Δ4-dihydroceramide desaturase 2 to produce phytoceramide in mammalian cells [46]. Hydroxylation and desaturation at other positions have also been reported [62].

Functional group addition at the 1-hydroxy position of dihydroceramide or ceramide provides another level of structural diversity. Headgroups may be primarily linked by phosphodiester bonds at the 1-hydroxyl position yielding sphingomyelin (ceramide-1-phosphocholine, SM), ceramide phosphoethanolamine (CPE), and ceramide

phosphoinositiols). Ceramide may also be 1-O modified via phosphorylation or acylation to yield ceramide-1-phosphate [63] or 1-O-acyl ceramide [64], respectively. One alternative to *de novo* biosynthesis for the generation of sphingoid bases is the De-N-acylation of dihydroceramide to produce sphinganine. Likewise, de-N-acylation of ceramide and phytoceramide produces sphingosine and phytosphingosine, respectively. These sphingoid bases are therefore derived from the "turnover" or "salvage" pathway, and are subject to further metabolism as described above [65-67].

Glycosphingolipids

By far the most structurally diverse sphingolipids are the glycosphingolipids (GSLs). Here the carbohydrate headgroup is O-linked to the 1-hydroxyl position yielding a monohexosylceramide, which may be either glucosylceramide (GlcCer) or galactosylceramide (GalCer). Collectively called cerebrosides, these molecules serve as foundations for hundreds of unique molecular structures generated by the repeated glycosylation of a growing carbohydrate "tree" using different carbohydrate monomers (i.e. glucose, galactose, N-acetylglucosamine, N-acetylgalactosamine, fucose, N-acetylneuraminic acid, etc.). The GSL family may be subdivided into broad classes of neutral and acidic lipids based on the absence or presence of ionizable moieties such as a carboxylic acid or sulfate. GSL may be further subdivided into the ganglio- (Gg), globo- (Gb), isoglobo- (iGb), lacto- (Lc), neolacto- (nLc), arthro- (At), and mollu- (Mu) series, each of which is defined by a unique tetrasaccharide core (Figure 1.2).

Root Name	Abbreviation	Core Structure
Ganglio	Gg	Galβ1-3GalNAcβ1-4Galβ1-4Glcβ1-1'Cer
Lacto	Lc	Galβ1-3GalNAcβ1-3Galβ1-4Glcβ1-1'Cer
Neolacto	nLc	Galβ1-4GalNAcβ1-4Galβ1-4Glcβ1-1'Cer
Globo	Gb	GalNAcβ1-3Galα1-4Galβ1-4Glcβ1-1'Cer
Isoglobo	iGb	GalNAcβ1-3Galα1-3Galβ1-4Glcβ1-1'Cer
Mollu	Mu	GalNAcβ1-2Manα1-3Manβ1-4Glcβ1-1'Cer
Arthro	At	GalNAcβ1-4GlcNAcβ1-3Manβ1-4Glcβ1-1'Cer

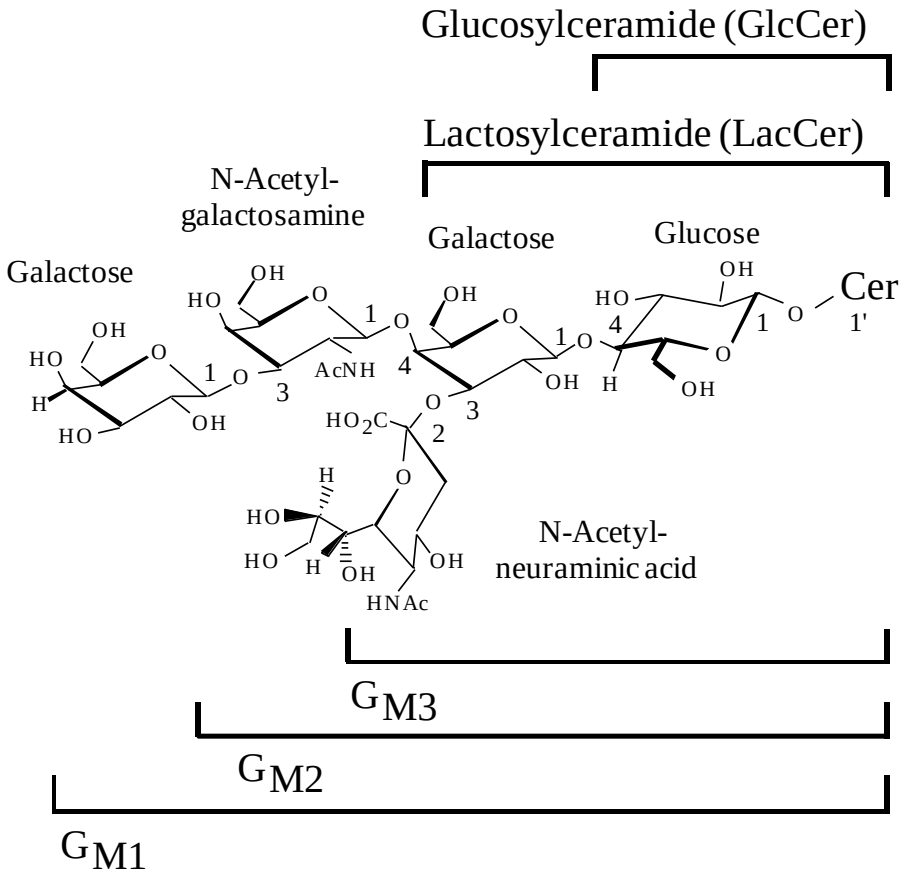

Figure 1.2. Glycosphingolipid nomenclature. The core tetrasaccharide structures that define each GSL group are listed, and a portion of ganglioside biosynthesis is shown.

One nomenclature for GSL is the Svennerholm system [68] where G is used to denote ganglioside, and M, D, and T represent the number of sialic acid residues (mono-,

di-, and tri-sialyl GSL, respectively) and the relative position of the species after resolution by thin-layer chromatography (for example the relative migrations of the G_M series are $G_{M3} > G_{M2} > G_{M1}$). Another more explicit nomenclature system sequentially lists saccharide subunits from the non-reducing end to the ceramide moiety, and specifies both the branching carbon atom linkage and the anomeric configurations of inter-saccharide bonds. For example, the core tetrasaccharide structure of ganglio-series GSL may be written Galβ1-3GalNAcβ1-4Galβ1-4Glcβ1-1'Ceramide, or simply Gg_4Ceramide. Because some GSLs are isomeric (the same set of saccharide subunits but different anomeric linkages or different branching), this nomenclature system uses Roman numerals and Arabic superscripts to designate the root saccharide and its specific position(s), respectively, which are substituted, and abbreviates the core tetrasaccharide moiety. For example, G_{D1a} may be written $IV^3Neu5AcII^3Neu5AcGg_4$Ceramide and its isomer $G_{D1a\alpha}$ as $III^6Neu5AcII^3Neu5AcGg_4$Ceramide. As an alternative to Roman numerals and Arabic superscripts, branch saccharides may be written in parentheses after the saccharide to which they are linked. The multiple anomeric linkages between carbohydrate monomers and further carbohydrate modifications such as sulfation and acetylation increase the number of potential GSL structures beyond 1000, indicating considerable room for discovery and characterization.

Lysosphingolipids

Other types of sphingoid base derivatives have recently garnered a great deal of attention because they have been found to be highly bioactive [69]. These lipids include the 1-phosphates and the "lyso" sphingolipids such as lyso sphingomyelin (sphingosyl-phosphocholine) and psycosine (glucosylsphingosine). Additionally, the N-methyl-

derivatives (N-methylsphingosine, N,N-dimethylsphingosine, and N, N, N-trimethylsphingosine) have also been observed [70], however, their route of synthesis and biological function have not been fully determined.

Cellular Biology

Sphingolipids are bioactive compounds that serve not only as components of biologic structures such as membranes and lipoproteins, but also as regulators of cell proliferation, differentiation, cell-cell and cell-matrix interactions, cell migration, intracellular (and extracellular) signaling, membrane trafficking, autophagy and cell death[2, 71, 72]. For most of these functions, there is structural specificity with respect to the major sphingolipid subclass (for example, in many cases ceramides are growth inhibitory whereas sphingoid base 1-phosphates usually stimulate growth)[73]. And within subclasses, changes as minor as the presence or absence of a double bond can have a major impact on function[74]. Methodologies which have the ability to distinguish and quantitate many sphingolipids rapidly, such as LC-MS/MS, are particularly suited for elucidating sphingolipids that affect biochemical behavior.

While sphingolipids are ubiquitous amongst eukaryotes, only some viruses prokaryotes contain sphingolipids[75]; however, general trends in sphingolipid structure exists in organisms of increasing evolutionary complexity. For example, plants are characterized as having both phytosphingosine (t18:1) as well as a higher occurrence of sphingodienes (d18:2)[76-78]. Yeast are characterized as having phytosphingosine as well as d20:1 and d20:0 sphingoid bases[79]. Insects have been shown to have d14:1 and d14:0 as their primary sphingoid bases[49, 80]. Insects have also been shown to have high quantities of ceramide phosphoethanolamine in contrast to sphingomyelin observed in

mammals[81] Mammals have been shown to have mainly d18:1 and d18:0 sphingoid bases; however, d20:1 and d20:0 are observed in tissues such as skin[47] and brain[82-84].

Sphingolipid biosynthesis and turnover take place in several organelles and cellular compartments. The committed step in sphingolipids biosynthesis is the condensation of a plamitoyl-CoA and a serine by serine palmitoyl transferase to form 3-keto-sphinganine, which is rapidly reduced to sphinganine by 3-keto-sphinganine reductase. Sphinganine can then be acylated by a number of (dihydro)ceramide synthases (discussed later). Dihydroceramides can then be desturated by dihydroceramide desaturases which leads to ceramide formation on the cytosolic surface of the endoplasmic reticulum[85]. Ceramides are then transfered to the Golgi by either vesicular[86] or non-vesicular transport, the latter mediated by ceramide transfer protein (CERT)[87]. The Golgi is the major site for the biosynthesis of complex sphingolipids such as glucosylceramide and sphingomyelin, except for galactosylceramide, which is made on the lumen side of the ER after ceramide is transfered inside by a flipase. The complex sphingolipids products are then transferred to the plasma membrane by vesicular transport. Turnover of sphingolipids takes place mainly in lysosomes[88]; however, some degradation takes place in the plasma membrane, such as sphingomyelinases[89]. Sphingolipids are degraded into sphingoid bases in the lysosome, which are then released to the cytosol where they can be phosporylated to sphingoid base 1-phosphates by sphingosine kinase or recycled back into the ER for use by ceramide synthases. Sphingoid base 1-phosphates can also be cleaved into ethanolamine phosphate and hexadecenal or hexadecanal (d18:1 and d:18:0 bases respectively) by sphingosine phosphate lyase in order to remove sphingolipids from the pathway.

Classical Methods of Sphingolipid Analysis

Thin Layer Chromatography (TLC)

TLC has been used for the qualitative study of sphingoid bases and their phosphates [90], ceramides [91], sphingomyelin [92] and more complex GSLs [93]. Advances in high performance TLC (HPTLC) have allowed improved resolution of some molecular species [94, 95]. However, TLC does not offer sufficient structural specificity to guarantee homogeneity within a single spot.

High Performance Liquid Chromatography (HPLC)

HPLC has also been employed for separation and identification of derivatized and underivatized sphingoid bases [96-98], sphingoid base 1-phosphates [99], ceramides, sphingomyelins [100], and monohexosylceramides [101]. HPLC has the advantage of being relatively inexpensive while providing resolution of SL's based on headgroup (normal phase) or N-acyl chain length (reverse phase). Detection of SL's has been primarily performed by UV or fluorescence after deacylation (for complex SL's) and modification of the free amine via addition of a chromophore such as ortho-phthaldehyde [102]. However, recent advances in evaporative light-scattering detection (ELSD) [103] avoid any necessity for derivatization. Ceramides or other complex SL can also be analyzed either by O-benzylation derivatization using benzoyl chloride [104, 105] or benzoic anhydride [106] or by synthetic derivatives (such as short chain analogues with 7-nitro-2-1,3-benzoxadiazol-4-yl (NBD) moieties [107, 108]. However, accurate quantitation often depends on definitive resolution of SL species, which HPLC alone cannot guarantee. This disadvantage exemplifies the requirement for more specific techniques of structural elucidation.

Immunochemical methodologies

Immunochemistry techniques have yielded information on sphingolipids such as GD3[109] and ceramides [110]. These methods typically employ antibody affinities for isolation of SL's for quantitation or standard protein isolations through gel electrophoresis coupled to blotting. However, these methods do not have a guaranteed high level of specificity, because the antibody may have affinity for the desired target as well as undesired targets. Certainly protein work is valuable for understanding the expression of regulatory enzymes and their precursor genes; however, these studies prove much more valuable when coupled to more rigorous quantitative analysis on the species in the sphingolipid biosynthetic and regulatory pathways.

Sphingolipid Analysis via Mass Spectrometry

Electron Ionization (EI) Mass Spectrometry

Ions are produced in EI by the interaction of analytes and electrons in the gas phase. Electrons are produced by heating a wire, which has a current running through it. Electron ionization mass spectrometry was initially used to elucidate the structures of ceramides [111, 112] and neutral GSL species [113, 114]. These early experiments permitted the analysis of SL's as intact molecular species, and yielded diagnostic fragmentations that could distinguish isomeric SL structures [115, 116]. Because these molecules were either relatively large or polar they required derivatization of the SL to trimethylsialyl [117] or permethyl ethers to reduce their polarity and increase their volatility for efficient transfer to the gas phase. However, in some cases observation of intact higher mass molecular ions was precluded because EI induced extensive fragmentation owing to its relatively high-energy imparted during ionization. Additionally, resolution of complex mixtures of

SL's with varying headgroups, sphingoid bases, and N-acyl combinations was particularly challenging using these methods as resulting spectra displayed multiple fragments from multiple precursors.

Fast Atom Bombardment (FAB) and Liquid Secondary Ionization Mass Spectrometry (LSIMS)

FAB and LSIMS are techniques for the ionization of non-volatile lipids in which SL's are ionized off a probe tip by collisions with a beam of either accelerated atoms or ions [78, 118-120]. FAB and LSIMS are considered to be much "softer" ionization techniques than EI as they ionize lipids directly without need for derivatization and yield intact molecular ions with a lesser degree of fragmentation. These ionization techniques allowed analysis of complex mixtures of monohexosylceramides [121], sphingoid bases [122] and sphingomyelins [123] as individual molecular species could be distinguished by mass.

Structural information could also be obtained from mass spectrometric analysis, especially if tandem mass spectrometric analyses were employed to select an ion of interest, collisionally dissociate it, and detect the resultant product ions. When either $(M + H)^+$ or $(M - H)^-$ precursor ions fragment, they do so at specific positions to yield product ions distinctive for the structural sections of SL: headgroup, sphingoid base, and N-acyl fatty acid [124]. These pathways of fragmentation can be influenced by the inclusion of alkali metal ions as $(M + Metal)^+$ where the metal may be Li^+, Na^+, K^+, Rb^+, or Cs^+ [125].

FAB and LSIMS have some limitations for SL analysis. Both of these methods require a matrix to solubilize the analyte of interest and aid in its ionization. These matrices induce a significant amount of background chemical noise, which can limit

sensitivity, especially for lower molecular mass species, such as the free sphingoid bases. Methods such as Dynamic FAB [126, 127] partially solved this problem with continuous application of solvent and matrix to the probe tip; however, the ~ 100-fold reduction in background noise was not enough to completely eliminate background chemical noise from matrix at low analyte concentrations.

Electrospray Ionization

Electrospray ionization (ESI) allows SL's in solution to be continuously infused directly into the ion source of a mass spectrometer [128-130]. The central component of this ion source is a hollow metal needle, which is held at a high positive or negative potential. At the ending tip of the needle, highly charged solvent droplets containing SL's are formed and are subsequently drawn into the orifice of the mass spectrometer via both a potential and atmospheric pressure difference. During transition from atmospheric pressure to vacuum the solvent is pumped away and the analyte of interest is ionized in the gas phase. This ionization technique results in a much softer ionization, and when optimized yields primarily intact ions with little or no fragmentation.

Early ESI ion sources required low flow rates and multiple pumping stages to remove excess solvent. However, ESI provided greatly reduced chemical noise and yielded sensitivity orders of magnitude lower than either FAB or LSIMS. Structural information could likewise be obtained via tandem mass spectrometry, whereby specific headgroup, sphingoid base, and fatty acid combinations may be determined.

High Performance Liquid Chromatography Mass Spectrometry (HPLC-MS) and Tandem Mass Spectrometry (MS/MS)

ESI's method of direct sample introduction and ionization via solution naturally lends itself to coupling HPLC prior to mass spectrometric analysis for added separation and analytical robustness for quantitation. When analyzed in this manner SL's may be de-salted, chromatographically focused, and selectively eluted enhancing sensitivity. HPLC also serves to reduce the complexity of the eluent at any given elution time, which greatly reduces ionization suppression effects from other species further improving quantitative accuracy and sensitivity. Additionally, HPLC allows the separation of isomeric and isobaric species, which are often indistinguishable by mass spectrometry alone.

HPLC-MS/MS has been used to identify, quantify, and determine the structures of free sphingoid bases, free sphingoid base phosphates [131-133], ceramides, monohexosylceramides (both galactosylceramides and glucosylceramides), lactosylceramides, sphingomyelins [134, 135] and more complex glycosphingolipids [136, 137]. Complete chromatographic resolution of all individual species is not required in LC-MS/MS because the mass spectrometer is able to differentiate between many components present in a mixture by their mass and structure (for example, all of the N-acyl chain length variants of Cer). Sphingolipidomic separations have mainly been distributed between two types of HPLC: reversed phase LC [138, 139] for separations based on the length and saturation of N-acyl chains (for example, to separate sphingosine and sphinganine) and normal phase LC [138, 140] to separate compounds primarily by their headgroup constituents (for example, resolving ceramide from sphingomyelin, etc.). The

requirement for some LC separations many not be immediately realized, for example, sphingosine and sphinganine have easily resolved precursor and product ions. However, typically in biological samples sphingosine is much more abundant than sphinganine, and the (M + 2) isotope of sphingosine will have the same precursor *m/z* as sphinganine, and so will interfere with the quantitation of sphinganine unless the sphingoid bases have been separated by LC [138].

Matrix Assisted Laser Desorption Ionization Mass Spectrometry and Tandem Mass Spectrometry

Matrix assisted laser desorption ionization (MALDI) has been used to identify ceramide, monohexosylceramide, and sphingomyelin [141] as well as complex GSLs, including lactosylceramide and gangliosides [142]. Samples are prepared for MALDI by mixing a solution containing the analyte with a solution containing a matrix compound often in much greater concentration. MALDI matrices are typically small substituted organic acids that contain a moiety that absorbs the photonic energy of the laser [143]. Absorption of the laser energy causes the matrix to become vibrationally excited and volatilize taking analyte molecules with it into the gas-phase. Here the analyte and matrix molecules under go charge exchange reactions and the analyte becomes ionized. Matrix choice is key to successful generation of intact molecular species with minimal fragmentation and has been thoroughly reviewed [144].

MALDI ion sources are typically used in conjunction with time-of-flight (ToF) mass analyzers because the laser pulse and resulting ion plume provides a discreet event which is compatible with ToF mass analysis [145]. Because of the nature of MALDI ionization, studies of more complex GSL have often utilized this technique [146, 147].

MALDI efficiently produces singly charged ions, which in conjunction with the high *m/z* range of ToF instruments, has aided in the observation of higher molecular weight GSLs [148]. One downside to this ionization technique is that many matrices produce abundant background chemical noise at lower *m/z* values, which precludes analysis of smaller free sphingoid bases and similarly sized SLs. However, new advances in matrix choices and high pressure sources may provide an opportunity to study these lower molecular weight SLs by MALDI.

Sphingolipidomics

In order to perform investigations on a biological scale, analyses must encompass a "sphingolipidomic" scale, for which mass spectrometry is the analytical tool of choice for several important reasons. First, mass spectrometry provides a high level of specificity with regard to identification of complex molecular species via molecular mass. This is especially true with either high resolution and accurate mass measurement, which yields empirical formula [147], or tandem mass spectrometry (MS/MS) [149], which yields structural information. Second, mass spectrometry provides levels of sensitivity that are orders of magnitude lower than that of classical techniques (sub fmol detection limits). This enables detection of SL's present in minute quantities (~ fmol or less) in small sample amounts (~10^6 cells). Third, the signal response of SL's analyzed by mass spectrometry can be correlated to their concentration yielding quantitative information. [It should be noted that accurate and precise quantitation via mass spectrometry requires use of appropriate internal standards to control for sample losses in extraction, and normalization for differences in ionization and fragmentation of various individual molecular species.] Finally, mass spectrometry provides a wide dynamic range, typically

several orders of magnitude for quantitation of SL's. This allows analysis of SL's which vary in abundance over this range in biological systems (i.e. sphingomyelin versus sphingosine-1-phosphate). In spite of all these positive attributes, poor choices in analytical techniques and experimental design can yield erroneous results. These include sample handling and extraction protocols, separation of isomeric and isobaric species prior to mass analysis, internal standards, ionization technique, instrument (mass analyzer, interface, and tuning), and mass spectrometry analysis technique.

CHAPTER 2

Quantitative analysis of sphingolipids for lipidomics using a triple quadrupole mass spectrometer and a quadrupole linear ion trap mass spectrometer in the triple quadrupole mode

Many methods have been used for sphingolipid analysis, from classic methods such as TLC [150] and HPLC [151], to mass spectrometry, which has proven to be useful for analysis of broad categories of sphingolipids from sphingoid bases and their 1-phosphates [130, 131, 152, 153] to ceramides (Cer) [128, 131, 135, 154, 155] and simple mono- and dihexosylceramides [127, 138, 142, 156, 157], sphingomyelins (SM) [138, 158-161], and more complex glycosphingolipids [114, 137, 162-166].

Some of the methods are able to profile subspecies in multiple categories [130, 131, 138, 167-170]. Chromatographic resolution of specific subsets of sphingolipid allows for focused analysis of each subset [130, 138]. These methods allow for quantitation through the use of internal standards, which are required to elute in a similar time window and follow similar fragmentations.

For quantitation of sphingolipids it is essential to have internal standards that are valid for each of the subspecies that the method reports to quantify [131, 169]. These can be stable isotope, N-acyl chain length variants, or sphingoid base variants. This study compares the validity of an internal standard cocktail that is commercially available and contains species to quantify sphingoid bases, sphingoid base 1-phosphates, and several families of complex sphingolipids. Short chain, d17:1 and d17:0, sphingoid bases and sphingoid base 1-phosphates are used for quantitation of the 18:1 and 18:0 species; whereas, complex species are quantified by comparison to C12:0 N-acyl species.

It is common in mass spectrometry to have various categories of instruments available for identification and quantitation of analytes, which involve using different combinations of modes of ionization and mass analyzers. This dissertation describes the optimization and validation of a sphingolipid internal standard cocktail on both a triple quadrupole and a quadrupole linear-ion trap mass spectrometer operating in the triple quadrupole mode, both equipped with electrospray sources. Because it is an intrinsic feature of mass spectrometry that ion yields tend to vary considerably among different compounds, source, methods, and instruments, an analysis that purports to be quantitative will not be conclusive unless the methods involved are validated. By first optimizing the ionization and fragmentation conditions for a wide range of N-acyl chain length analytes as well as the internal standards used to quantify them on both instruments, LC-MS/MS methods could be developed for quantitative analysis.

By using syringe infusion analysis to characterize the sphingolipid profile of RAW264.7 cells, LC-MS/MS methods were adjusted to quantify the major sphingolipid species found to be present. Internal standards were then evaluated for their ability to quantify the naturally occurring species in RAW264.7 cells.

Materials and Methods

Materials

Synthetic internal standards were obtained from Avanti Polar Lipids (Alabaster, AL). These standards were provided in sealed ampules at concentration dated and certified by Avanti polar lipids as an internal standard cocktail (named LM-6002) (d17:1 So, d17:0 Sa, d17:1 sphingosine 1-phosphate (S1P), d17:0 sphinganine 1-phosphate (Sa1P), d18:1/C12:0 Cer, d18:1/C25:0 Cer, d18:1/C12:0 GlcCer, d18:1/C12:0 lactosylceramide, d18:1/C12:0 ceramide 1-P and d18:1/C12:0 SM) by Avanti Polar

Lipids (Alabaster, AL). The sulfatide internal standard (d18:1/C12:0 sulfatide) and d18:1/C12:0 galactosylceramide were obtained from Avanti Polar Lipids (Alabaster, AL) as an individual compounds. For comparison additional internal standards were obtained from commercial providers as follows. Sulfatides (d18:1/16:0 and d18:1/C18:0) were obtained from Matreya (Pleasant Gap, PA). All other chain length sphingolipids were either obtained from Avanti Polar Lipids (Alabaster, AL), or commercially unavailable d18:0 sphingolipids were synthesized by bubbling hydrogen gas through solutions containing the d18:1 sphingolipid and 10% Pd on charcoal (Sigma St. Louis, MO). All solvents used were HPLC grade. Methanol (HPLC grade) VWR (Catalog # EM-MX0475), acetonitrile (HPLC grade) VWR (Catalog # EM-AX0145), chloroform (HPLC grade) VWR (Catalog # EM-CX1058), hexanes (HPLC grade) VWR (Catalog # JT9304-33), formic acid (ACS grade) VWR (Catalog # EM-FX0440-7), acetic acid (ACS grade) Fisher (Catalog # A38C-212). VWR (West Chester, PA) and Fisher (Pittsburgh, PA).

Cell Culture

RAW264.7 is a macrophage-like cell line derived from tumors induced in male BALB/c mice by the Abelson murine leukemia virus. Cells were obtained from ATCC laboratories (cat# TIB-71; lot# 3002360). RAW264.7 cells were grown in 60-mm plastic culture dishes in DMEM supplemented with 10% FBS, 4 mM L-glutamine, and 4.5 g/L glucose. RAW264.7 cells were cultured at 37°C, 95% relative humidity, and 5% CO_2 with 1.5 g/L sodium bicarbonate, 100 U/mL penicillin, and 0.1 mg/mL streptomycin in ThermoForma Steri-cult CO_2 incubators. Cells were passaged at 80% confluence and seeded at 2.5 x 10^6 cells in 5 mL of media. Cells were never passaged more than 20 times.

Extraction of cells

RAW264.7 cells were washed twice with PBS to remove excess media, scraped from the dish using Nalgene cell scraper (Rochester, New York) and transferred by pipette into a 13 x 100 mm borosilicate tube with a Teflon-lined cap (VWR, West Chester, PA). Additions of 0.5 mL CH_3OH and 0.25 mL $CHCl_3$, followed by internal standards (500 pmol) dissolved in 0.02 mL ethanol were added to the test tube then the extracts were dispersed using a Brinson 1510 ultra sonicator at room temperature for 30 s, and incubated at 48°C overnight in a heating block. After cooling, 75 µl of 1 M KOH in CH_3OH was added, mixed briefly by sonication, and incubated in a shaking water bath for 2 h at 37°C. A fraction of 0.4 mL was transferred to a new test tube and solvent was evaporated using a Savant AES2000 Automatic Environmental Speedvac. The dried residue was reconstituted in LC-MS/MS mobile phase (identical A:B composition to initial chromatographic conditions) for sphingoid base and sphingoid base 1-phosphate analysis. The remainder of the initial extract was neutralized with 3 µl of glacial acetic acid, and 3 ml 1:2 (v/v) of $CHCl_3/H_2O$ was added. Samples were mixed and then centrifuged. The lower layer was removed by a Pasteur pipet, and transferred to a new tube. The dried residue was reconstituted in LC-MS/MS mobile phase (identical A:B composition to initial chromatographic conditions) for complex sphingolipid analysis

Instruments

Two different LC-MS/MS systems were used for lipidomic analysis: a Perkin Elmer Series 200 MicroPump system coupled to a PE Sciex API 3000 triple quadrupole mass spectrometer (Applied Biosystems, Foster City, CA), and a Shimadzu LC-10 AD

VP binary pump system coupled to a Perkin Elmer Series 200 autoinjector coupled to an ABI 4000 QTrap (Applied Biosystems, Foster City, CA).

Liquid Chromatographic Separation

Sphingoid Bases, Sphingoid Base 1-Phosphates, and Ceramide 1-Phosphates

Free sphingoid bases, sphingoid base 1-phosphates and the Cer-1-P were separated by reverse phase HPLC using a binary solvent system and a Supelco 2.1 x 50 mm Discovery C18 column (Sigma St. Louis, MO) at a flow rate of 1 mL/min. Mobile phase A consisted of $CH_3OH/H_2O/HCOOH$ (58:41:1) (v,v,v) with 5 mM ammonium formate. Mobile phase B consisted of $CH_3OH/HCOOH$ (99:1) (v,v) with 5 mM ammonium formate. Prior to the injection, the column was equilibrated for 0.4 min with 60:40 (A/B). After sample injection (50 μL), the analytes were eluted with 60:40 A/B for 0.5 min, followed by a 1.8 min linear gradient to 100% B, which was held for 5.3 min and followed by a 0.5 min wash of the column with 60:40 A/B to re-equilibrate the column before the next run.

Complex Sphingolipids

The Cer, monohexosylceramides (HexCer), SM, sulfatide (ST), LacCer, and Cer-1-P were separated by normal phase HPLC using a binary solvent system and a Supelco 2.1 x 50 mm LC-NH_2 column at a flow rate of 1.0 mL/min. Mobile phase A consisted of $CH_3CN/CH_3OH/HCOOH$ (97:2:1) (v,v,v) with 5 mM ammonium formate. Mobile phase B consisted of $CH_3OH/H_2O/HCOOH$ (89:6:5) (v,v,v) with 50 mM triethylammonium acetate. Prior to injection, the column was equilibrated for 1.0 min with 100% A. After sample injection, analytes were eluted with 100% A for 3 min, followed by a 1.0 min linear gradient to 100% B, which was held for 3.0 min, and then followed by a 1.0 min

linear gradient to 100% A. The column was then re-equilibrated at 100% A for 1.0 min.

Glucosylceramide and Galactosylceramide

Because glucosylceramide and galactosylceramide coelute by the above method, biological samples that contain both can be analyzed by a separate method. Dried samples are re-dissolved in $CH_3CN/CH_3OH/H_3CCOOH$ (97:2:1) (v,v,v) with 5 mM ammonium acetate. The LC-Si column (Supelco 2.1 x 250 mm LC-Si) is pre-equilibrated with $CH_3CN/CH_3OH/H_3CCOOH$ (97:2:1) (v,v,v) with 5 mM ammonium acetate for 1.0 min at 1.5 mL per min, sample is injected, and the column is isocratically eluted for 8 min. GlcCer elutes at 2.56 min and GalCer at 3.12 min using this isocratic normal phase system; however, column age and previous sample load can influence the retention times of HexCer's by this method. Periodic retention time confirmation with internal standards allows the monitoring of column stability and subsequent effectiveness.

Quantitative LC-MS/MS

Ion source temperature varied between 300 and 500 °C depending on solvent composition and mass spectrometer. Q3 was set to pass molecularly distinctive product ions. A multiple reaction monitoring (MRM) method was created by setting Q1 and Q3 to pass the precursor and product ions of the most abundant sphingolipid molecular species and fragment ion. In both instruments N_2 was used to collisionally induce dissociations in Q2, which was offset from Q1 by 30-120 eV. For example, for Cer, these transitions occur at *m/z* 538.7/264.4, 566.5/264.4, 594.6/264.4, 622.7/ 264.4, 648.7/264.4, 650.7/264.4, which correspond to Cer with a d18:1 sphingoid base and

C16:0, C18:0, C20:0, C22:0, C24:1, and C24:0 N-acyl chain, respectively. The dwell time was 25 ms for each transition.

Infusion Experiments

Identification of ionization and fragmentation parameters for standards

Prior to running of standard curves on either instrument, each analyte was diluted to a concentration of 1 to 10 pmol/µL in CH_3OH and infused into the ion source at a rate of 0.6 mL/h to optimize ionization and fragmentation conditions for each sphingolipid species. Once the LC elution was optimized, this procedure was repeated for each analyte dissolved in the solvent mixture at the appropriate ratios in which they elute from the column. This optimization allows for correction of ionization conditions, as might be anticipated due to the differences in mobile phase composition.

The optimization procedure was identical for each analyte. Ionization conditions were first varied to produce the maximum signal with the mass spectrometer functioning in only MS mode. In the QQQ these settings were declustering potential (DP) and focusing potential (FP), and in the QTrap the settings were DP and entrance potential (EP). After the Q1 settings are determined, product ion spectra are taken across a range of collision energies (CE). Structurally specific product ions are identified. One structurally indicative product ion is then chosen for optimization. Collision energies and collision cell exit potentials (CXP) are then varied to produce optimal signal for the product ion of choice. With optimal settings determined, the precursor/product ion pairs are placed in an MRM method for validation.

Survey of species in biological samples profile

Cellular extracts are resuspended in 0.5 mL CH_3OH and infused into the QTrap at a rate of 0.6 mL/h to determine sphingoid base and fatty acid combinations within the sample. Several different precursor scans are used to determine sphingolipid composition. Precursor ion scans of *m/z* 184.4 are indicative of SM. Precursor scans of *m/z* 264.4 and 266.4 are then performed over a wide range of collision energies (35-75 eV) and mass ranges to check for other classes of sphingolipids and the corresponding d18:1 and d18:0 subspecies (Cer, HexCer, LacCer, etc). Precursor ion scanning also allowed the evaluation of the N-acyl chain length distribution as well as presence of hydroxylation. Precursor scans of *m/z* 264.4 and 266.4 +/- n*(14) are used to identify the sphingoid base profile within samples that have different chain lengths. Similarly, precursor scans of *m/z* 262.4 and 262.4 +/- n*(14) are used to identify the presence of d18:2 species.

Standard Curves

Unless shipped as a 1 mg sealed ampule, powder of each sphingolipid was placed in a decicator overnight to ensure that each weighed amount was a true dry weight. Each analyte was dissolved in methanol in concentrated stocks of approximately 0.5 mg/mL. These were then serially diluted to 0.5 to 1000 pmol in 50 µL solvent. Each concentration was run by LC-MS/MS in triplicate. Identical samples were analyzed on both mass spectrometers.

Evaluation of Sphingolipid Recovery

The non-soluble material from cellular extracts was re-extracted three times using the above method, and each extract was analyzed by LC-MS/MS for sphingoid base and sphingoid base 1-phosphate analysis. The upper layer from the final step of the cellular

extracts was re-extracted 3 times with1 ml $CHCl_3$. The dried residue was reconstituted in LC-MS/MS mobile phase for complex sphingolipid analysis.

Thioglycollate Elicited Macrophages

Thioglycollate elicited macrophages were produced by collaborators using the following Lipid Maps protocol (http://www.lipidmaps.org/protocols/PP0000001400.pdf). Samples were shipped dry and extracted by the above protocol.

Results

The goal of these experiments was to develop reverse phase (Figure 2.1) and normal phase (Figure2.2) LC-MS/MS methods for the quantitation of sphingolipids on both an API 3000 triple quadrupole (QQQ) and ABI 4000 quadrupole linear-ion trap (QTrap) mass spectrometers using a commercially available internal standard cocktail.

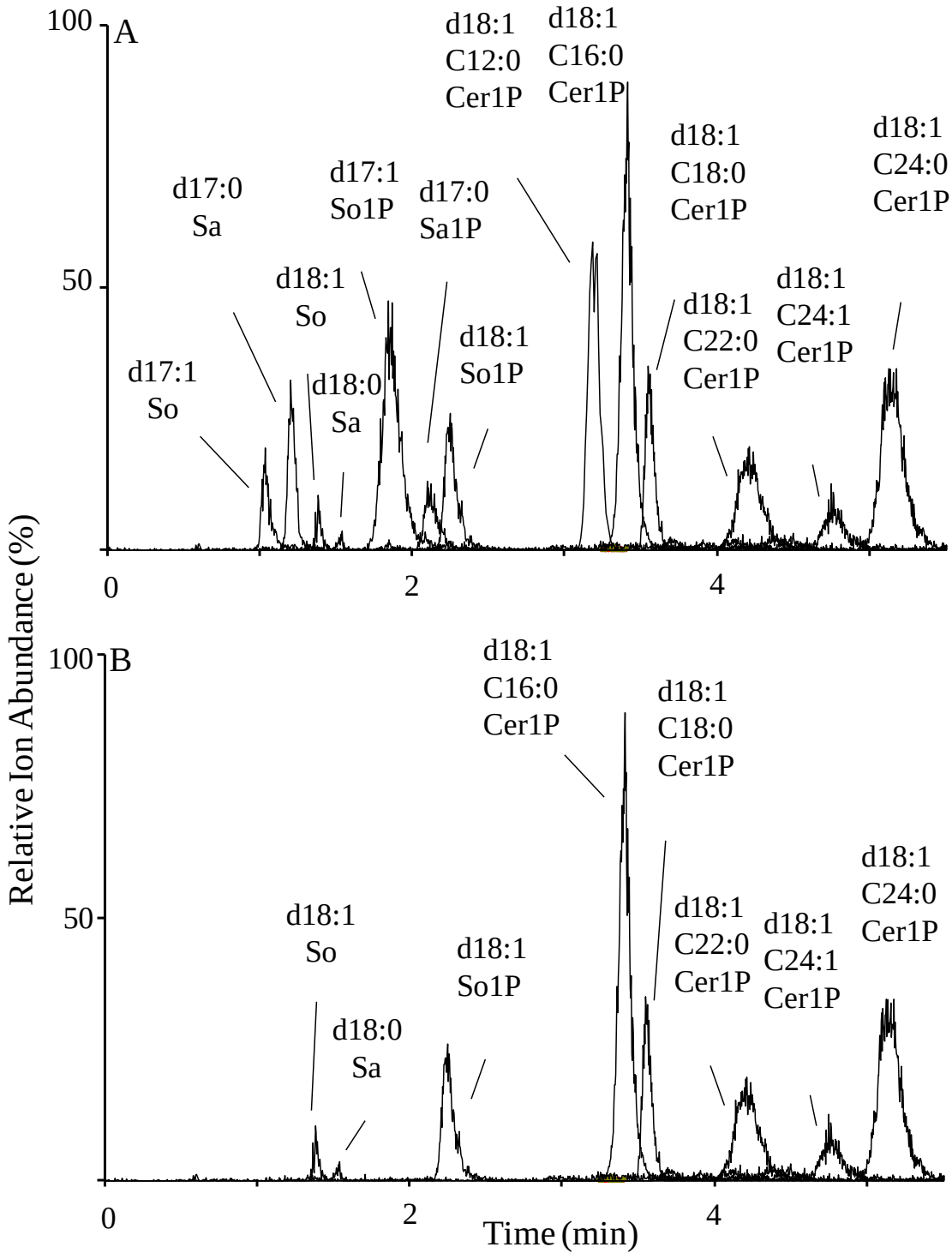

Figure 2.1. Reverse phase LC-MS/MS of sphingoid bases, base 1-phosphates, and Cer1P from RAW264.7 cells. A) with internal standards and B) without internal standards.

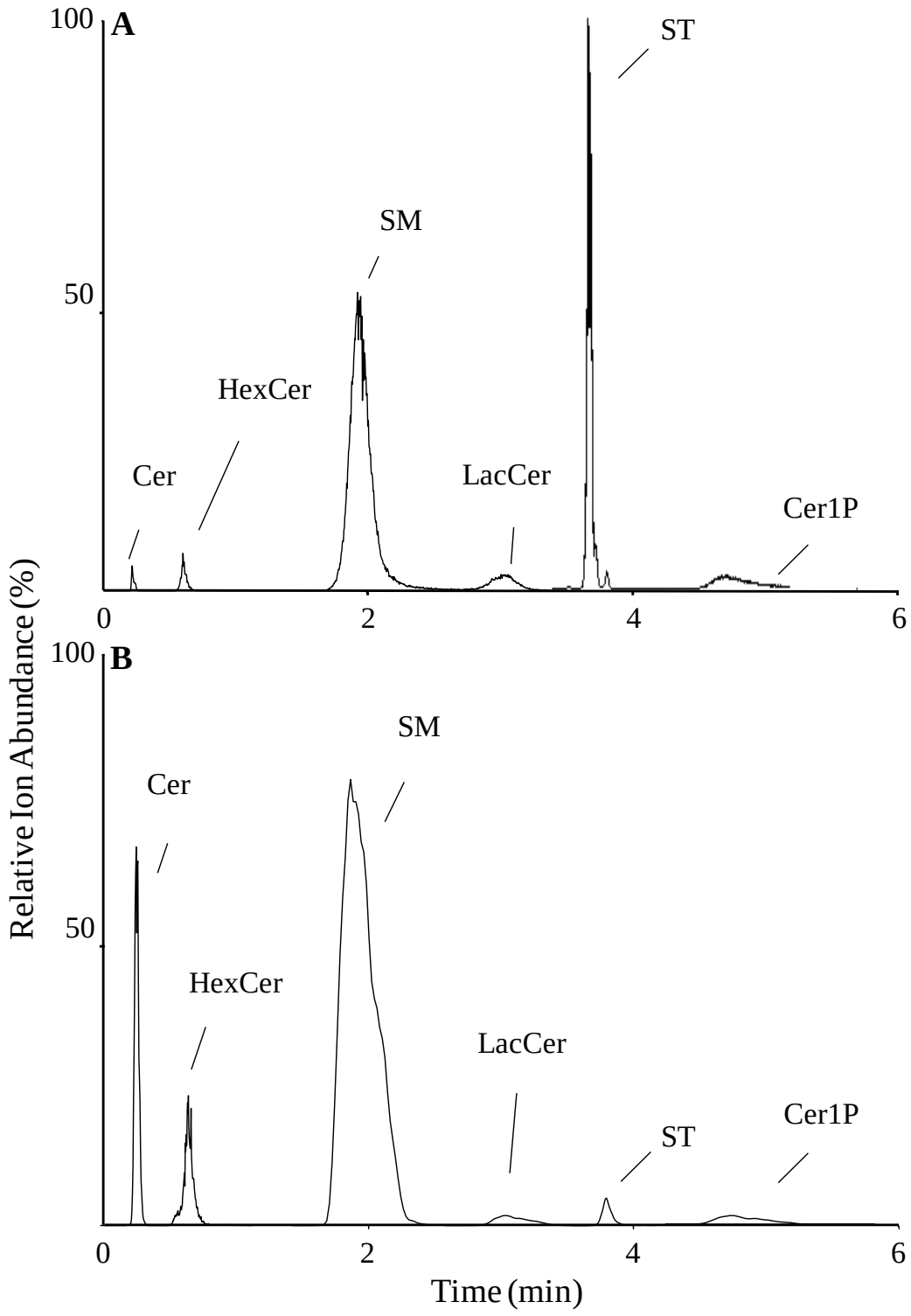

Figure 2.2. Normal phase LC-MS/MS total ion chromatogram of Cer, GlcCer, SM, LacCer, sulfatide, and Cer1P. Internal standards **A)** and RAW264.7 cells with internal standards **B)** without internal standards.

Initial Ion Characterization

Syringe infusion was initially used to characterize sphingolipid ionization and fragmentation behavior on the QQQ and QTrap. In the QQQ, d17:1 and d18:1 So doubly dehydrate to form fragment ions of *m/z* 250.3 and 264.4 respectively (Figure 2.3); whereas, in the QTrap the most abundant product ion is the single dehydration product ion of *m/z* 268.3 and 282.3 respectively. Both instruments displayed formation of a $[M-CH_4O_2]^+$ product ions for So and Sa *m/z* 252.2 and 254.2 respectively, which resulted from cleavage of the 1 carbon and the hydroxyl at that position as well as dehydration at the 3 position. Sa species on the QTrap undergo a loss of C_2H_6NO to produce a primary product ion of *m/z* 60 (Figure 2.4). Sphingoid base 1-phosphates fragment via cleavage of the phosphate group and dehydration at the 3 position on both instruments yielding fragment ions of *m/z* 264.4 and *m/z* 266.4 for d18:1 and d18:0 sphingoid bases, respectively [169]. A general fragmentation mechanim is proposed in Figure A2.1.

Cer fragments via cleavage of the headgroup from the 1 position, dehydration at the 3 position, and cleavage of the N-acyl chain to either *m/z* 264.4 for d18:1 species or *m/z* 266.4 for d18:0 species (Figure 2.5) Other product ions are observed in the CID spectrum of d18:1/C12:0 Cer, including a single dehydration at *m/z* 464.5, double dehydration at *m/z* 446.4, loss of CH_4O_2 at *m/z* 434.4, cleavage of the N-acyl chain and a single dehydration at *m/z* 282.2, and loss of CH_4O_2 along with cleavage of the N-acyl chain and a dehydration at *m/z* 252.3.

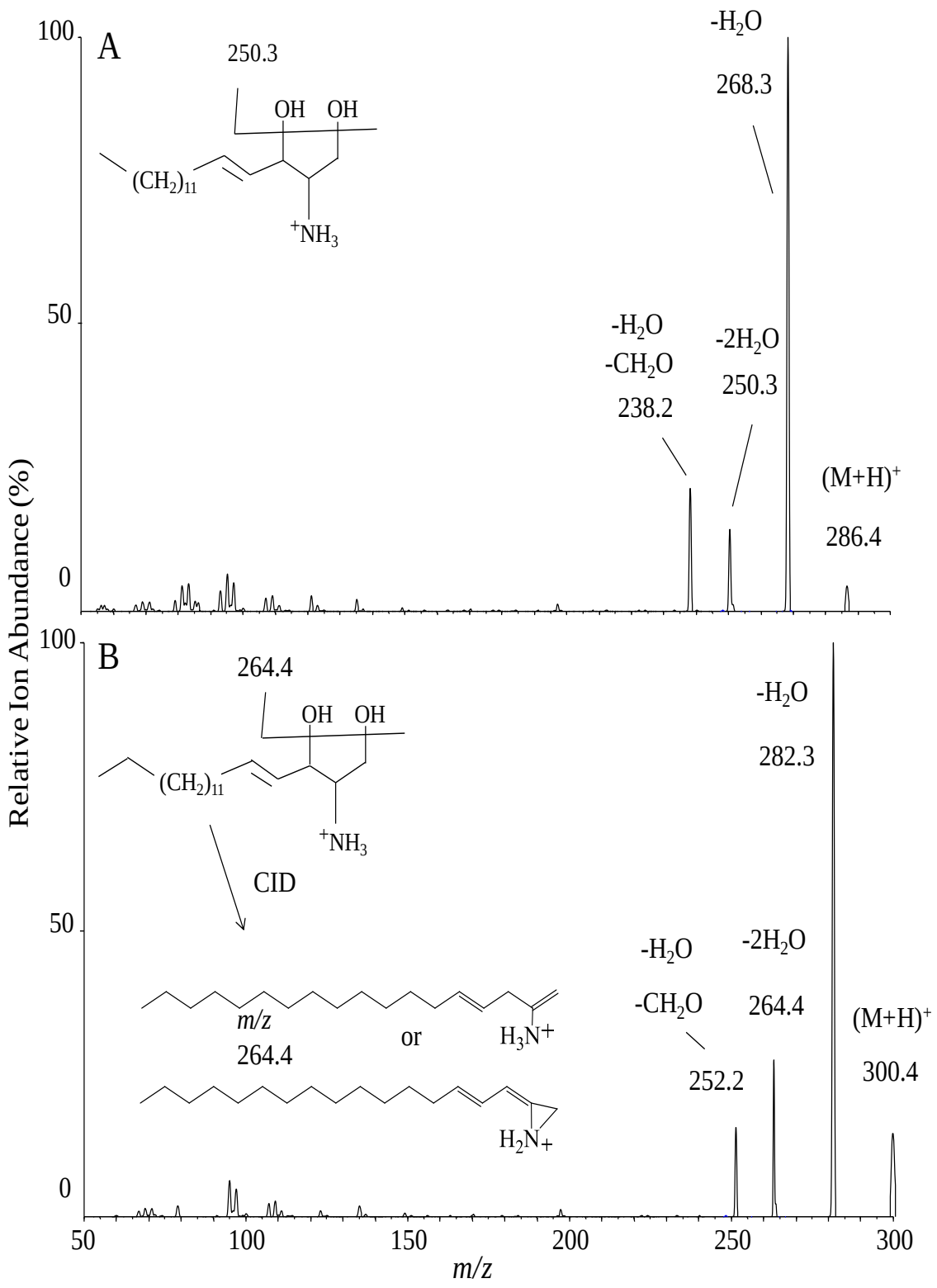

Figure 2.3. Product ion scan of A) d17:1 and B) d18:1 So by QQQ.

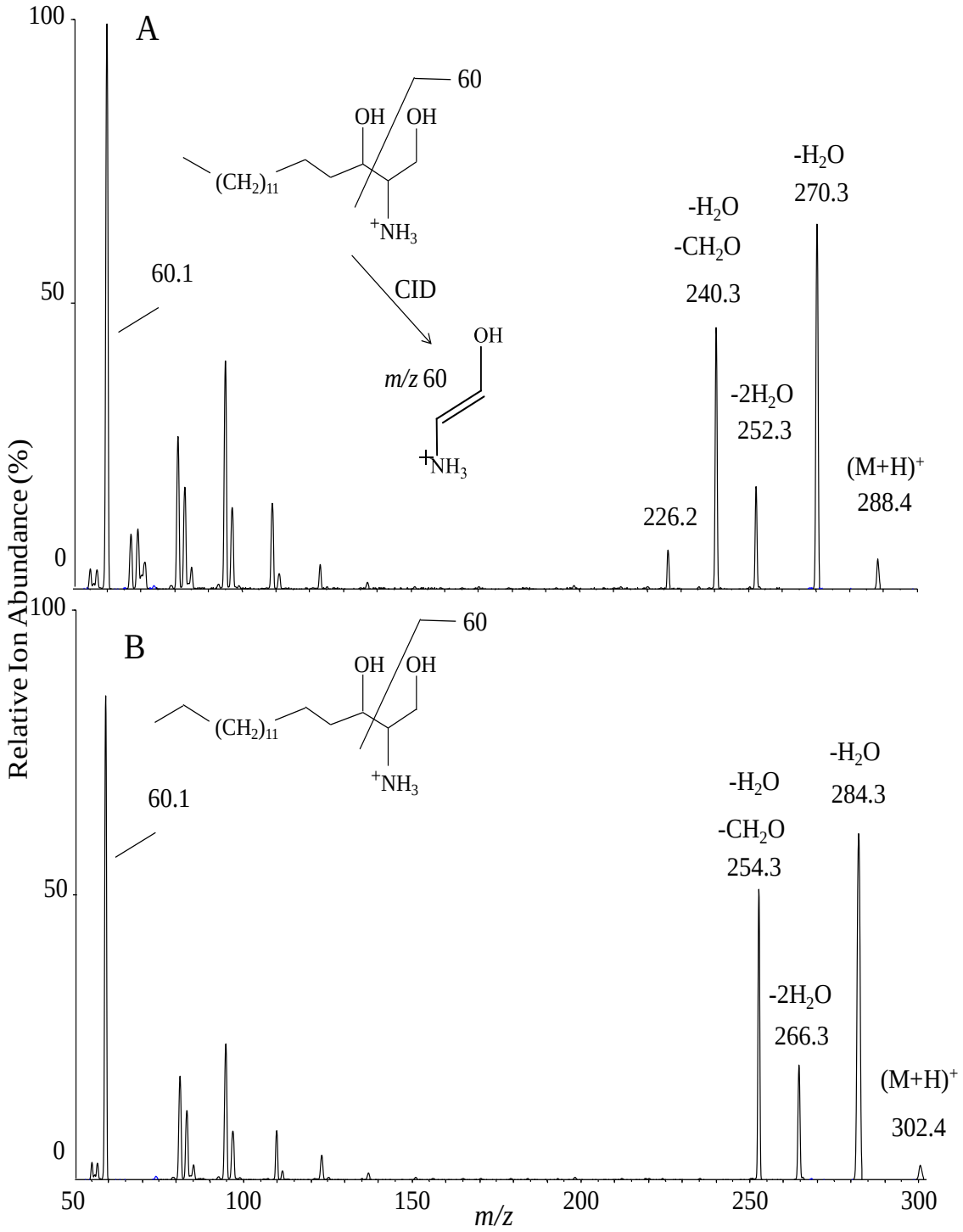

Figure 2.4. Product ion scan of A) d17:1 and B) d18:1 Sa by QTrap.

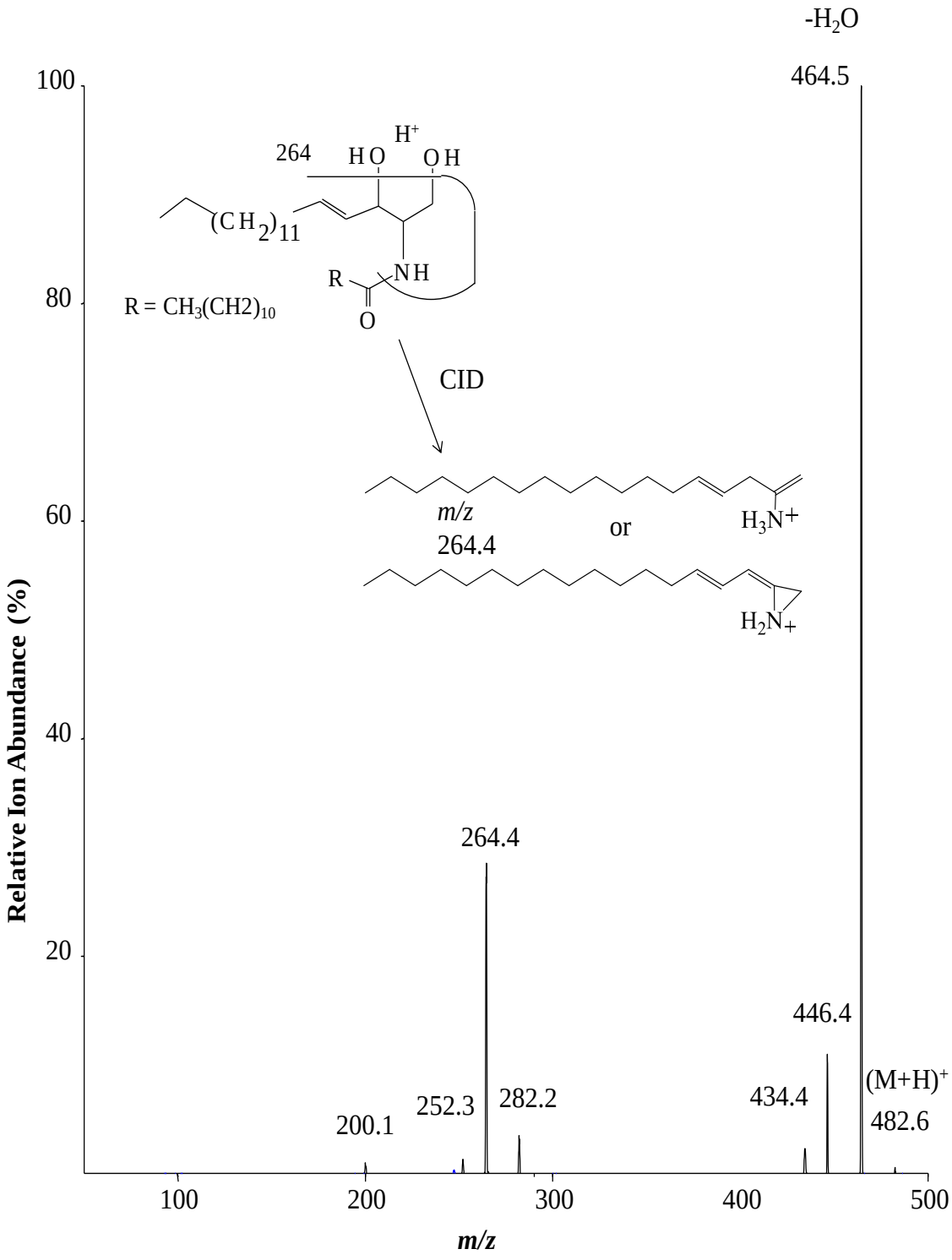

Figure 2.5. Product ion scan of d18:1/12:0 Cer by QTrap.

HexCer fragmented via cleavage of the hexode from the 1 position, dehydration at the 3 position, and cleavage of the N-acyl chain to either *m/z* 264.4 for d18:1 species or *m/z* 266.4 for d18:0 species (Figure 2.6). Other product ions are observed in the CID spectrum of d18:1/C12:0: single dehydration at *m/z* 626.6, deglycosylation and cleavage of the N-acyl chain at *m/z* 300.4, deglycosylation along with cleavage of the N-acyl chain and a single dehydration at *m/z* 282.2, and deglycosylation followed loss of CH_4O_2 along with cleavage of the N-acyl chain and a dehydration at *m/z* 252.3.

In positive ion mode, LacCer fragment by cleavage of the lactose from the 1 position, dehydration at the 3 position, and cleavage of the N-acyl chain to form a product ion *m/z* 264.4 (*m/z* 266.4 for dihydrolactosylceramides) (Figure 2.7) [171]. cleavage of the N-acyl chain to either *m/z* 264.4 for d18:1 species or *m/z* 266.4 for d18:0 species (Figure 2.6). Other product ions are observed in the CID spectrum of d18:1/C12:0: single dehydration at *m/z* 626.6, deglycosylation and cleavage of the N-acyl chain at *m/z* 300.4, deglycosylation along with cleavage of the N-acyl chain and a single dehydration at *m/z* 282.2, and deglycosylation followed loss of CH_4O_2 along with cleavage of the N-acyl chain and a dehydration at *m/z* 252.3.

SM fragment by cleavage and charge retention by the phosphocholine headgroup to produce abundant *m/z* 184.4 ions; however, a significantly less abundant structurally significant product ion can be observed at *m/z* 264.4, which corresponds to the previously discussed sphingoid base product (Figure 2.8).

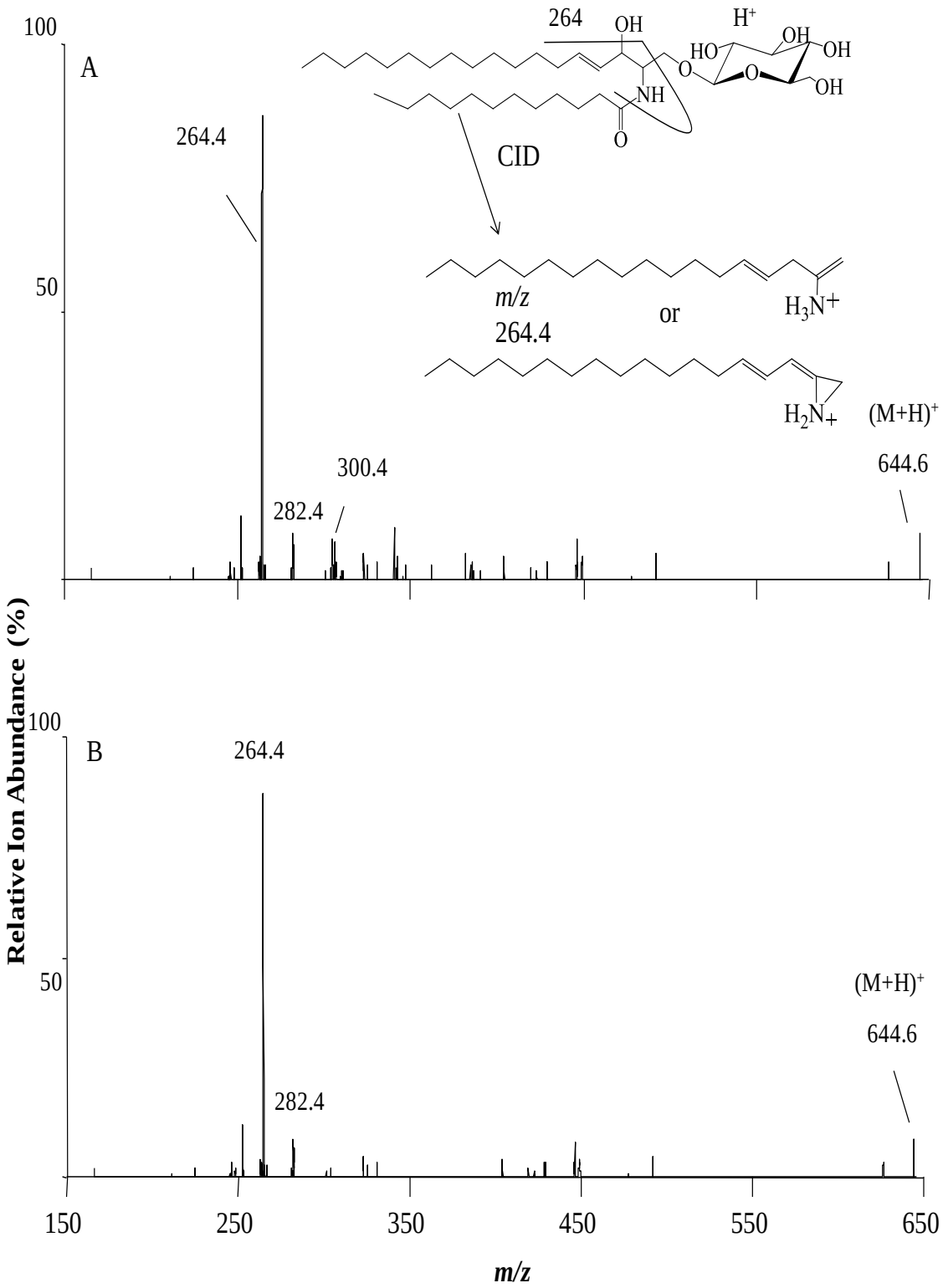

Figure 2.6. Product ion scan of d18:1/12:0 A) GlcCer and **B) GalCer.**

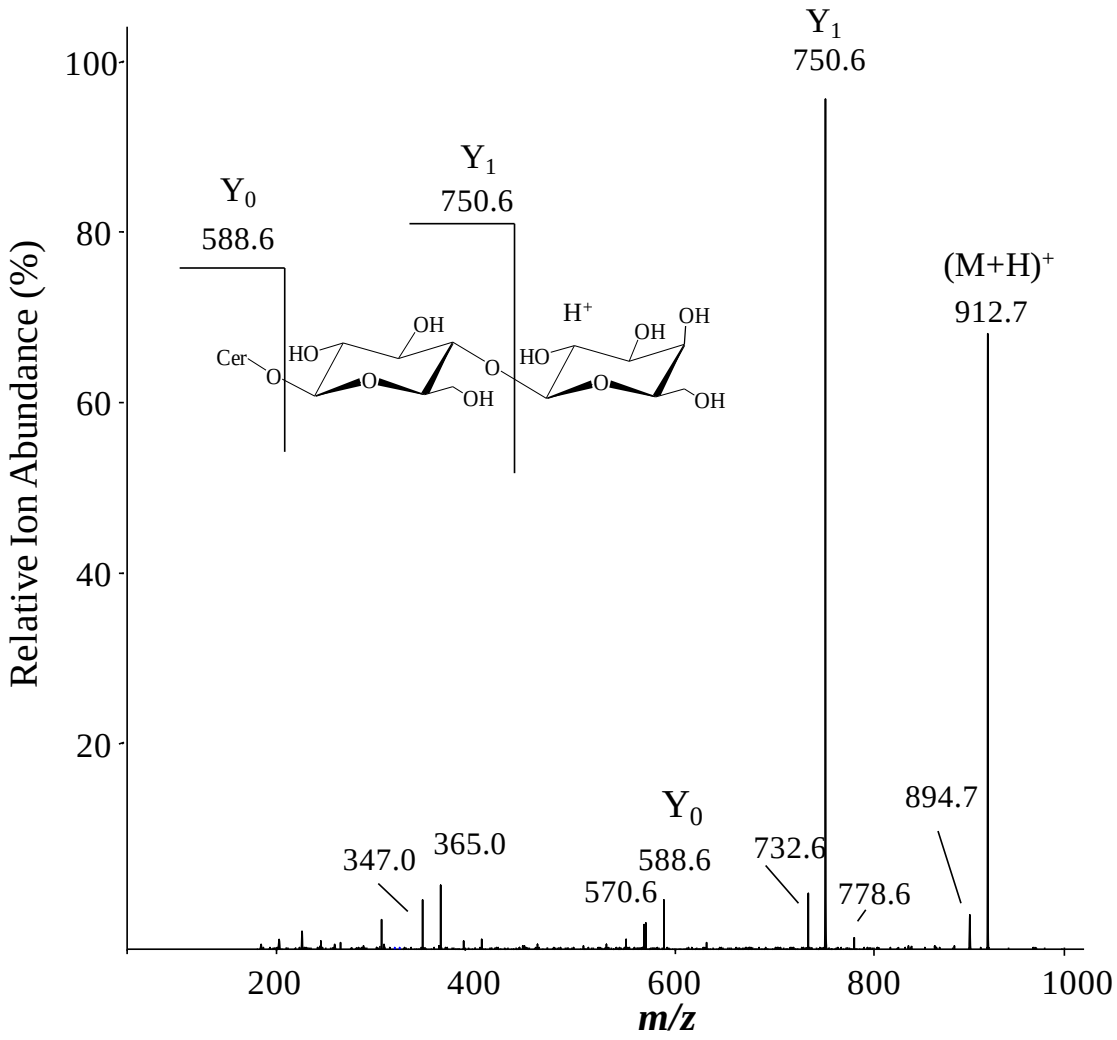

Figure 2.7. Product ion scan of d18:1/12:0 LacCer by QTrap. Positive ion mode fragmentation of LacCer involves a dehydration, deglycosylation, and cleavage of the N-acyl chain.

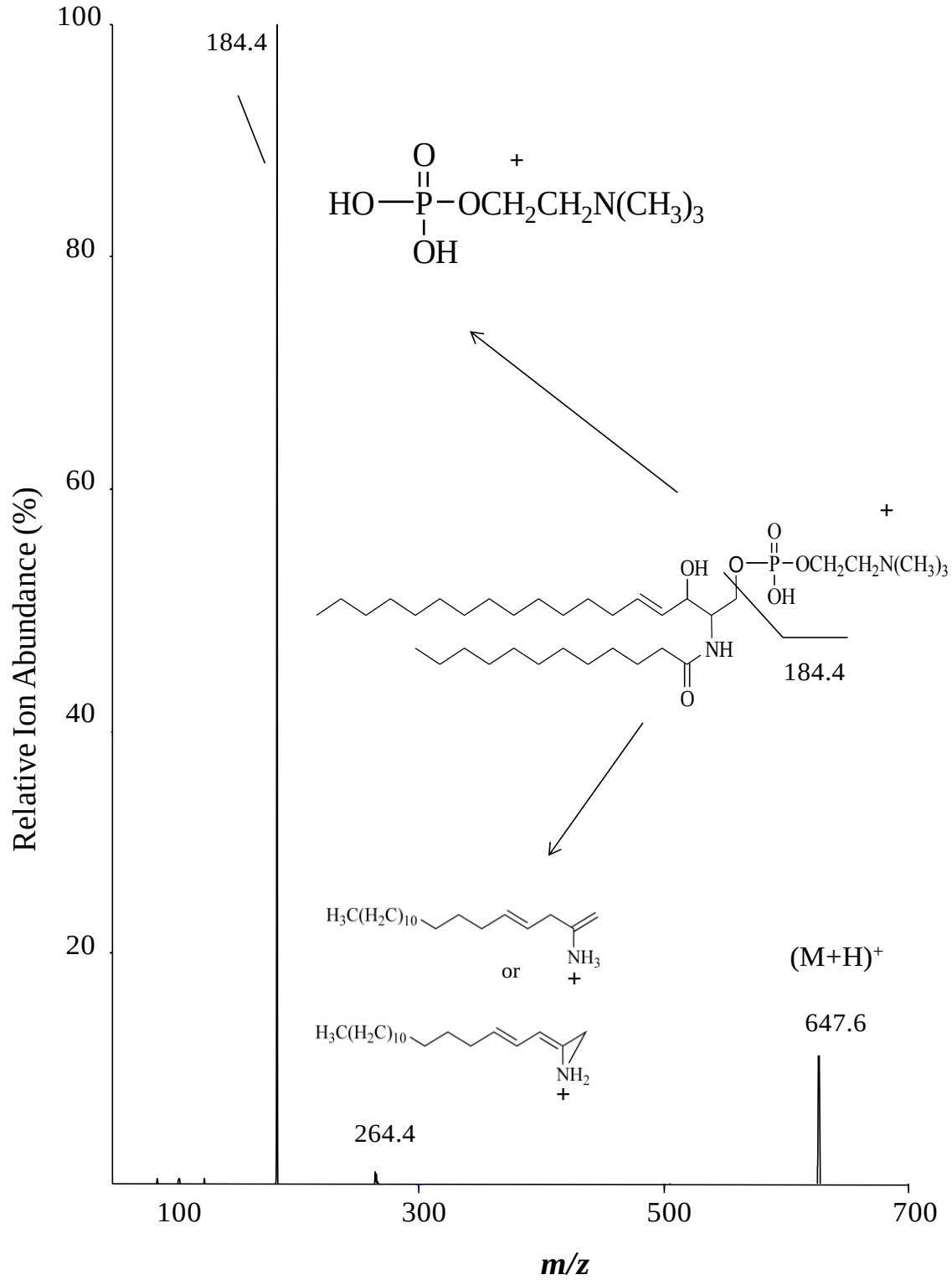

Figure 2.8. Product ion scan of d18:1/12:0 SM by QTrap.

Cer1P fragment in positive ion mode to *m/z* 264.4 for d18:1 species; however, other product ions are observed. (Figure 2.9A) [138]. Other product ions observed are a single dehydration at *m/z* 544.4, -HPO_3 at 482.2, phosphate loss at *m/z* 464.5, and phosphate loss with a dehydration at *m/z* 446.5. Negative ion mode loss of a charged PO_3^- at *m/z* 78.9 was the primary product ion (Figure 2.9B) [172]. Other negative mode product ions included dehydration at *m/z* 542.3, amide bond cleavage at *m/z* 378.2, amide bond cleavage and dehydration at *m/z* 360.2, and charged phosphate loss at *m/z* 97.0.

Sulfatides fragmented in a similar manner in negative mode with charge retention of the sulfate group at *m/z* 96.9 (Figure 2.10) [173]. Other product ions were more structurally indicative, such as *m/z* 390.2, which represents the N-acyl fatty and portion of the sphingoid base or *m/z* 240.9, which represents the sulfated galactose.

Unnatural d17 species were used as internal standards for sphingoid bases and sphingoid base 1-phosphates. Similarly, unnatural C12:0 variants were used as internal standards for complex species. These non-naturally occurring sphingolipids were chosen in place of stable isotope internal standards due to cost and lack of availability. Because these internal standards very rarely were observed in biological samples, background signal did not affect their use for quantitation.

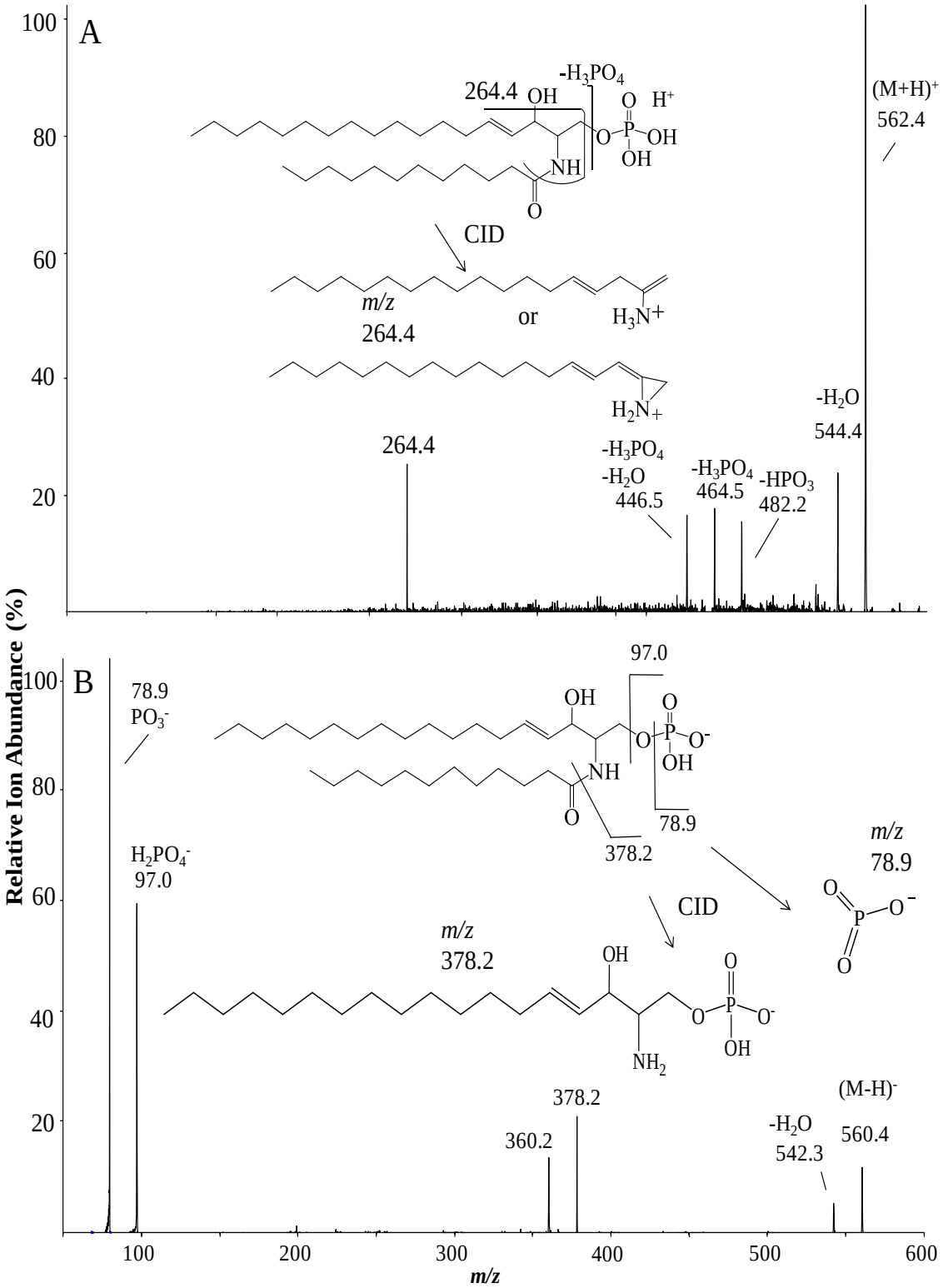

Figure 2.9. Product ion scan of d18:1/C12:0 Cer1P. A) Positive ion mode B) Negative ion mode

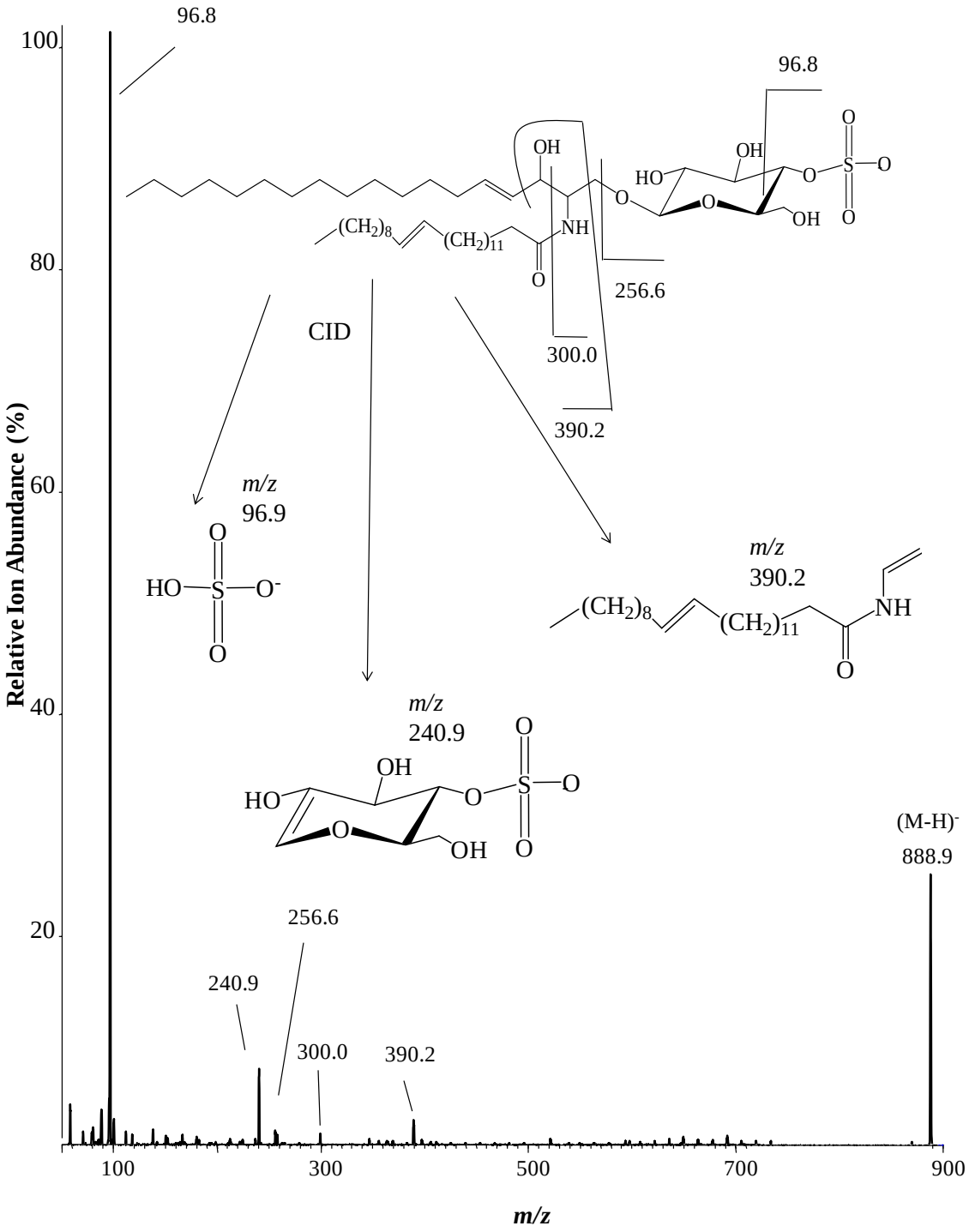

Figure 2.10. Product ion scan of d18:1/24:1 ST by QTrap.

Ion selection within RAW264.7 cells

Prior to selecting MRM pairs for each cell type, the variation in fatty-acyl chain length needs to be determined, which allows the MRM transitions to be tailored for the major N-acyl species within the sample. This is initially accomplished by syringe infusion of one sample dissolved in 1 mL of CH_3OH/HCOOH (99:1) (v,v) with 5 mM ammonium formate. Precursor ion scans of *m/z* 184.4, the structure specific fragmentation indicative of SM, were first performed because SM are typically abundant and are indicative of both d18:1 and d18:0 based species (Figure 2.11). Given the relative abundance of SM to other complex sphingolipids, lower abundance variations in sphingoid base of N-acyl fatty acid (i.e. α-OH, diene, methylation, etc) would be more easily observed. In RAW 264.7 cells, the major N-acyl chain length SM are C16:0, C18:0, C20:0, C22:0, C24:1, C24:0, C26:1, and C26:0. Precursor scans of *m/z* 264.4 and 266.4 were then performed over a wide range of collision energies (35-75 eV) and masses to check for other classes of sphingolipids and the corresponding subspecies (Cer, HexCer, LacCer, etc) and verify that no significant variance in major N-acyl chain lengths was observed (Figure 2.12). N-acyl chain lengths chosen for observation in RAW264.4 cells were C16:0, C18:0, C20:0, C22:0, C24:1, and C24:0. Analysis of sulfatides via precursor *m/z* 96.9 scans revealed that α-OH transitions also needed to be included for sulfatide analysis.

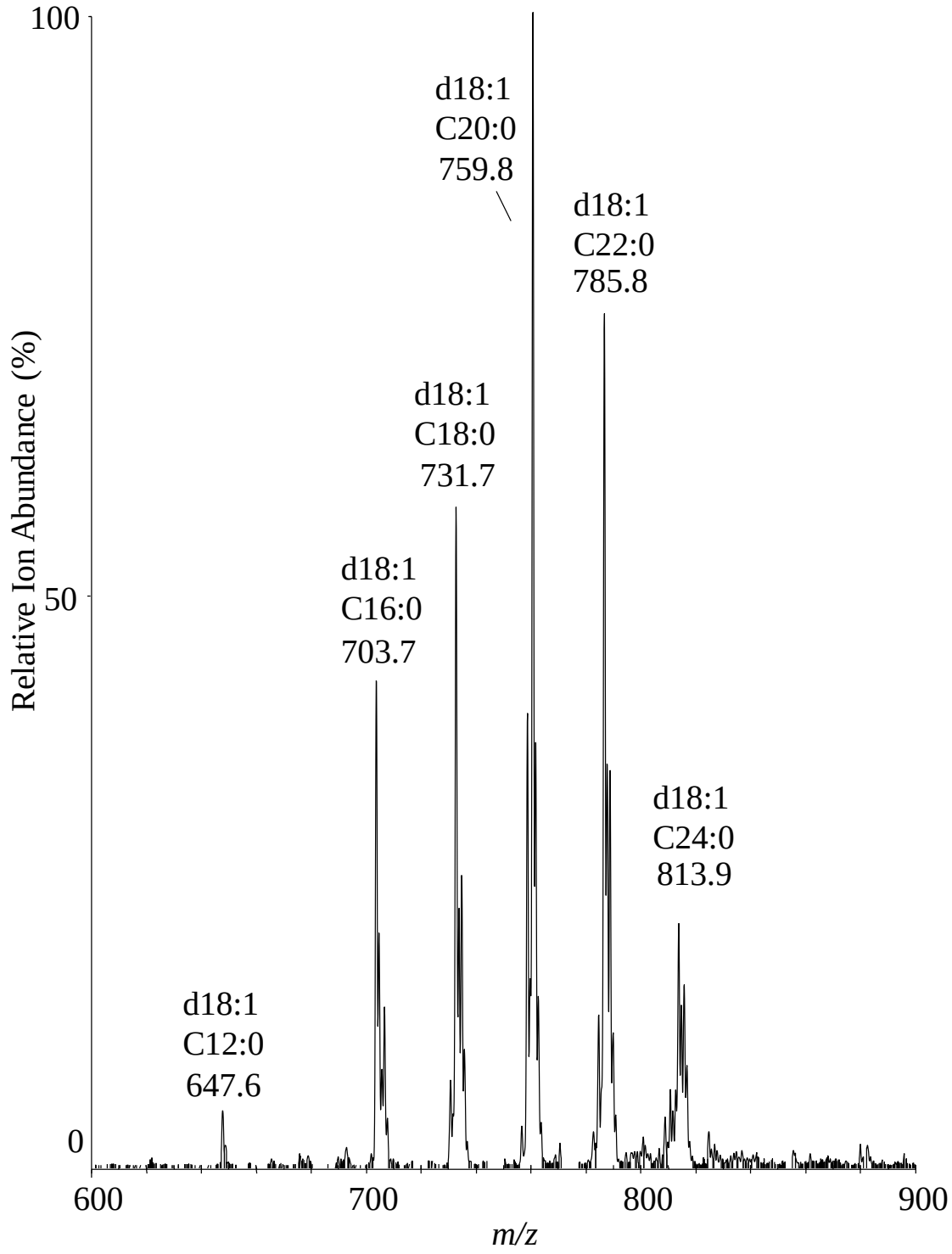

Figure 2.11. Precursor ion scan of *m/z* 184.4 scan by QTrap of RAW264.7 cells.

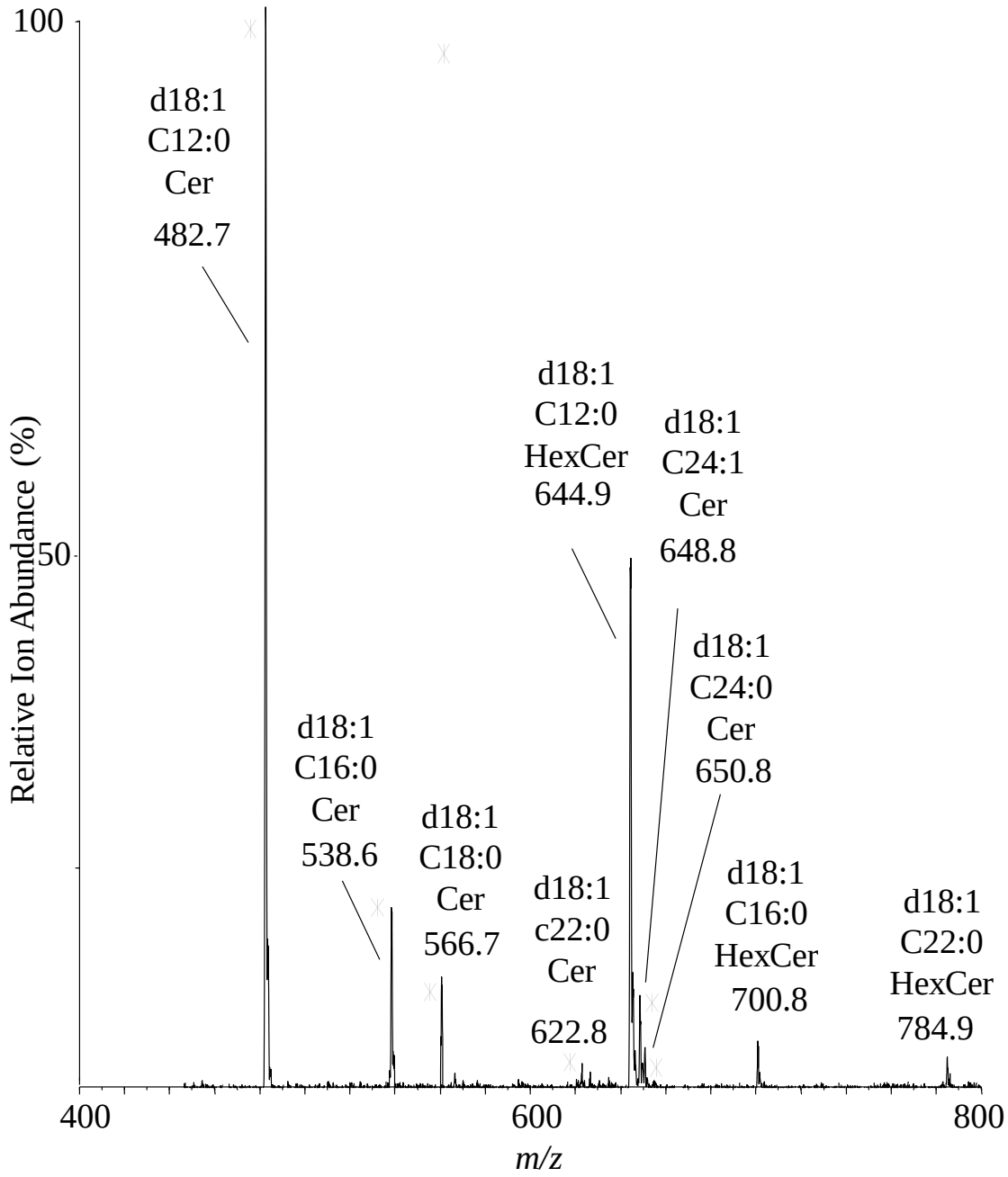

Figure 2.12. Precursor ion scan of *m/z* 264.4 scan by QTrap of RAW 264.7 cells.

Sphingoid bases and sphingoid base 1-phosphates

All species showed a linear signal response from 0.5 to 1000 pmol on both on both the QQQ (Figure 2.13A) and QTrap (Figure 2.13B). Sphingosine 1-phosphates were observed to have the highest signal response on both instruments; however the Sa1P had a similar signal response to sphingoid bases. Signal response for all species on the QTrap were 3 to 4 orders of magnitude greater than the QQQ. Signal response for d17 and d18 species were similar for each pair; however, differences in signal response in S1P and Sa1P demonstrate the need for individual internal standards for saturated and unsaturated species.

Odd chain (d17:1 and d17:0) sphingoid bases and sphingoid base 1-phosphates provided accurate quantitation as internal standards for d18:1 and d18:0 sphingoid bases and sphingoid base 1-phosphates because the background natural abundance of d17 species is less than 2 pmol per million cells. This fact in conjunction with both LC elution window and similar shifts between So and Sa species increased confidence in quantitative assignment. Ionization and CID conditions for these species are summarized in Appendix A. Internal standards and naturally occurring chain lengths were evaluated on both the QQQ (Figure 2.13A) and QTrap (Figure 2.13B). Major differences in product ion abundances were observed between the QQQ and QTrap. Increased collision energy in the QTrap made the double dehydration the major product ion; however, the overall signal was lower. Sa and other saturated species had weaker signal on the QQQ than So, although they still fragmented via double dehydration.

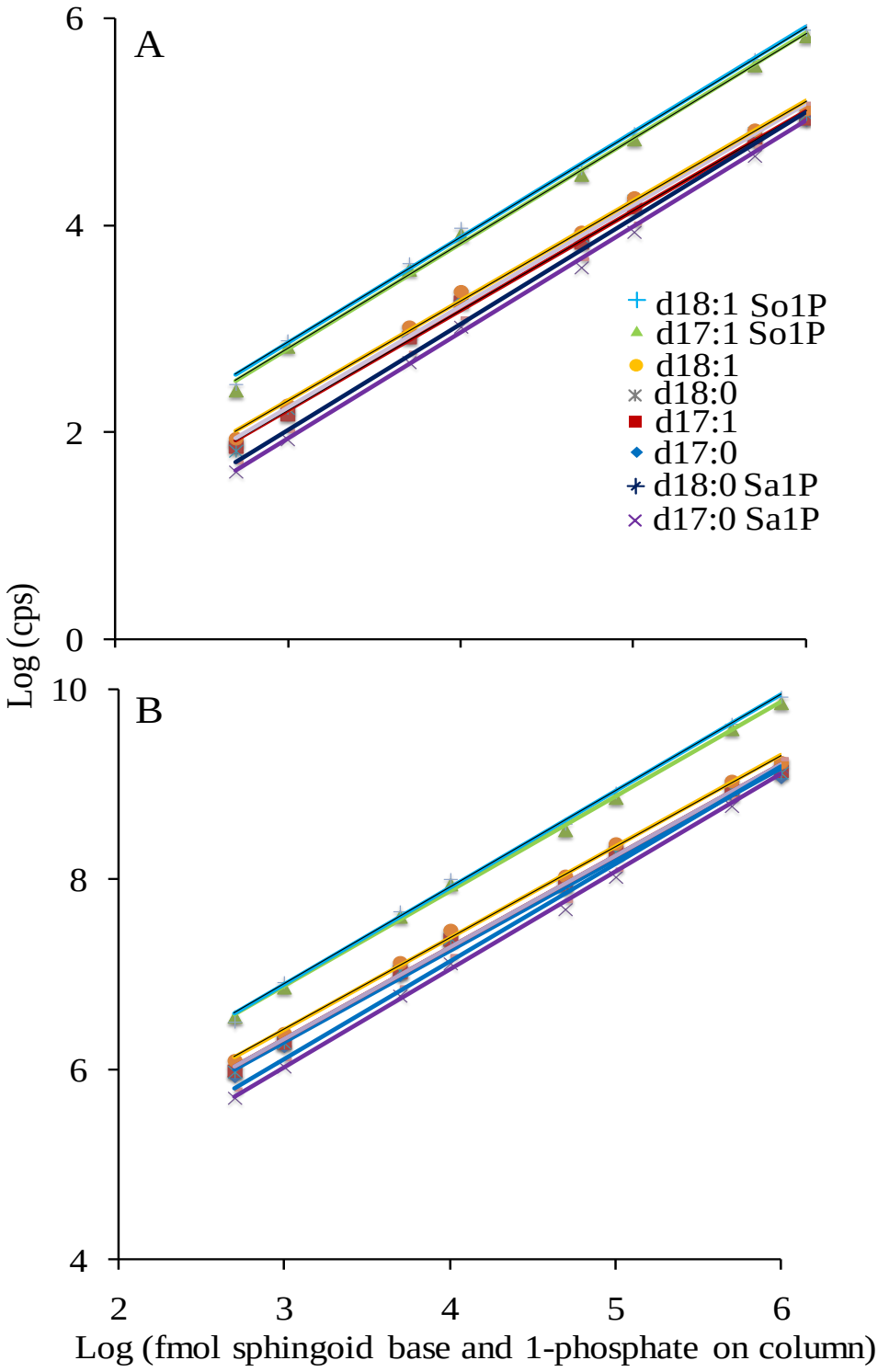

Figure 2.13. Signal response for sphingoid bases and sphingoid base 1-phosphates using a A) API 3000 triple quadrupole and B) ABI 4000 quadrupole linear-ion trap mass spectrometer.

Ceramides

Signal response from 0.5 to 1000 pmol of Cer (Figure 2.14A and 2.14B) and dihydroceramide (DHCer) (Figure 2.14C and 2.14D) species were plotted. Ionization and CID conditions for Cer (as well as other complex species) are summarized in Tables A.3. and A.4. Ion yield for DHCer on the QQQ were 6 to 8 times lower than their respective Cer as observed in figures 2.14A and 2.14C. For example, the area under the peak at 100 pmol on column for C16:0 Cer is seven times greater than that of C16:0 DHCer. Fragmentation on the QTrap did not reveal a similar relationship as shown in figure 2.14B and 2.14D, where signal response for DHCer subspecies is ~85% of the corresponding Cer subspecies. Signal response for all DHCer and Cer species was linear from 0.5 to 1000 pmol on both instruments; however, signal response for Cer on the QTrap was 3 orders or magnitude higher than the QQQ. Signal response for DHCer species were almost 4 orders of magnitude greater on the QTrap. There were virtually no difference in signal response based on N-acyl chain length, and the majority of the difference between chain lengths can be accounted for by the shifts in isotopic abundance induced by the addition of carbons in longer chain species.

Hexosylceramides

Ion yield for dihydroglucosylceramides on the QQQ (Figure 2.15C) was ~7 times lower than their respective GlcCer (Figure 2.15A) (500 pmol of C16:0 GlcCer on column resulted in an area under the peak of 1.29e05, while C16:0 dihydroglucosylceramide resulted in an area under the peak of 1.74e04). Signal for GlcCer was ~2 orders of magnitude higher on the QTrap (Figure 2.15B and 2.15D) than the QQQ (500 pmol of C12:0 GlcCer on column on the QQQ resulted in an area under the peak of 1.36e05,

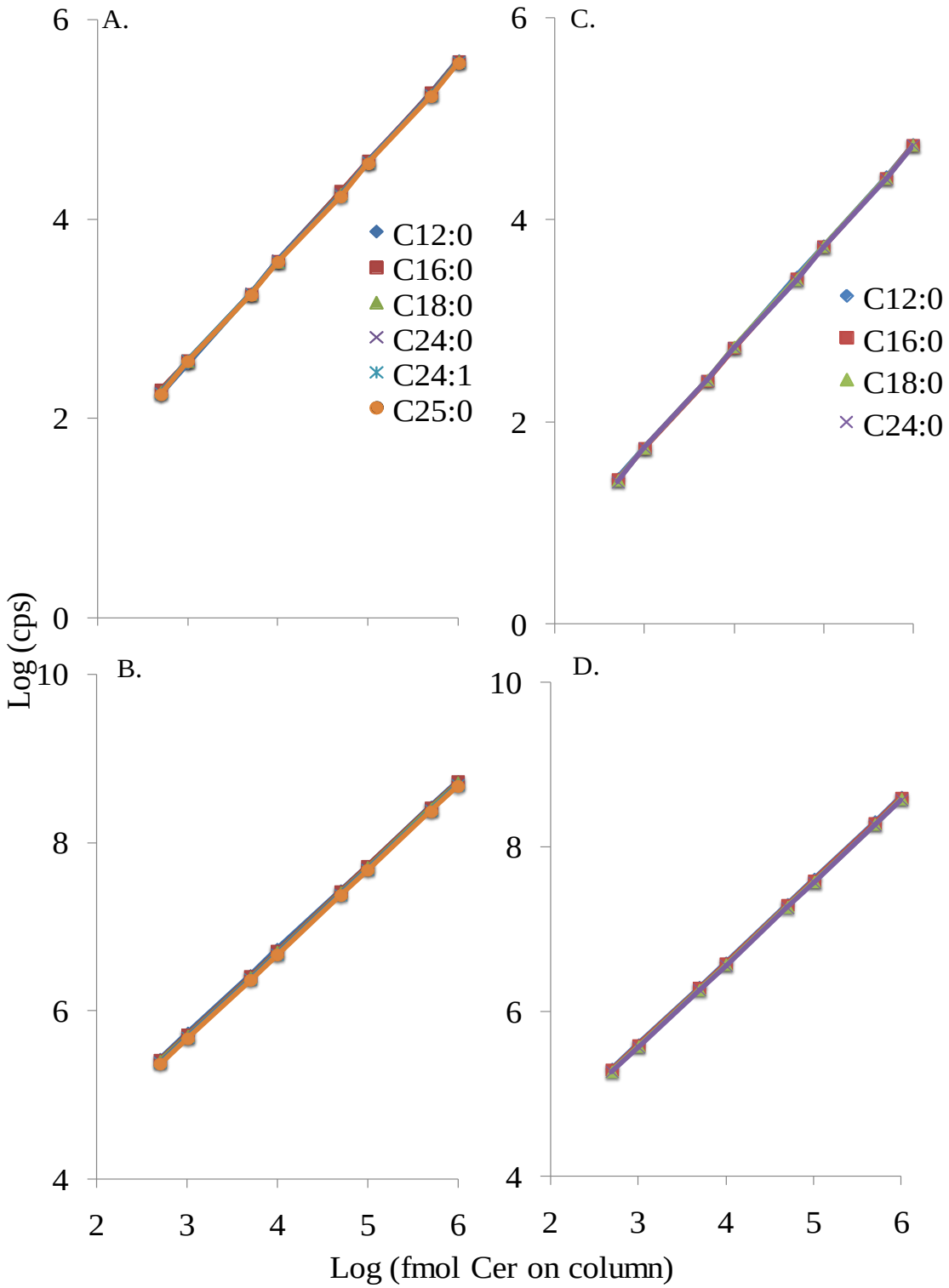

Figure 2.14. Signal response for varying N-acyl chain length Cer on the A) API 3000 triple quadrupole and B) ABI 4000 quadrupole linear-ion trap mass spectrometer and dihydroceramides on the C) API 3000 triple quadrupole and D) ABI 4000 quadrupole linear-ion trap mass spectrometer.

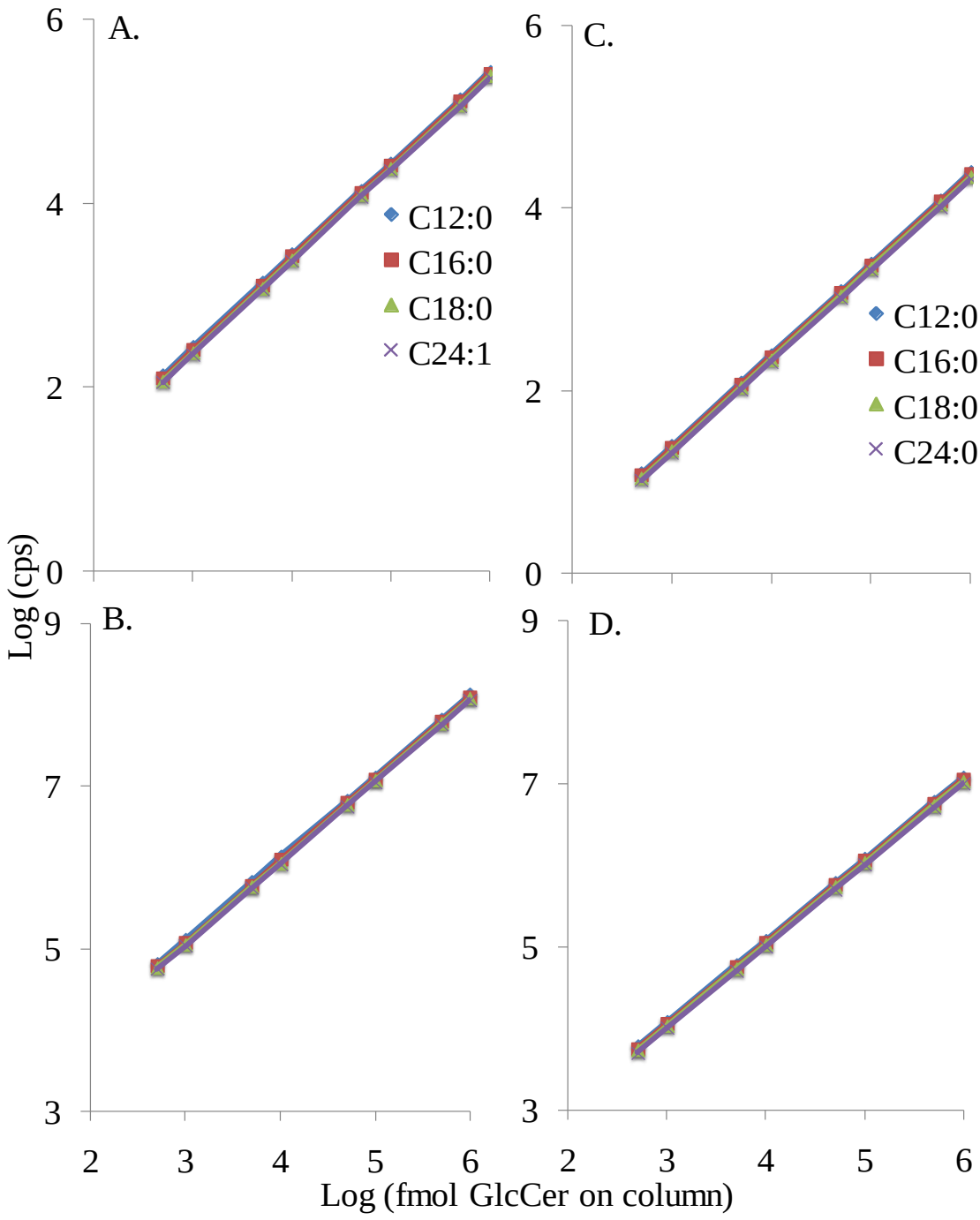

Figure 2.15. Signal response for varying N-acyl chain length GlcCer on the A) API 3000 triple quadrupole and B) ABI 4000 quadrupole linear-ion trap mass spectrometer and dihydroglucosylceramides on the C) API 3000 triple quadrupole and D) ABI 4000 quadrupole linear-ion trap mass spectrometer.

while C12:0 GlcCer resulted in an area under the peak of 2.64e07). All N-acyl chain lengths were linear over the range of 0.5 to 1000 pmol) on both instruments. Saturated species had a lower signal response on the QTrap as well, although N-acyl chain length did not significantly impact signal response on either instrument.

Sphingomyelins

Signal response for SM on the QTrap (Figure 2.16B) was only an order of magnitude higher than observed for the QQQ (Figure 2.16A) (3.42e8 versus 2.91e07 for 500 pmol on column of C16:0 SM on the QTrap and QQQ, respectively). Dihydrosphingomyelin had similar signal response to SM on both the QQQ (Figure 2.16C) and QTrap (Figure 2.16D). N-acyl chain length did not significantly impact the signal response on either instrument.

Lactosylceramides

N-acyl chain length did not significantly impact ionization on either instrument, and signal response was linear for each species from 0.5 to 1000 pmol on column. Signal response for LacCer (Figure 2.17A and 2.17B) is the lowest of the sphingolipids observed in positive ion mode. This lower signal response is caused by increase in the B mobile phase, which contains TEAA. While a decrease in solvent hydrophobicity is required to elute the LacCer, the TEAA component reduces ionization efficiency of the LacCer. Analyzing LacCer on the QTrap improved signal by an order of magnitude with signal response for 500 pmol of C16:0 LacCer on column being 1.78e05 on the QTrap and 1.48e04 on the QQQ. Dihydrolactosylceramides were 5 fold lower than LacCer on the QQQ; however, signal response for dihydrolactosylceramides on the QTrap were only ~ 20% lower than LacCer.

Ceramide 1-phosphates

Neither N-acyl chain length nor saturation significantly affected signal response, which was linear from 0.5 to 1000 pmol on column for both instruments. Reverse phase separation (Figure 2.1) with positive mode ionization allows separation of varied Cer1P by chain length as well as production of a structurally specific product ion (*m/z* 264.4). As with other sphingolipids, an increase in N-acyl chain length increased the collision energy required to optimize formation of the N" ions (Table A3-4).

Normal phase separation with negative mode ionization provides an orthogonal method for comparison with the reverse phase positive ion mode data. Here chain length variants (Figure 2.2B) elute at virtually the same chromatographic time as the internal standard (Figure 2.2A). In negative ion mode, Cer1P fragment by cleavage of the C1-O1 bond to yield PO_3^- and charge retention by PO_3^- [172]. While this product ion is not structurally indicative, it is extremely abundant and allowed for sub-pmol detection limits (Figure 2.18). Signal response for 100 pmol on column of C16:0 Cer1-P by normal phase was 7.15e06 on the QTrap and 2.52e5 by reverse phase. Signal response was over an order of magnitude higher on the QTrap than the QQQ.

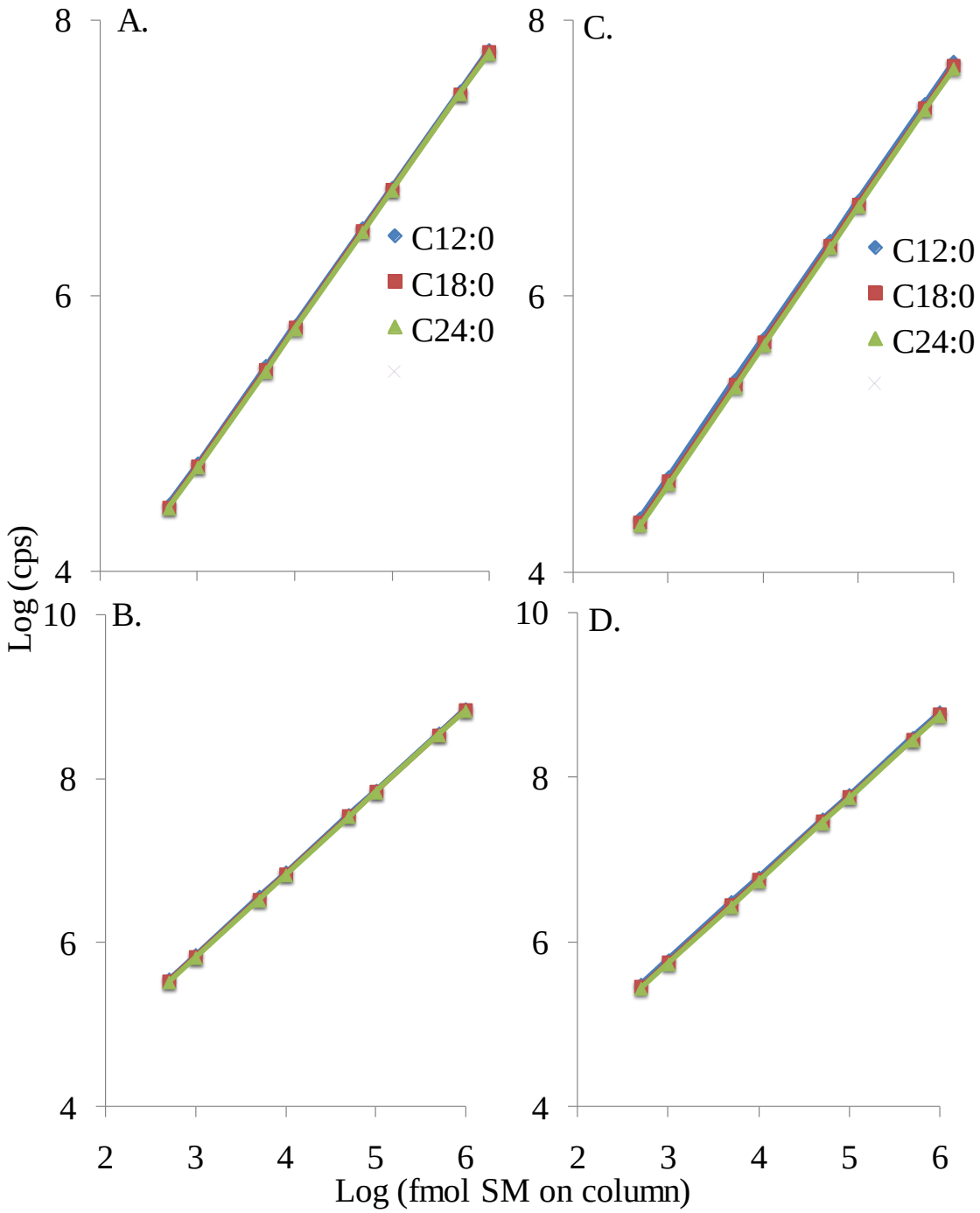

Figure 2.16. Signal response for varying N-acyl chain length SM on the A) API 3000 triple quadrupole and B) ABI 4000 quadrupole linear-ion trap mass spectrometer and dihydrosphingomyelin on the C) API 3000 triple quadrupole and D) ABI 4000 quadrupole linear-ion trap mass spectrometer.

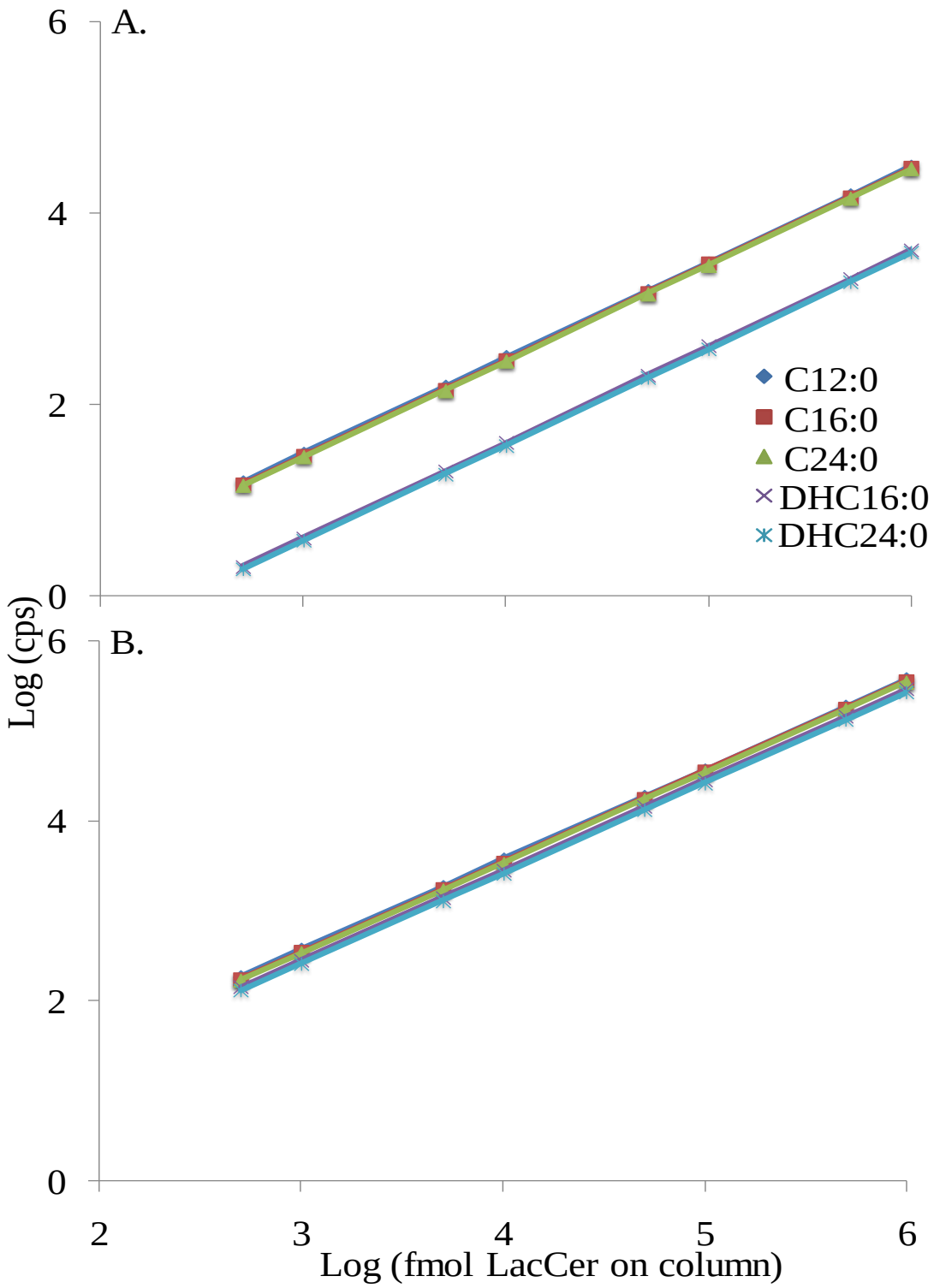

Figure 2.17. Signal response for varying N-acyl chain length LacCer and DHLacCer on the A) API 3000 triple quadrupole and B) ABI 4000 quadrupole linear-ion trap mass spectrometer.

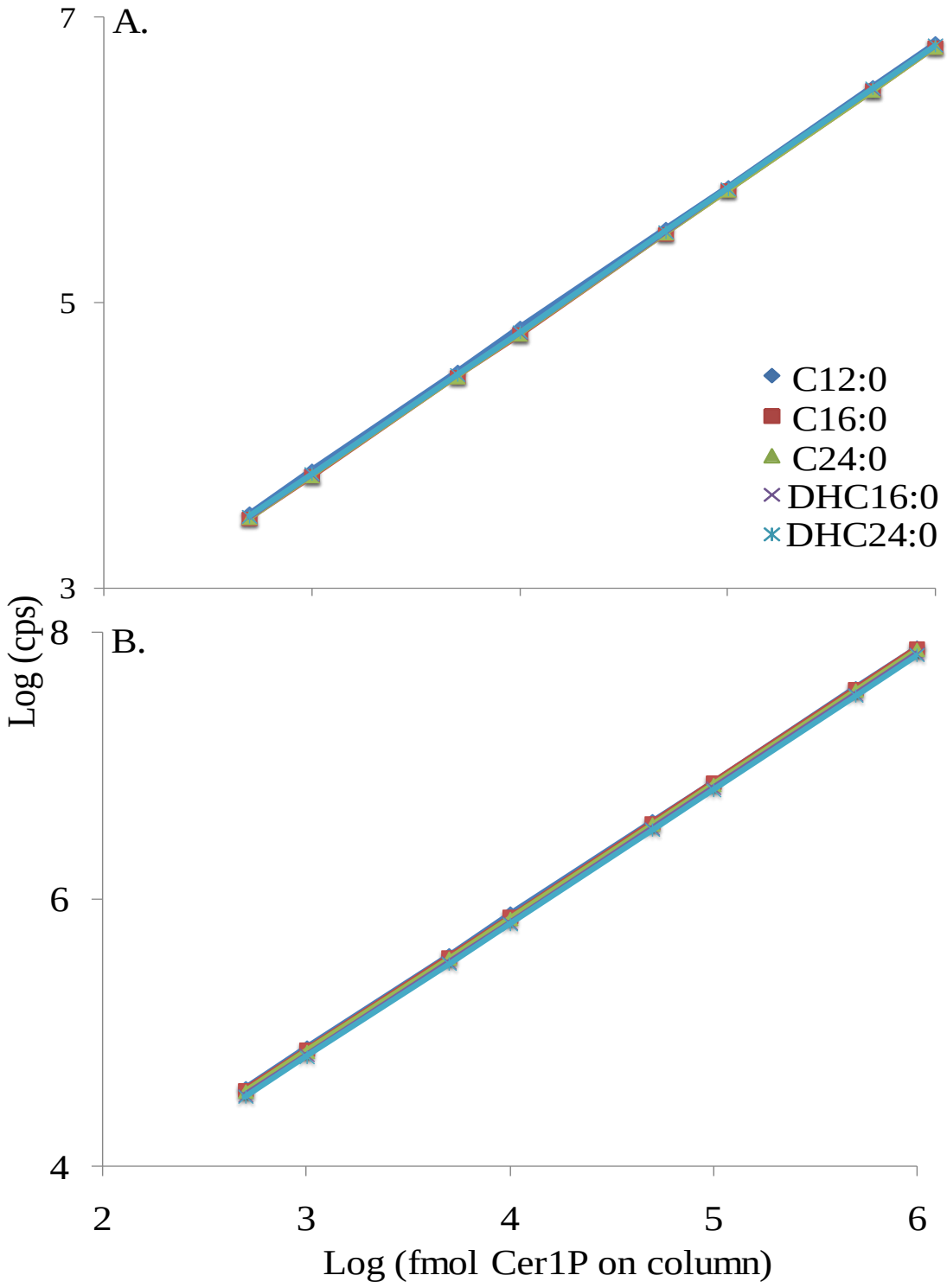

Figure 2.18. Signal response for varying N-acyl chain length Cer1P and DHCer1P on the A) API 3000 triple quadrupole and B) ABI 4000 quadrupole linear-ion trap mass spectrometer.

Sulfatides

Sulfatide species yielded significant signal in negative ion mode because sulfatides fragment via cleavage of C1-O1 bond to yield HSO_4^- and charge retention by the sulfate [174]. The negatively charged sulfate product ion is highly abundant and allows for fmol detection limits. However, this product ion does not differentiate fatty acid and sphingoid base combinations. The much less abundant fatty acid fragment ion (i.e. *m/*z 390.2 in Figure 2.10) slowed for structural characterization at a higher limit of detection. Ionization conditions were identical for all sulfatide species (Table A3-A4). Signal response for sulfatides on the QTrap (Figure 2.19B) was approximately an order of magnitude higher than the QQQ (Figure 2.19A) (signal response for 500 pmol of C16:0 sulfatide on column was 1.18e07 for the QQQ versus 8.17e07 for the QTrap). Neither N-acyl chain length nor saturation significantly affected signal response, which was linear from 0.5 to 1000 pmol on column for both instruments.

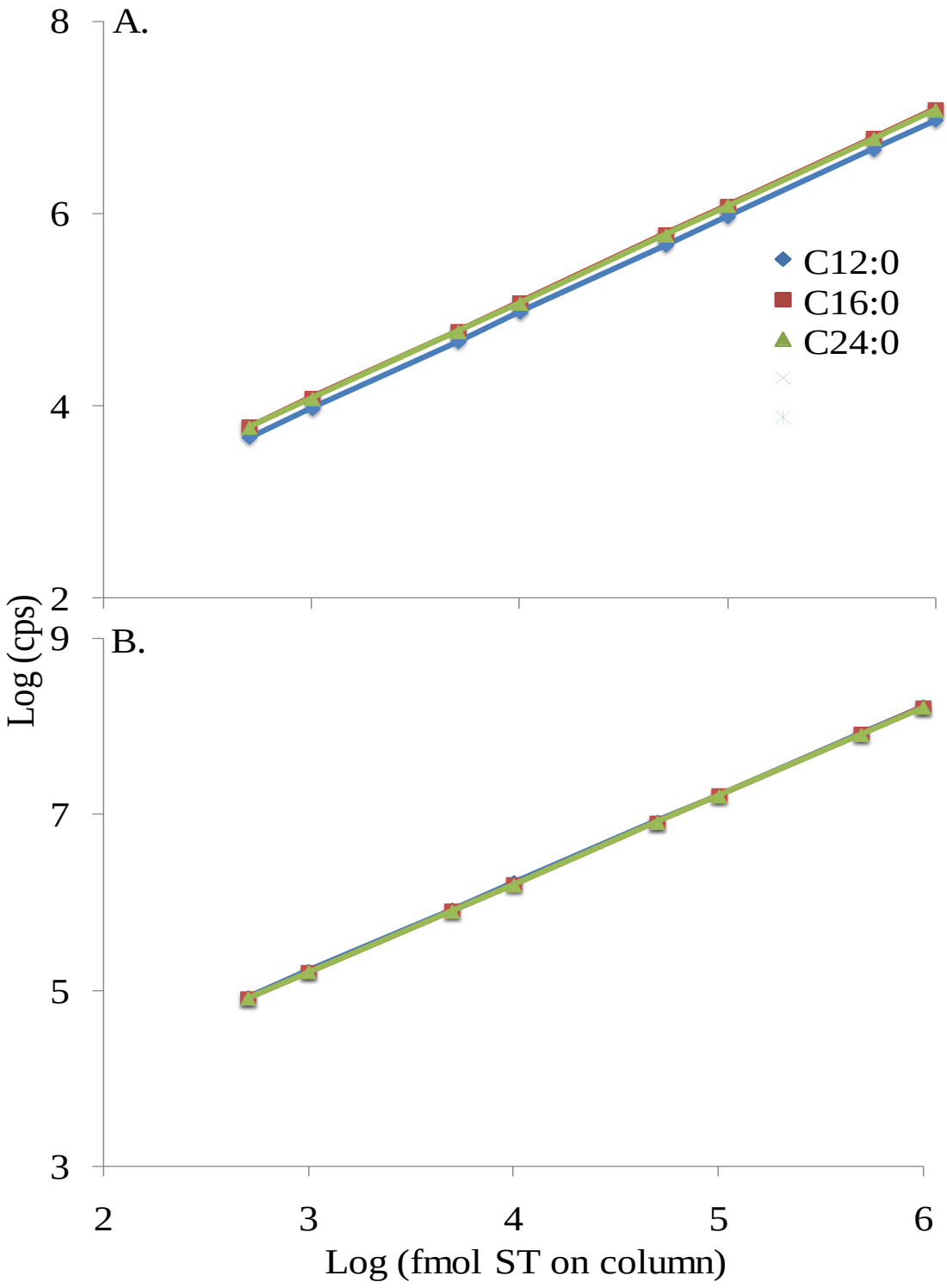

Figure 2.19. Signal response for varying N-acyl chain le length Cer1P on the A) API 3000 triple quadrupole and B) ABI 4000 quadrupole linear-ion trap mass spectrometer.

Recovery of sphingolipids and internal standards from RAW 264.7 cell extracts

To validate the extraction protocol, ~ 3.0 x 10^6 RAW 264.7 cells (N=6) were spiked with internal standards and extracted. Both the aqueous and organic layers were subjected to repeated re-extraction. For long chain bases and their 1-phosphates greater than 90% of the total signal was recovered in the initial extraction, 5-8% in the second extraction and ~1% in the third (Figure 2.20). The same percentages were recovered for the internal standard as for the endogenous analyte (Figure 2.20). The presence or absence of the Δ4 double bond had no effect on recovery as d17:1 and d17:0 species were recovered similarly (427 ± 21 pmol for d17:1 and 413 ± 11 pmol for d17:0).

The complex sphingolipid extraction had approximately 80% of the total extracted complex sphingolipids in the initial extract with the first and second re-extractions containing approximately 15% and 5%, respectively (Figure 2.21). N-acyl chain length distribution of the analytes did not vary between washes, so the relative ratios of analyte N-acyl chain length molecular species were not altered by the extraction protocol. Initial recoveries were 85%, 83%, and 79% for SM, Cer, and HexCer respectively..

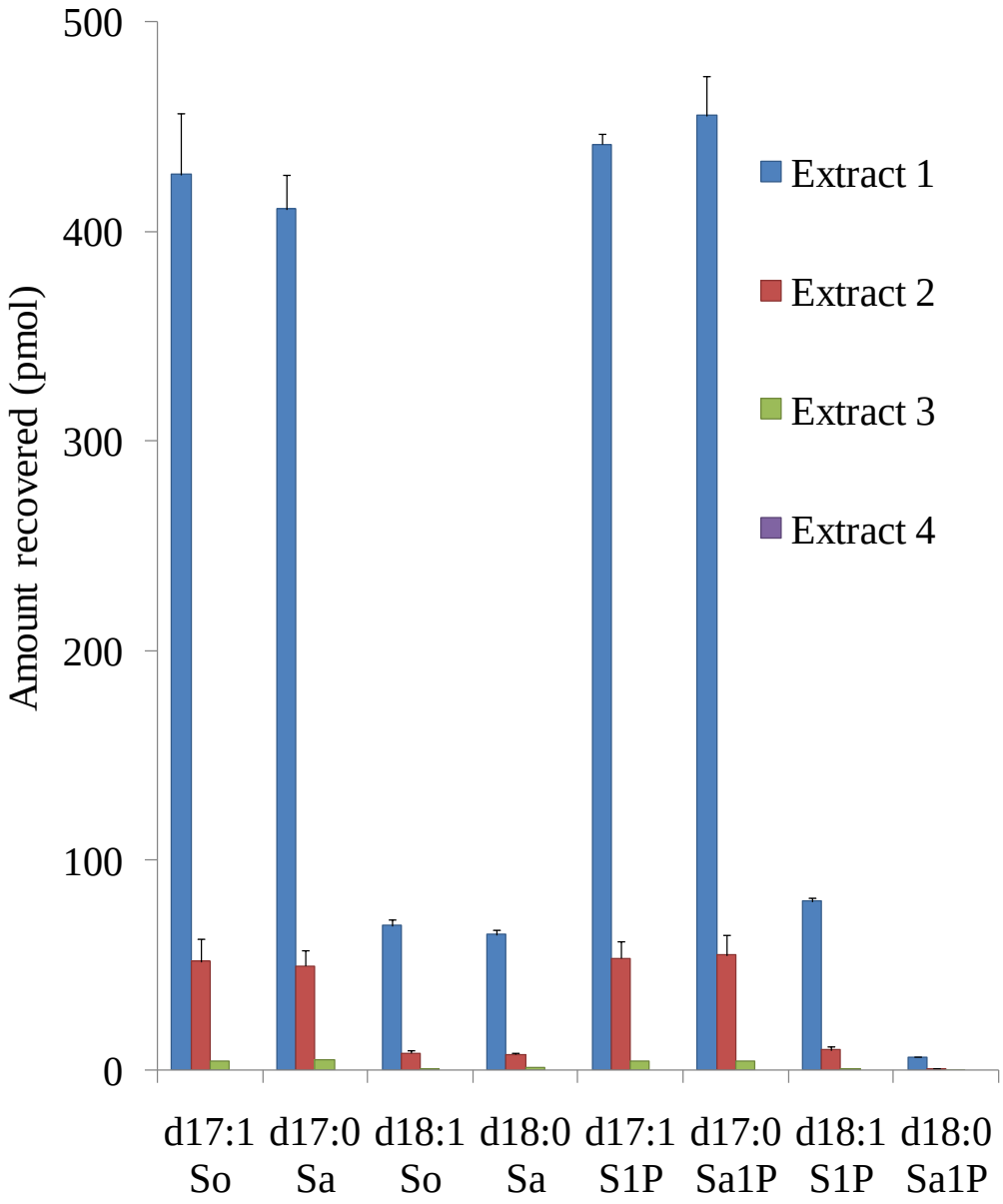

Figure 2.20. Recovery of sphingoid bases and their 1-phosphates during cell extraction. RAW264.7 cells were spiked with 500 pmol of internal standards and extracted four times, and recoveries were analyzed using LC-MS/MS on an ABI 4000 quadrupole linear-ion trap mass spectrometer. Samples were analyzed as an N=6 and means and standard deviations are shown.

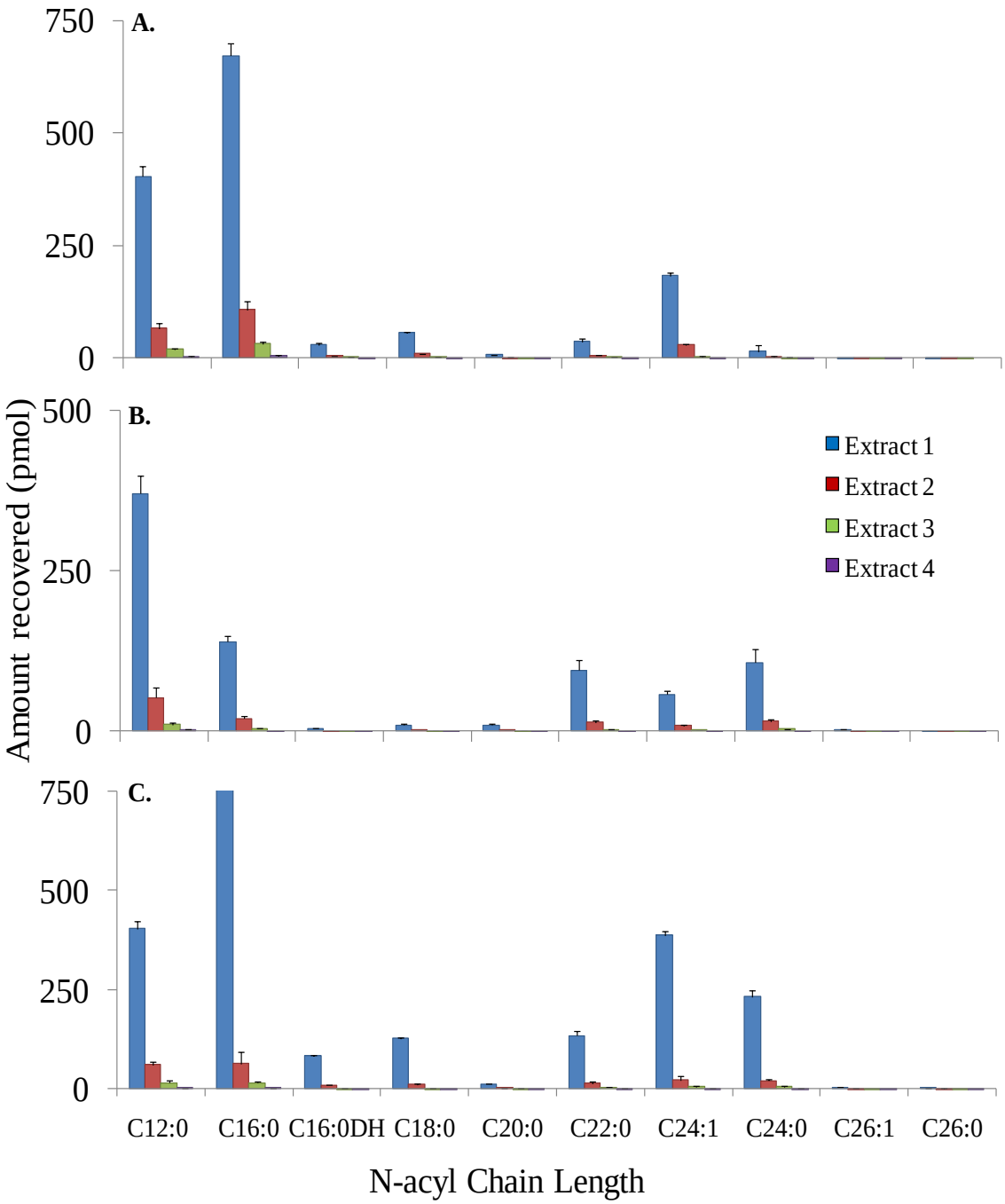

Figure 2.21. Recovery of complex sphingolipids during cell extraction. RAW264.7 cells were spiked with 500 pmol of internal standards and extracted four times and recoveries were analyzed using LC-MS/MS on an ABI 4000 quadrupole linear-ion trap mass spectrometer using a Supelco 2.1mm x 5 cm LC-NH_2 column. Samples were analyzed as an N=6 and means and standard deviations are shown.

Correction of signal for quantitation

Several factors were considered when quantifying molecular subspecies of sphingolipids, which included similarity in ionization and fragmentation behavior between analyte and internal standard, elution profile relative to internal standard, and potential internal standard background within biological samples. Internal standards were used for each sphingoid base and sphingoid base 1-phosphate, which had shorter chain length variants (d17:1 and d17:0). With complex sphingolipids, synthetic d18:1/C12:0 internal standards were used as a single standard for each family of complex sphingolipids. These internal standards were structurally similar enough to endogenous species to both ionize and fragment at similar settings (i.e. a shift of 5 or less DP and FP and an ~ 2.5 eV difference in CE per addition of 2-4 CH_2 to an N-acyl chain). Both d17 and C12 sphingolipids are typically thought of as very low abundance and unnatural species. Choice of these unnatural chain length variants minimized the background of false internal standard signal within samples. Shorter chain sphingoid bases and sphingoid base 1-phosphates maintained their chromatographic resolution between saturated and unsaturated species. Complex analytes such as SM eluted in the same chromatographic window as their internal standard (Figure 2.2), which allowed for use of a single internal standard for each family of complex sphingolipid. Therefore, if there was any ionization suppression by interfering analytes, it is more likely to be uniform for all chain length subspecies including the internal standard.

The areas under the peaks generated for both analytes and internal standards can then be integrated with mass spectrometer software (i.e. Analyst 1.4.2 for both Applied Biosystems instruments). Using identical integration settings (number of smoothes = 2-3,

bunching factor = 5-10, and noise threshold = 1 x 10^4) to integrate both internal standard and analyte allowed quantitation using the formula (area unknown / area internal standard)*amount internal standard added. Spiking the sample with internal standards prior to extraction serves as a control for extraction recovery. Relative ionization and dissociation conditions between sphingoid base variants can also be corrected for by using standard curves for analytes, such as C12:0 Cer in figure 2.14A and C16:0 DHCer in 2.14B, if a known discrepancy exists between internal standard and analyte (such as the 8x difference in signal between Cer and DHCer on the QQQ). Analytes can also be corrected for slight differences in isotopic abundance resulting from differences in chemical formula, most notably extra carbons from longer N-acyl chains. The difference between C12:0 and C24:0 N-acyl chains is 12 additional carbon atmos, which contributes ~13 % to a higher relative abundance of the $(M+H+1)^+$ peak. This lost signal can be factored back in by calculation of the differences in isotope abundance. This is accomplished by first calculating the ratio of $(M+H)^+$, $(M+H+1)^+$, and $(M+H+2)^+$ for both internal standards and analytes (larger molecules such as longer N-acyl chain length species will have relatively higher $(M+H+1)^+$, and $(M+H+2)^+$ ratios than shorter N-acyl chain length variants). These ratios are then converted to a total percent and the signal observed for the analyte is divided by the percent for its $(M+H)^+$ and multiplied for the typically higher $(M+H)^+$ percent from the internal standard.

Sphingolipid Amounts in RAW264.7 cells and Thioglycollate Elicited Macrophages

Recovery of sphingolipids from extracts of RAW264.7 can be viewed [Table 2.1-2.2] as well as explored in depth at www.lipidmaps.org. Discussion of the following data represents the ability of these methodologies to detect and quantify sphingolipid amounts

across a timecourse (RAW264.7 0 and 24 h) as well as between different cell lines and treatments (RAW264.7 cells vs. thioglycolate elicited macrophages). All data represents an N =3-4 and were integrated and quantitated according to the above described methodologies.

So varied between 31.7 and 48.2 pmol/µg DNA, while Sa was an order of magnitude lower and varied between 3.9 and 2.6 pmol/µg DNA. Sphingoid base 1-phosphates followed a similar trend with So1P varying between 10.0 and 16.8 pmol/µg DNA, and Sa1P varying between 0.7 and 1.3 pmol/µg DNA. TGEM samples had significantly lower abundances of So, So1P, and Sa1P (39%, 11%, and 8% relative to RAW264.7 0 h respectively), while Sa was 79% of the RAW264.7 0 h time point.

Complex sphingolipids were more abundant than the sphingoid bases and the sphingoid base 1-phosphates. The data revealed that N-acyl chain length profiles of Cer and SM were similar with C16:0, C24:0, and C24:1 as the major N-acyl species. GlcCer had a higher percentage of C22:0 relative to other complex sphingolipids; however, C16:0 and C24:0 were still major species. Cer1P had C16:0, C18:0, and C24:1 as the two major species. Quantitation of Cer and HexCer revealed that only minor variations were calculated between RAW264.7 at both 0 and 24 h and TGEM samples. The one exception was d18:1/C24:0 Cer in RAW264.7 cells at 0 and 24h (decrease from 12.3 to 5.3 pmol/µg DNA from 0 to 24 h). In RAW264.7 cells SM was the most abundant complex sphingolipid, having 15 times more total SM than total Cer (539.5 and 37.1 pmol/µg DNA respectively). TGEM had a higher abundance of SM relative to RAW264.7 cells at 0 h with individual increases in N-acyl chain length for 23% (C18:0) to 53% (C24:1). TGEM samples displayed a notably different Cer1P N-acyl profile than

Table 2.1. Quantitation of sphingoid bases and sphingoid base 1-phosphates from RAW264.7 cells cultured for 24 h and thioglycolate elicited macrophages.

		So (pmol/µg DNA)	Sa (pmol/µg DNA)	So1P (pmol/µg DNA)	Sa1P (pmol/µg DNA)
RAW264.7	0 h	38.8 ± 4.2	3.9 ± 1.0	10.0 ± 2.1	1.3 ± 0.2
RAW264.7	24 h	48.2 ± 4.4	2.6 ± 0.6	16.8 ± 1.8	0.7 ± 0.1
TGEM	0 h	15.2 ± 2.3	3.1 ± 0.0	1.1 ± 0.2	0.1 ± 0.0

Table 2.2. Quantitation of complex sphingolipids from RAW264.7 cells cultured for 24 h and thioglycolate elicited macrophages.

	C16:0 (pmol/µg DNA)	C18:0 (pmol/µg DNA)	C20:0 (pmol/µg DNA)	C22:0 (pmol/µg DNA)	C24:1 (pmol/µg DNA)	C24:0 (pmol/µg DNA)
Cer						
RAW 0 h	12.1 ± 4.2	0.6 ± 0.1	0.4 ± 0.1	3.9 ± 0.3	7.8 ± 0.7	12.3 ± 1.0
RAW 24 h	9.2 ± 1.4	0.4 ± 0.1	0.2 ± 0.0	2.1 ± 0.5	6.3 ± 1.3	5.3 ± 1.4
TGEM 0 h	10.0 ± 1.0	0.8 ± 0.3	0.5 ± 0.1	4.6 ± 1.6	6.1 ± 1.2	10.4 ± 0.4
HexCer						
RAW 0 h	7.8 ± 0.9	0.6 ± 0.1	0.5 ± 0.1	7.1 ± 0.6	2.6 ± 0.3	5.1 ± 0.8
RAW 24 h	8.4 ± 0.5	0.4 ± 0.1	0.4 ± 0.0	4.1 ± 0.2	2.9 ± 0.2	4.4 ± 0.2
TGEM 0 h	7.9 ± 2.9	0.3 ± 0.1	0.2 ± 0.0	1.2 ± 0.3	3.2 ± 0.5	2.3 ± 0.4
SM						
RAW 0 h	340.6 ± 30.7	17.9 ± 1.2	9.8 ± 0.8	28.1 ± 2.1	98.1 ± 7.0	45.0 ± 3.3
RAW 24 h	359.3 ± 49.5	11.6 ± 1.7	6.3 ± 1.1	27.3 ± 5.6	120.9± 9.8	63.7 ± 8.4
TGEM 0 h	456.0 ± 42.2	22.0 ± 2.8	11.6 ± 1.8	37.9 ± 7.7	150.1± 9.2	69.2 ± 9.3
Cer1P						
RAW 0 h	104.7 ± 7.5	11.3 ± 1.0	2.3 ± 5.1	2.8 ± 1.5	56.0 ± 2.0	2.1 ± 0.3
RAW 24 h	85.6 ± 6.8	6.4 ± 0.2	1.1 ± 1.3	2.1 ± 0.7	51.2 ± 8.6	2.8 ± 0.5
TGEM 0 h	33.4 ± 5.4	23.6 ± 1.5	2.0 ± 0.2	10.0 ± 1.0	18.0 ± 6.4	7.3 ± 0.6

RAW264.7, although quantities of Cer1P in TGEM samples were only 53% of Cer1P in RAW264.7 cells at 0 h. C16:0 Cer1P was 58% of total Cer1P in RAW264.7 cells at 0 h; whereas, C16:0 Cer1P was on 35% of total Cer1P in TGEM samples. However, the percent of C18:0 Cer1P relative to total Cer1P was elevated in TGEM samples versus RAW264.7 cells at 0 h(25% and 6% respectively).

Discussion

Because of the structural complexity of sphingolipids, mass spectrometry has been used for decades to identify individual species. Concurrently application of these techniques to quantitative analysis has also been explored [138, 175, 176]. These developments have driven a need in the sphingolipid community for not only high quality internal standards, but also validation that these internal standards are applicable to quantitation of naturally occurring sphingolipids. Verification requires exploration of ionization and fragmentation conditions of both internal standards and the analytes they are supposed to represent. Fortunately, most fragmentation mechanisms of sphingolipids arise via cleavage of the amide bond (removal of N-acyl fatty acid) and do not vary with the length of the fatty acid cleaved (other than requiring increasing collision energy with increasing chain length). This behavior allows use of synthetic non-natural chain length species, which are significantly less cost prohibitive than stable-isotope labeled internal standards for each individual molecular species. Evaluation of these methodologies across a range of possible mass spectrometers and manufacturers provides for identification of differences in ionization, fragmentation, and mass analyzers [177].

Coupling liquid chromatography to mass spectrometric analysis has many advantages. LC can be used for de-salting of the compounds of interest in biological

samples as well as providing a mechanism to focus the sample in a small volume via column retention and elution. LC also has the ability to separate isomers that might not be distinguished by MS or MS/MS alone [178, 179]. LC also reduces the ionization suppression typically observed in infusion experiments [180] by reducing the complexity of the eluent at any given elution time [181] as coeluting analytes having greatly different gas phase basicity or acidity can suppress the ionization of one or the other.

To validate internal standards for quantitation of a biological experiment, first one must know the range of fatty acid and sphingoid base combinations in the cell or tissue type in order to verify that internal standard choice allows quantitation of all observable species. This is accomplished by precursor ion scans of the structure specific fragments indicative of the various classes of sphingolipids. SM are typically looked for first via precursor *m/z* 184.4 scans (positive mode cleavage of charged phosphocholine headgroup) because they are abundant and often indicate the presence of both So and Sa based species. For example, in RAW 264.7 cells, the major N-acyl chain length SM were C16:0, C18:0, C24:0 and C24:1, which comprised 93% of total SM. Following the SM analysis, other classes of sphingolipids may be identified using a structure-specific precursor ion scan of *m/z* 264.4, which corresponds to doubly dehydrated d18:1 sphingoid bases [130]. Likewise classes of dihydrosphingolipids, which lack the Δ4 double bond, can be identified via precursor scans for 266.4 [130, 131, 181]. Other complex sphingolipid variants can be detected with modifications to the precursor ion scan *m/z* value based on the presence of absence of additional double bonds, oxidation, increasing or decreasing chain length, or other alterations. For example precursor ion scan of *m/z* 262.4 scans will detect sphingadiene-based lipids (d18:2), such as the ones found in

plants [78]. Precursor ion scan of *m/z* 208.4 and 210.4 can detect d14:1 and d14:0 based species, such as the ones found in insects [49]. These precursor scan will also detect the α-hydroxy fatty acid species [182] and N-acyl chain length variants. However, a single collision energy will not produce optimized signal over a large range, so spectra will not necessarily be indicative of relative amounts of sphingolipids. Once the combination of sphingoid bases and N-acyl variants within a system are determined, the corresponding transitions should be incorporated into a MRM method to allow quantitation of all identified species (assuming suitable internal standards are available).

After data is collected, post-processing must be done to account for any potential isotopic interference. Because sphingolipids have a high number of carbons, $[M+H+2]^+$ and $[M-H+2]^-$ isotopes are very common and must be considered [153] as potential contributors of false signal. For example, So and Sa only differ by 2 Da (a single double bond). So species are usually much more abundant; therefore, the $[M+H+2]^+$ signal from So-based species, will lead to increased signal for Sa-based species. Reverse phase LC resolves this problem in sphingoid base and sphingoid base 1-phosphates if the species are baseline resolved chromatographically as in Figure 2.1. However, normal phase separations do not always offer baseline resolution of So and Sa-based species [138]. In these cases, the So-based species are integrated first and the theoretical $[M+H+2]^+$ abundances are calculated. The calculated $[M+H+2]^+$ values are then subtracted from the integrated signal observed for Sa-based sphingolipids. This method allows the accurate quantitation of dihydrosphingolipids.

By optimizing ionization and dissociation conditions for a wide range of N-acyl chain lengths (C12:0 to C24:0) of each subspecies such as Cer, corrections can be made

to account for decreases in signal response associated with an increase in N-acyl chain length. Previously, these corrections were applied to syringe infusion relative to internal standards [128, 183]. The LC-MS/MS methods described, allow for reduction in the amount of species observed in a given chromatographic period (reduction in MRM cycle time) as well as insuring identical conditions for MRM analysis of analytes and internal standards. In summary, these methods provide a template to analyze sphingolipids on either a triple quadrupole or quadrupole linear-ion trap mass spectrometer. Applying a similar template for other similar instruments will allow optimization for accurate, precise, and reproducible quantitative studies.

CHAPTER 3

SIMPLE: Sphingolipid isotopic metabolic precursor labeling experiments using U-[^{13}C] palmitate to estimate *de novo* sphingolipid biosynthesis and turnover

Recently LC-MS/MS methods [37, 52, 130, 138] have been developed to quantify sphingolipids. Quantitative studies of sphingolipids provide some insight into cellular mechanisms such as apoptosis; however, many mechanisms could be more fully elucidated by distinction between biosynthesis and turnover [184-187].

Analysis of stable isotope incorporation into sphingolipids by mass spectrometry has been explored previously [188-190]; however, here several advantages versus these previous methods are discussed. In this method uniformly-labeled [^{13}C]-palmitate is used to distinguish between pre-existing sphingolipids and *de novo* biosynthesized sphingolipids. Labeled palmitate was chosen because it can be incorporated into the pathway at two points: initially by serine palmitoyltransferase [191, 192], which catalyzes the condensation of serine and palmitoyl-CoA to form 3-keto-sphinganine, and later by one of several (dihydro)ceramide synthase isoforms [41, 59, 193]. This treatment produces labeled and unlabeled d18:0 and d18:1 sphingoid bases (sphinganine and sphingosine respectively), as well as four sets of complex sphingolipid species. These may be completely unlabeled, labeled in only their sphingoid base, labeled in only their N-acyl fatty acid, or labeled in both their sphingoid base and N-acyl fatty acid. MS and MS/MS analysis distinguishes both the number and the position of label incorporation. Here mass shifts in precursor and product ion pair *m/z* values by either 16 or 32 Da reveal whether the label is present in either the sphingoid base, N-acyl fatty acid, or both.

The utility of this sphingolipid isotope metabolic precursor labeling (SIMPLE) method is demonstrated by the quantitation of sphingolipids in HEK293 and RAW264.7 cells treated with U-^{13}C-palmitate. Coupling SIMPLE with quantitation of labeled and unlabeled precursor fatty acyl-CoA pools allows correction of labeled sphingolipid values based on isotopic enrichment (i.e. specific activity) of the precursor pool.

Materials and Methods

Materials

The internal standards as defined in chapter two were obtained from Avanti Polar Lipids (Alabaster, AL). U-[^{13}C]-palmitate (98%) was purchased from Cambridge Isotope (Andover, MA). Phospholipase D (*Streptomyces chromofuscus*) was purchased from Biomol (Plymouth Meeting, PA). Fumonisin B1 was obtained from Matreya (Pleasant Gap, PA). All solvents were HPLC grade. The HEK293 cells (ATCC # CRL-1573) were obtained from the ATCC (Manassas, VA). Tissue culture dishes were obtained from VWR (Buffalo Grove, IL). Fetal bovine serum was supplied by Hyclone (Logan, Utah).

Cell Culture

HEK293 cells were grown in 60-mm plastic culture dishes in DMEM F12 (50:50 v/v) media with 10% fetal calf serum in ThermoForma Steri-cult CO_2 incubators with 5% CO_2 and 90% relative humidity at 37°C. In labeling experiments cells were incubated with 0.1 mM U-^{13}C-palmitate in a 1:1 molar complex with fatty acid-free bovine serum albumin. In experiments involving FB1, an ethanol stock of FB1 was added to the cell culture media to a final concentration of 50 μM.

Extraction of cells

Cells were extracted for sphingolipids analysis as defined in chapter 2.

Phospholipase D Treatment

1000 units of Phospholipase D (*Streptomyces chromofuscus*) were suspended in 0.1 ml of 3 mM decylglucopyranoside (Sigma) and 100mM Tris HCl (pH 8.0). An aliquot of the complex fraction was treated with PLaseD and incubated for 15 min at 37°C in a heating block. Samples were then dried under vacuum in a Savant AES2000 Automatic Environmental Speedvac and reconstituted in LC-MS/MS mobile phase for analysis.

Liquid Chromatography Electrospray Tandem Mass Spectrometry of Sphingolipids

All sphingolipids data was collected by LC-MS/MS as defined in chapter 2.

Cell extraction for Fatty acyl-CoA Determination

The medium was aspirated from dishes of adherent HEK293 cells, which were then washed twice with ice-cold PBS. Cells were scraped up in 1 mL PBS using a Nalge Nunc cell scraper (Rochester, New York) and transferred by pipette into 13 X 100 mm borosilicate screw cap test tubes using 0.5 ml CH_3OH. Cells were extracted by a modified Folch procedure. Internal standard (10 μL of 50 pmol/μL 15:0-CoA in CH_3OH) was added, followed by sonication using a Brinson 1510 ultra sonicator three times for 30 s each. An additional 250 μL of $CHCl_3$ was added, and sonicated for 30 sec. The extract was placed in a 50° C heating block for 30 min and then cooled to room temperature. $CHCl_3$ (250 μL) was added and vortexed for one minute, then 250 μL H_2O was added and vortexed for 1 min. After centrifugation (2500 rpm, 5 min), the upper (aqueous) layer was carefully removed with a Pasteur pipet and transferred into an HPLC vial. A quantity

of CH_3OH was added to the extract to increase its volume by 10% of the initial extract, which increased the solubility of very long-chain acyl-CoA (22 to 26 carbon atoms) in the extract.

Liquid Chromatography Electrospray Tandem Mass Spectrometry of Fatty acyl-CoA Species

Fatty acyl CoAs were separated by reverse phase HPLC using a Shimadzu SCL-10A VP system controller, two LC-10AD VP pumps, DGU-14A degassing unit, and a Perkin-Elmer Series 200 autosampler. The column was an XTerra 2.1 x 30 mm MS C18 column with 2.5 μm particles used at a flow rate of 0.2 mL/min. Mobile phase A consisted of CH_3OH/H_2O (70:30) (v,v) with 10 mM triethylammonium acetate [TEAA]. Mobile phase B consisted of $CH_3OH/CH_3(CH_2)_2CH_2OH$ (90:10) (v,v) with 10 mM TEAA. The pump program was as follows: 100% A for 1.5 min to equilibrate column at 100%A, 10 μL injection, 100% A for 1.7 min, gradient to 100% B at 6.3 min, hold 100% B until 11.3 min, gradient to 100% A at 11.4 min, 100% A at 14.5 min.

An Applied Biosystems MDS Sciex 4000 QTrap triple quadrupole/linear ion trap instrument was used in positive ion mode with the Turbo V ESI source and N_2 was used for the nebulizing gas, desolvation, curtain, and collision gases. Fatty acyl-CoA precursor ions were $(M + H)^+$ species. Multiple reaction monitoring (MRM) methods selected $(M + H)^+$ precursor ions with Q1 and structure-specific product ions with Q3 (neutral loss of 507 Da).

Acyl-CoA standards (Avanti Polar Lipids, Inc., Alabaster AL) in 0.5 mg aliquots were dissolved in 1.0 mL CH_3OH up to arachidoyl-CoA and in 1.0 mL $CH_3OH/CH_3(CH_2)_2CH_2OH/CHCl_3$ for behenoyl-CoA and longer. After dilution to 10

pmol/μL, each standard was infused at 5 μL/min and compound-dependent parameters (desolvation potential [DP], collision energy [CE], and collision-activated dissociation [CAD] gas) were optimized. Flow injection analysis (FIA) of individual fatty acyl-CoAs was used to optimize source-dependent parameters (curtain gas, needle voltage, temperature, nebulizing gas, and desolvation gas).

Results

Mass spectrometry method development

Sphingolipids undergo structure specific fragmentation upon tandem mass spectrometry that allows analysis of large numbers of subspecies, including both biosynthetic (i.e. sphingomyelin and glucosylceramide) and signaling species (i.e. sphingoid base 1-phosphates [138]) and fragment as shown in chapter 2. Incorporation of U-^{13}C-palmitate gave rise to 4 label combinations for complex sphingolipids referred to as unlabeled (i.e.^{12}C-d18:1/^{12}C-C16:0), base labeled (i.e.^{13}C-d18:1/^{12}C-C16:0), fatty acid labeled (i.e. ^{12}C-d18:1/U-^{13}C-C16:0), and dual labeled (i.e.^{13}C-d18:1/U-^{13}C-C16:0), (Figure 3.1).

SM, however, fragments much differently. Here the charge resides on the phosphocholine headgroup resulting in a product ion of *m/z* 184.4. Therefore, while the total carbon number can be known for a SM molecular species by the precursor *m/z*, the exact nature of the backbone sphingoid base and fatty acid cannot be inferred unless confirmed independently via other MS/MS methods (see later).

	Precursor Ion Shift	Product Ion *m/z*	Label Position
Unlabeled	$(M+H)^+$	264.4	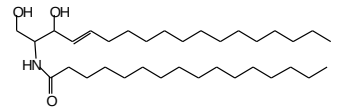
Base Labeled	$(M+H+16)^+$	280.4	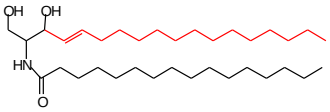
Fatty acid Labeled	$(M+H+16)^+$	264.4	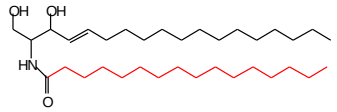
Dual Labeled	$(M+H+32)^+$	280.4	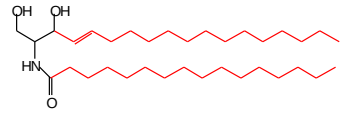

Figure 3.1. Complex sphingolipid labeling and identification scheme.

Incorporation of U-^{13}C-palmitate

Analysis of the acyl-CoA profile in HEK293 cells treated with 0.1 mM U-^{13}C-palmitate revealed that 55% of 16:0-CoA was labeled by 6 h and that the labeled palmitate CoA thioesters were both elongated and desaturated (Figure 3.2). The incorporation was rapid for 16:0-CoA (35% by 1 h), but elongated 18:0-CoA, and desaturated (16:1-CoA and 18:1-CoA) species showed a slower rate of incorporation. Both 18:0-CoA and 18:1-CoA appeared to reach a steady-state by 3 h at 19% and 8% respectively. Both 16:0-CoA and 16:1-CoA appeared to still be increasing after 6 h. The sphingolipid profile in extracts of HEK293 cells treated with 0.1 mM U-^{13}C-palmitate was first explored by precursor ion scans of highly abundant SM (*m/z* 184.4), which

allowed determination of possible sphingoid base and fatty acid combinations (Figure 3.3).

To verify these backbone and fatty acid combinations, precursor ion scans were performed for *m/z* 264.4 (d18:1) and *m/z* 266.4 (d18:0) to detect the corresponding free unlabeled sphingoid bases, Cer, and HexCer. Major N-acyl chain lengths in HEK293 cells were C16:0, C18:0,C 20:0, C22:0, C24:1, C24:0,C 26:1, and C26:0 with d18:1 and d18:0 sphingoid base backbones. The presence of elongated U-^{13}C-palmitate in N-acyl chains was also detected.

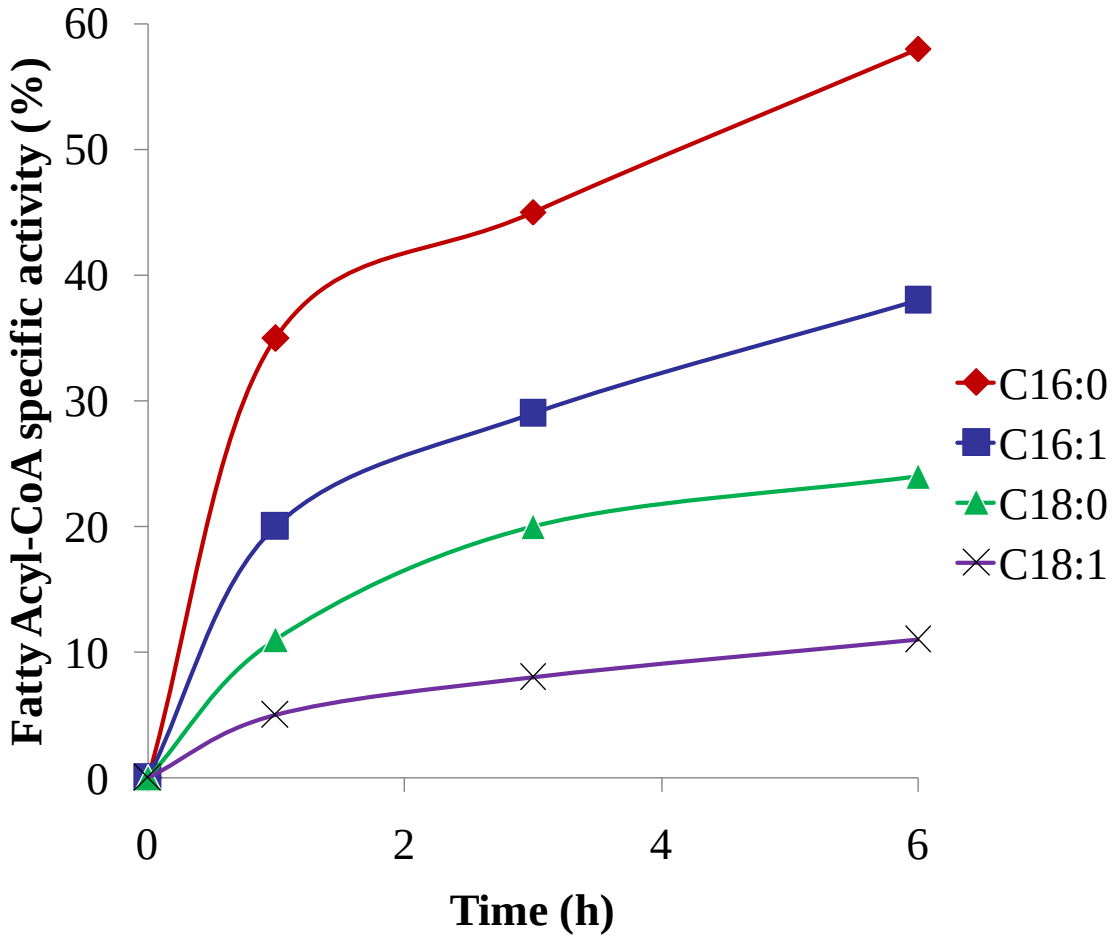

Figure 3.2. Fatty acyl-CoA species in HEK293 cells treated with 0.1 mM U-^{13}C-palmitate for 0 to 6 h.

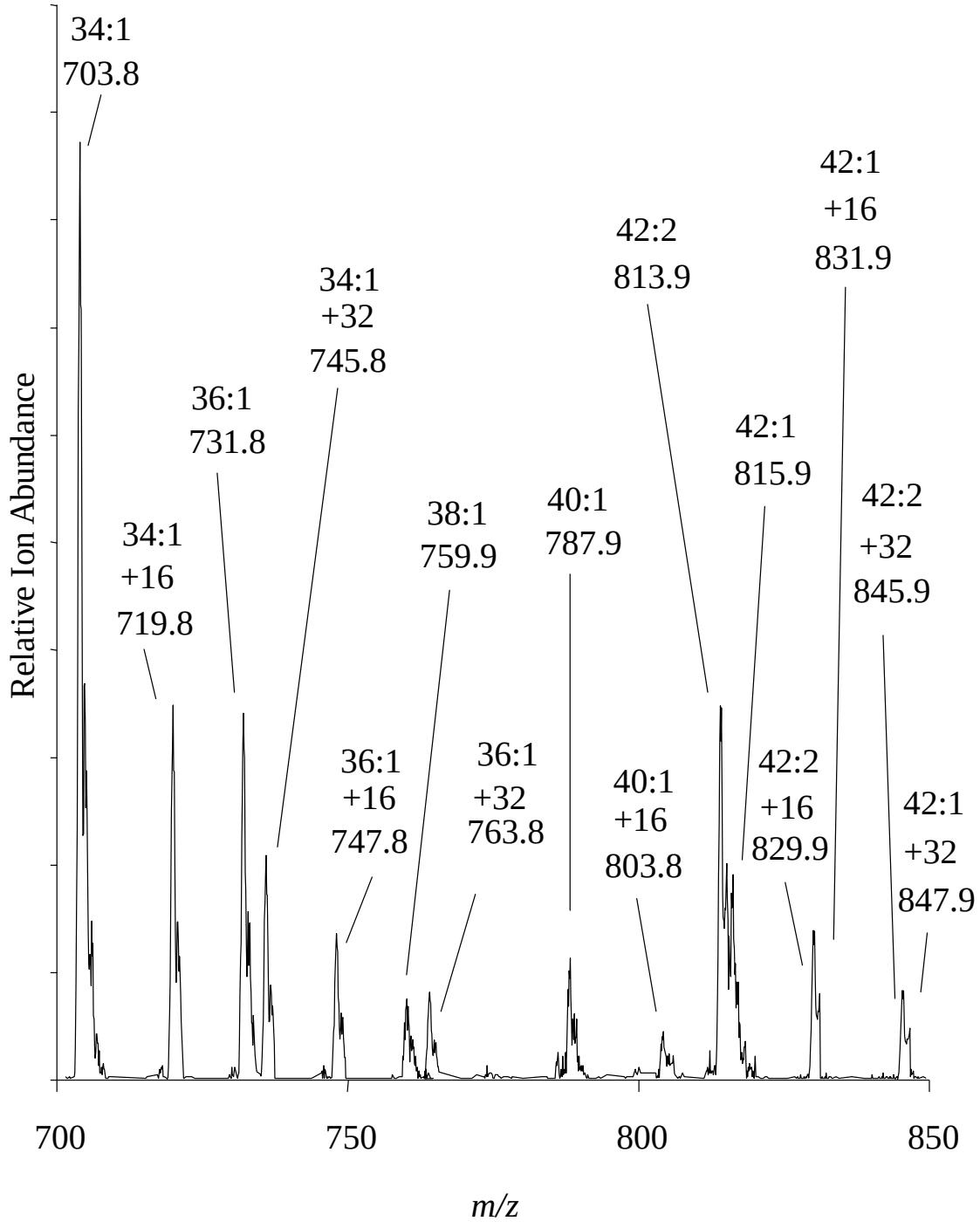

Figure 3.3. Positive mode precursor ion scan of extracts of HEK293 cells treated with 0.1 mM U-[^{13}C]-palmitate.

Time points were taken over 6 h at 1 h intervals. A distribution of chain lengths is observed in the unlabeled [^{12}C]-Cer (Figure 3.4). The major Cer, d18:1/16:0 Cer, decreases from 100 ± 20 to 50 ± 10 pmol/mg protein from t=0 to 1 h, while amounts level off by 3 h at 30 ± 5 pmol/mg protein. Other chain lengths of unlabeled Cer produced similar patterns. Decrease in d18:1/24:1 Cer was observed from 50 ± 10 to 40 ± 10 pmol/mg protein from 0 to 1 h, and the quantity stabilized at 20 ± 5 pmol/mg protein by 3 h. Total unlabeled Cer decreased from 250 ± 70 to 110 ± 20 pmol/mg protein. d18:1/20:0, d18:1/26:1, and d18:1/26:0 were minor species each being present at < 3 pmol/mg protein. Unlabeled Cer that was d18:1/24:0 decreased from 60 ± 10 to 40 ± 10 pmol/mg protein from 0 to 3 h and remained at that level until 6 h. Unlabeled Cer that was d18:1/16:0 and d18:1/24:0 Cer decreased by the largest percentage over 6 h. d18:1/24:1 Cer decreased the most to 20 ± 10 pmol/mg protein at 6h from the initial 60 ± 10 pmol/mg protein. d18:1/16:0 Cer levels had decreased at 6 h to 40 ± 10 pmol/mg protein from the initial 100 ± 20 pmol/mg protein.

Alteration in N-acyl chain length distribution over the time course was observed in unlabeled [^{12}C]-Cer. The d18:1/16:0 Cer decreased from 39% of total unlabeled [^{12}C]-Cer to 33% by 6 h; likewise, d18:1/24:0 Cer declined from 24% to 17% by 6 h. The percent lost was seen as an increase in d18:1/16:0 Cer, d18:1/18:0 Cer, and d18:1/22:0 Cer, which increased from 1% to 3%, 8% to 14%, and 7% to 9% respectively. d18:1/24:1 Cer remained constant at 20% over all time points. d18:1/20:0, d18:1/26:1, and d18:1/26:0 each comprised less than 2% Cer at all time points.

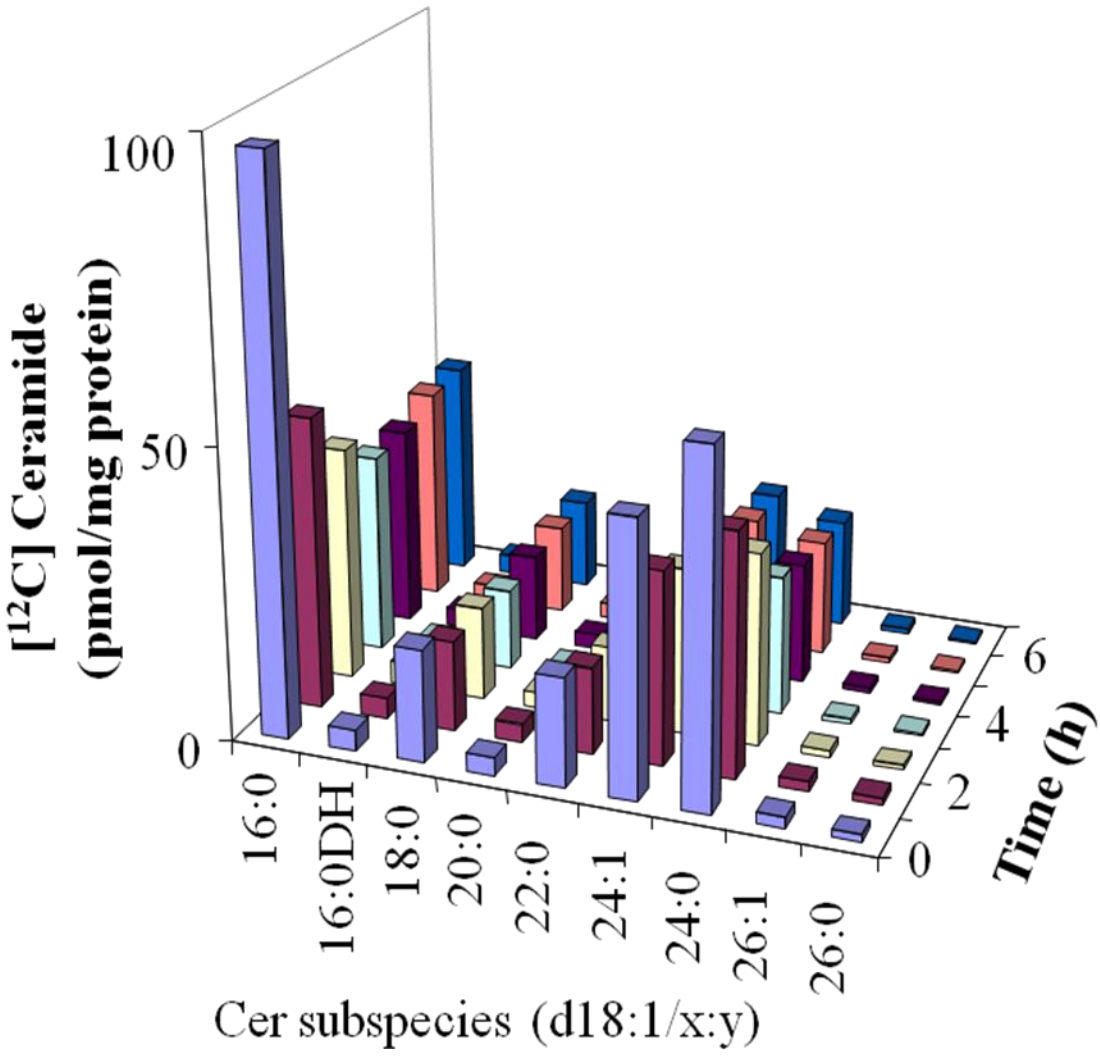

Figure 3.4. Unlabeled[^{12}C] ceramides from extracts of HEK293 cells treated with 0.1mM [^{13}C]-palmitate for 0 to 6 h.

U-[^{13}C]-palmitate was shown to be readily incorporated into sphingolipids in HEK293 cells. Incorporation into the N-acyl chains was examined and designated as the fatty acid labeled complex species in Cer (Figure 3.5), GlcCer, and SM.

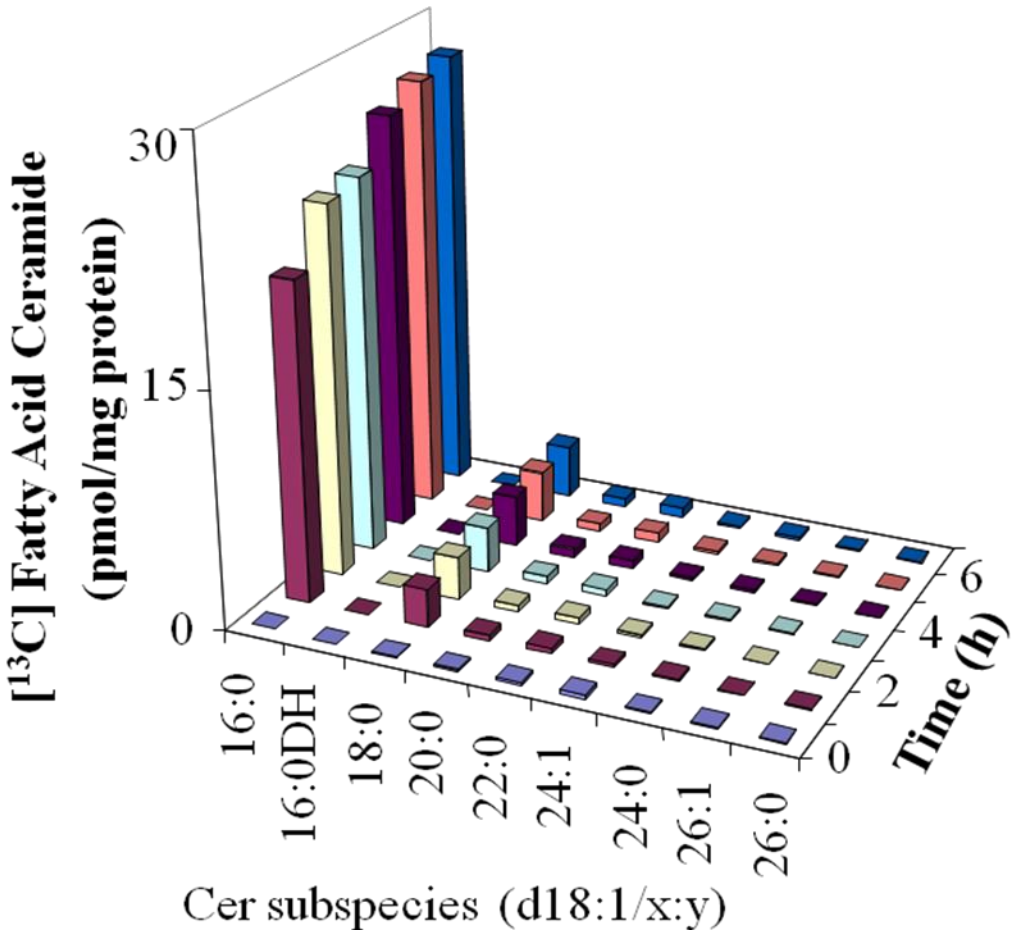

Figure 3.5. Fatty acid labeled ceramides from extracts of HEK293 cells treated with 0.1mM [^{13}C]-palmitate for 0 to 6 h.

Appreciable incorporation was seen in both d18:1/U-[^{13}C]-16:0 and ^{12}C-d18:1/[^{13}C]18:0 Cer. The ^{12}C-d18:1/[^{13}C]-16:0 Cer showed incorporation of 20 pmol/mg protein ± 5 pmol by 1 h, then amounts increased by 1.5 pmol/(mg protein*h) for a final concentration of 28 ± 6 pmol/ mg protein at 6h. d18:1/[^{13}C]-18:0 Cer amounts were above the limit of detection at 1 h, but did not reach amounts greater than 3 pmol/mg protein until the 3 h time point. Fatty acid labeled ^{12}C-d18:1/[^{13}C]-20:0, ^{12}C-d18:1/[^{13}C]-22:0, ^{12}C-d18:1/[^{13}C]-24:0, and ^{12}C-d18:1/[^{13}C]-24:1 Cer were greater than the limit of detection by 1 h; however, they did not accumulate to greater than 3 pmol/mg protein by 6 h. Fatty

acid labeled ^{12}C-d18:0/[^{13}C]-16:0 Cer as well as ^{12}C-d18:1/[^{13}C]-26:1 and ^{12}C-d18:1/[^{13}C]-26:0 Cer were not above the limit of detection by 6 h. Chain length distribution was not altered between 1 h and 6 h for ^{12}C-d18:1/[^{13}C]-16:0 Cer and ^{12}C-d18:1/[^{13}C]-18:0 Cer, which remained at 84% and 10% respectively. All other chain lengths of fatty acid labeled Cer were less than 2% total signal even when above the limit of detection.

Complex sphingolipids having incorporated label into both the fatty acid and sphingoid base were quantitatively the predominant labeled species. Incorporation into dual labled species was rapid with 36 ± 10 pmol/mg protein total dual labled Cer at 1 h. [^{13}C]-d18:1/[^{13}C]-16:0 and [^{13}C]-d18:1/[^{13}C]-18:0 Cer were the major labeled species (Figure 3.6). [^{13}C]-d18:1/[^{13}C]-16:0 Cer increased from an initial quantity of 25 ± 5 pmol/mg protein at 1 h to 50 ± 10 pmol/mg protein at 6 h. This increase represents a biosynthetic rate for [^{13}C]-d18:1/[^{13}C]-16:0 Cer of 5 pmol/(mg protein*h) from 1 h to 6 h as opposed ot the initial rapid incorporation of 27 pmol/(mg protein*h) from 0 h to 1 h. [^{13}C]-d18:1/[^{13}C]-18:0 Cer had a value at 1 h of 3 ± 1 pmol/mg protein, but did not increase to over 5 pmol/mg protein by 6 h. [^{13}C]-d18:1/[^{13}C]-22:0 Cer reached 3 pmol/mg protein by 6h, but was less than that value for all other time points. [^{13}C]-d18:1/[^{13}C]-20:0, [^{13}C]-d18:1/[^{13}C]-24:1, and [^{13}C]-d18:1/[^{13}C]-24:0 were also observed but were less than 3 pmol/mg protein for all time points.

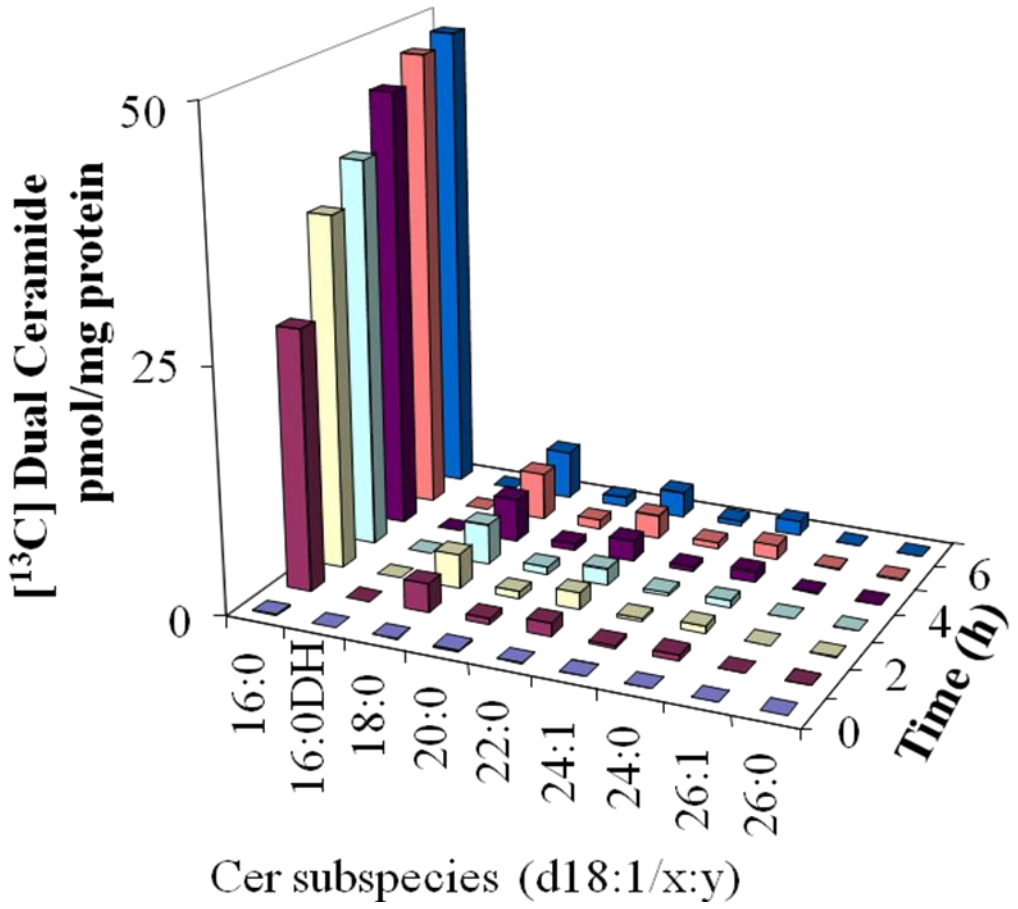

Figure 3.6. Dual labeled ceramides from extracts of HEK293 cells treated with 0.1 mM [^{13}C]-palmitate for 0 to 6 h.

[^{13}C] -d18:1/[^{13}C]-16:0 Cer was 82 ± 1 % of total dual-labeled ceramide for time points 1 h to 6 h, and [^{13}C]-d18:1/[^{13}C]-18:0 Cer remained between 8% and 9% of total dual-labeled ceramide for 1h to 6h. [^{13}C]-d18:1/[^{13}C]-22:0 was 4% for all time points as well. All other chain lengths were less than 2% of total dual-labeled ceramide each except for [^{13}C]-d18:1/[^{13}C]-24:0 which reached 3% by 5h.

Incorporation of U-[^{13}C]-palmitate into the sphingoid base, but not the fatty acid, in Cer over 6 h was 5 ± 1 pmol/mg protein or less; however, a trend of increasing quantity can be observed (Figure 3.7). Percentages of total Cer with label only in the sphingoid base backbone were maintained within ± 2 percent for all species with values

being 15%, 22%, 9%, 20%, 20%, and 12% for [^{13}C]-d18:1/16:0, [^{13}C]-d18:1/18:0, [^{13}C]-d18:1/20:0, [^{13}C]-d18:1/22:0, [^{13}C]-d18:1/24:1, and [^{13}C]-d18:1/24:1 Cer respectively.

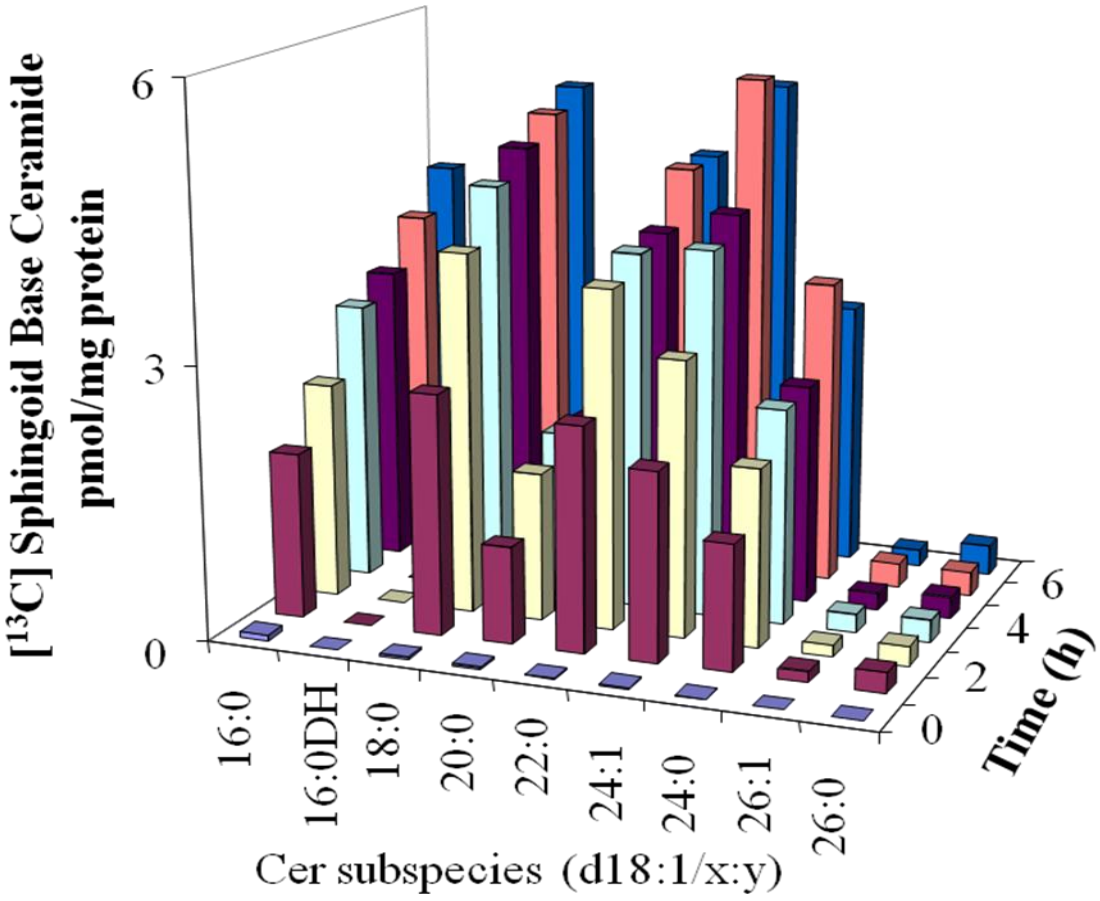

Figure 3.7. Base labeled ceramides from extracts of HEK293 cells treated with 0.1 mM [^{13}C]-palmitate for 0 to 6 h.

Phospholipase D Treatment

Incorporation of stable isotope label into Cer1P was not observed until after incorporation into SM; therefore, background levels of base and fatty acid labeled Cer1P were low. Total background quantities in 1 x 10^6 cells for HEK293 have consistently been less than 50 pmol. Therefore conversion of SM to Cer1P via phopholipase D treatmentwould allow elucidation of FA/LCB combinations.

Cells were grown in media containing 0.1 mM U-^{13}C-palmitate were analyzed for background singly labeled Cer1P. The total background concentration of singly-labeled Cer1P was 5 ± 2pmol/mg protein for both fatty acid and base labeled species. Total singly labeled SM was 690 ± 20 pmol/mg protein in extracts prior to phospholipase D treatment. After treatment with PLaseD, 70 ± 10 pmol/mg protein sphingoid base labeled Cer1P was observed along with 560 ± 20 pmol/mg protein of fatty acid labeled Cer1P. These summed to a total of 630 ± 20 pmol/mg protein, which represents a 91% recovery of labeled SM as Cer1P. N-acyl distribution was preserved with [^{13}C]-d18:1/16:0, [^{13}C]-d18:1/24:1, d18:1/[^{13}C]-16:0 and d18:1/[^{13}C]-24:1 being the most abundant chain lengths (Figure 3.8).

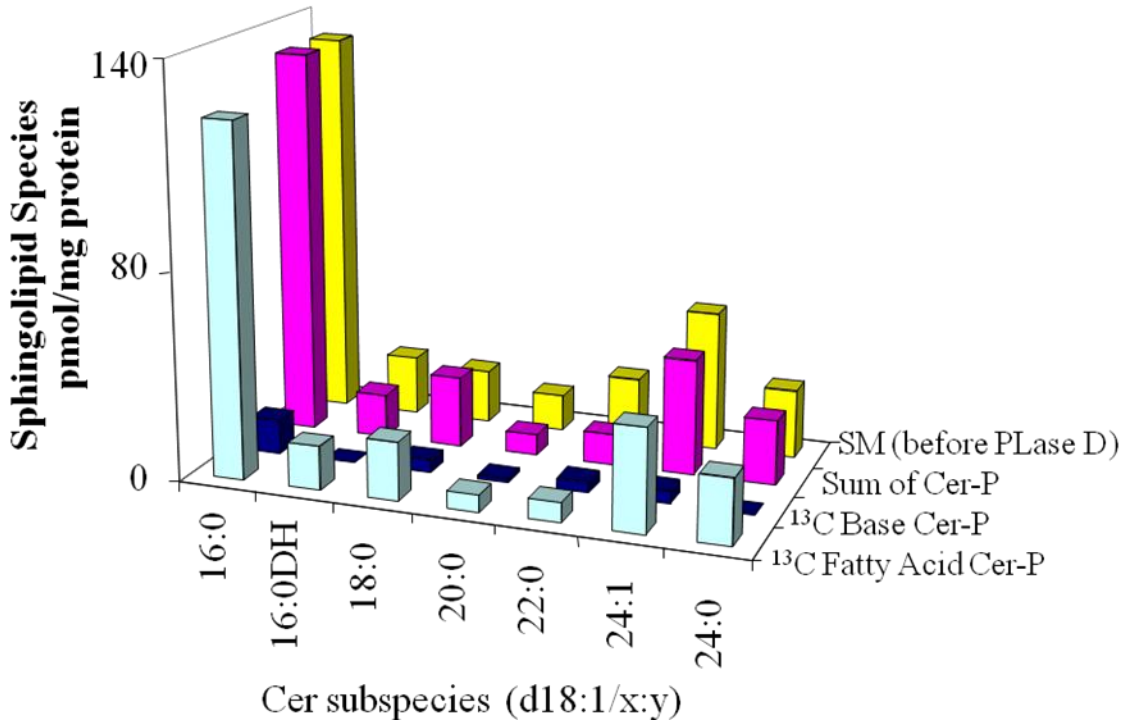

Figure 3.8. Determination of label position in singly labeled sphingomyelins was achieved by PLaseD treatment.

Incorporation of label into HEK 293 cells

Tables 3.1-3.3 show all the quantified sphingolipid species from HEK293 cells cultured for 3 h in media containing 0.1 mM U-^{13}C-palmitate. Quantitation was achieved by comparison of each peak within the sample to that of its appropriate internal standard. Base and fatty acid labeled SM were distinguished using PLaseD treatment. Incorporation of label into sphingosine-based species is rapid. The immediate product of serine palmitoyltransferase, 3-keto-sphinganine was quickly metabolized as evidenced by 3-keto-sphinganine amounts of < 10 pmol/mg protein. Likewise the incorporation of label into dihydroceramide is observed, but dihydroceramide is apparently quickly desaturated to ceramide, as evidenced by low dihydroglucosylceramide labeled amounts; however some labeled dihydrosphingomyelin is observed.

Differential rates of labeled palmitate incorporation into complex sphingolipids were observed between GlcCer and SM. While only 46% of total Cer was unlabeled at 3 h, total unlabeled GlcCer and SM were 85% and 93% respectively. SM made up the quantitative majority of the complex sphingolipids; however, label incorporation into SM by 3 h was low.

So and Sa also displayed different proportions of labeling. While the cells had a higher absolute concentration of So and So1P, Sa and Sa1P had greater relative incorporation of [^{13}C]-palmitate (Table 3.3). Of the 110 pmol/mg protein of So only 6 % was ^{13}C-d18:1; in contrast there was only 17 pmol/mg protein of Sa with 10% being [^{13}C]-d18:0.

Table 3.1. LC-MS/MS quantitation of complex sphingolipids with a sphingosine base in HEK293 cells treated with 0.1 mM U-[^{13}C]-palmitate for 3 h.

Sphingolipid	C16:0	C18:0	C20:0	C22:0	C24:1	C24:0
Cer	Mean ± SD pmol/mg protein	Mean ± SD pmol/mg protein	Mean ± SD pmol/mg protein	Mean ± SD pmol/mg protein	Mean ± SD pmol/mg protein	Mean ± SD pmol/mg protein
[^{12}C] t = 0	100 ± 20	20 ± 5	<10	20 ± 5	50 ± 10	60 ± 10
[^{12}C] t = 3	230 ± 10	120 ± 10	<10	30 ± 10	90 ± 10	40 ± 10
[^{13}C] FA	50 ± 10	40 ± 10	<10	<10	<10	<10
Dual [^{13}C]	150 ± 60	20 ± 10	<10	10 ± 0	<10	20 ± 10
[^{13}C] Base	70 ± 10	50 ± 10	<10	20 ± 10	20 ± 10	40 ± 10
GlcCer						
[^{12}C] t = 0	1230 ± 30	220 ± 10	<10	860 ± 40	210 ± 20	110 ± 20
[^{12}C] t = 3	1560 ± 50	340 ± 30	20 ± 10	890 ± 10	230 ± 60	120 ± 30
[^{13}C] FA	100 ± 30	20 ± 10	20 ± 10	30 ± 20	80 ± 10	50 ± 10
Dual [^{13}C]	70 ± 10	30 ± 10	50 ± 10	20 ± 10	30 ± 10	80 ± 10
[^{13}C] Base	20 ± 10	20 ± 10	40 ± 10	40 ± 10	80 ± 30	50 ± 20
SM						
[^{12}C] t = 0	1870 ± 90	200 ± 20	240 ± 10	80 ± 20	400 ± 10	340 ± 50
[^{12}C] t = 3	1780 ± 100	270 ± 60	50 ± 70	140 ± 60	630 ± 260	240 ± 10
[^{13}C] FA	130 ± 120	30 ± 60	50 ± 20	20 ± 10	30 ± 10	90 ± 20
Dual [^{13}C]	250 ± 230	20 ± 30	60± 10	30 ± 10	20 ±10	60 ± 10
[^{13}C] Base	70 ± 100	20 ± 50	20 ± 10	20 ± 10	40 ± 10	20 ± 10

Table 3.2. LC-MS/MS quantitation of complex sphingolipids with a sphinganine base in HEK293 cells treated with 0.1 mM U-[^{13}C]-palmitate for 3 h.

Sphingolipid	C16:0 DH	C18:0DH	C20:0 DH	C22:0 DH	C24:1 DH	C24:0 DH
Cer	Mean ± SD pmol/mg protein	Mean ± SD pmol/mg protein	Mean ± SD pmol/mg protein	Mean ± SD pmol/mg protein	Mean ± SD pmol/mg protein	Mean ± SD pmol/mg protein
[^{12}C] t = 0	100 ± 30	10 ± 5	<10	<10	20 ± 10	10 ± 5
[^{12}C] t = 3	90 ± 10	20 ± 10	<10	<10	40 ± 20	20 ± 10
[^{13}C] FA	<10	<10	<10	<10	<10	<10
Dual [^{13}C]	30 ± 10	<10	<10	<10	20 ± 10	<10
[^{13}C] Base	<10	<10	<10	<10	<10	<10
GlcCer						
[^{12}C] t = 0	<10	30 ± 10	<10	<10	150 ± 60	40 ± 20
[^{12}C] t = 3	60 ± 10	40 ± 10	<10	<10	70 ± 30	60 ± 30
[^{13}C] FA	<10	<10	<10	<10	30 ± 10	20 ± 10
Dual [^{13}C]	40 ± 10	80 ± 10	<10	<10	150 ± 20	110 ± 10
[^{13}C] Base	70 ± 30	<10	<10	<10	20 ± 30	<10
SM						
[^{12}C] t = 0	1150 ± 10	590 ± 20	<10	20 ± 10	230 ± 50	90 ± 30
[^{12}C] t = 3	1220 ± 80	680 ± 50	20 ± 10	120 ± 20	280 ± 70	70 ± 20
[^{13}C FA]	270 ± 40	120 ± 30	<10	20 ± 10	60 ± 20	20 ± 10
Dual [^{13}C]	310 ± 20	90 ± 20	10 ± 5	40 ± 10	110 ± 20	0 ± 10
[^{13}C] Base	90 ± 10	70 ± 40	<10	<10	20 ± 10	<10

Table 3.3. LC-MS/MS quantitation of long chain bases and their corresponding phosphates in HEK293 cells treated with 0.1 mM U-[^{13}C]-palmitate for 3 h.

Palmitate content	So Mean ± SD pmol/mg protein	Sa Mean ± SD pmol/mg protein	So1P Mean ± SD pmol/mg protein	Sa1P Mean ± SD pmol/mg protein
[^{12}C] t = 0	50 ± 10	10 ± 5	10 ± 5	<10
[^{12}C]	320 ± 40	22 ± 10	500 ± 20	30 ± 5
[^{13}C]	110 ± 20	17 ± 5	100 ± 20	60 ± 10

Treatment with fumonisin B1

Exposure to FB1 caused a decrease in the quantity of labeled Cer. Unlabeled Cer at 24 h were 46 ± 2 pmol/mg protein in control cells and 27 ± 1 pmol/mg protein in FB1 treated cells. A larger difference was seen in labeled Cer at 24 h. Control ^{13}C-d18:1 / [^{12}C]-(fatty acid) Cer was 13 ± 1 pmol/mg protein but FB1 treated cells had only 3 ± 1 pmol/mg protein base labeled Cer. d18:1/[^{12}C]-(fatty acid) Cer had a similar decrease with 7 ± 1 pmol/mg protein in control cells and < 3 pmol/mg protein for FB1 treated cells. [^{13}C]-d18:1/[^{13}C]-(fatty acid) Cer were 36 ± 1 pmol/mg protein for control cells and only 4 ± 1 pmol/mg protein in FB1 treated cells. These relationships were also observed in SM and GlcCer.

Changes in sphingoid base quantities provide an explanation of cellular responses to FB1 treatment (Figure 3.9).

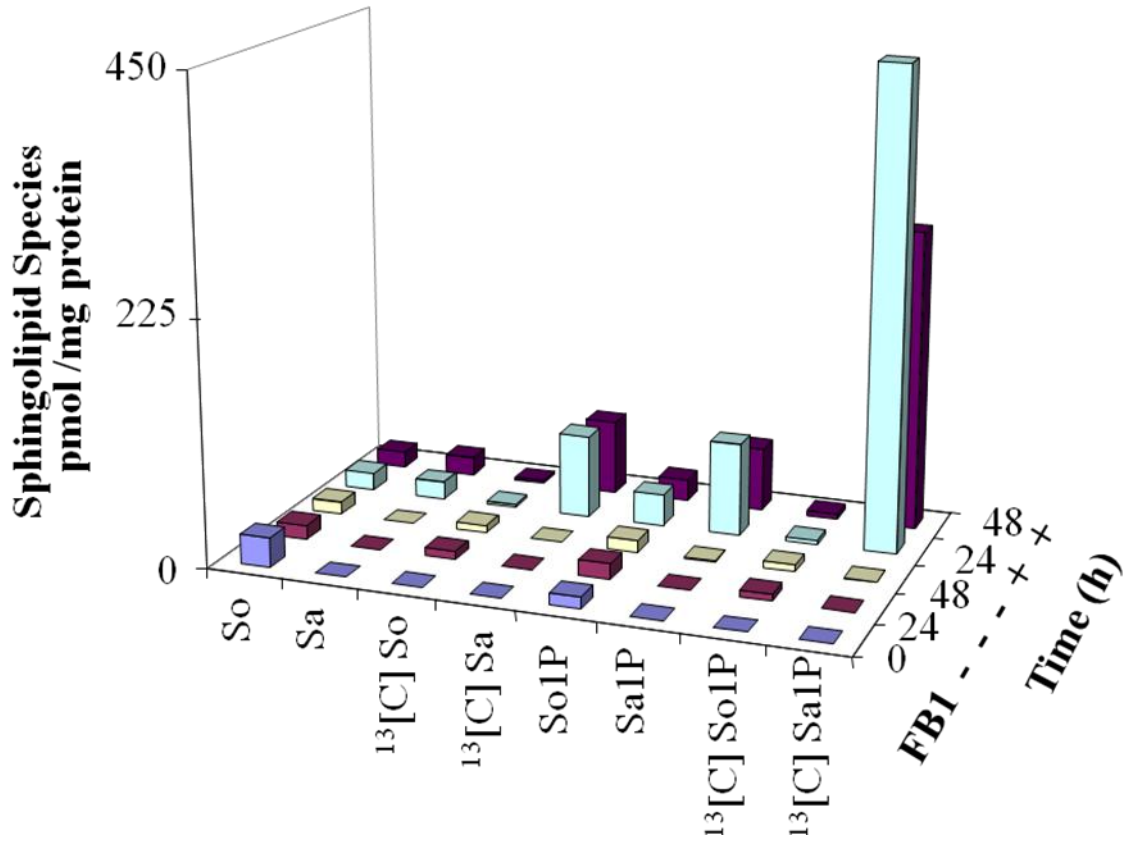

Figure 3.9. Sphingoid bases from HEK293 cells treated with 0.1 mM [^{13}C]-palmitate ± 50 uM FB1. FB1 was added to the cells by supplement to the media for 6 h due to its water solubility. Sphingoid bases of both [^{12}C] and [^{13}C] origins were analyzed simultaneously with reverse phase LC-MS/MS.

[^{13}C]-Sa and [^{13}C]-Sa1P were below quantification limits in control cells; however, they were the major sphingoid base species in FB1 treated cells at 79 ± 12 pmol/mg protein and 450 ± 67 pmol/mg protein, respectively. Unlabeled Sa and Sa1P were also observed to be 17 ± 4 pmol/mg protein and 88 ± 12 pmol/mg protein, respectively. These values correspond to an 82% labeling of Sa and and 84% labeling of Sa1P. This yields a 0.18 Sa/Sa1P ratio compared to a 0.19 [^{13}C]-Sa/[^{13}C]-Sa1P ratio.

Correction based on acyl-CoA pool

Analysis of the fatty acyl-CoA profile in HEK293 cells treated with 0.1 mM U-^{13}C-palmitate revealed that the 16:0-CoA was comprised of ~60% ^{13}C-16:0-CoA labeled by 6 h. One can also see that a portion of the ^{13}C-16:0-CoA was both elongated and desaturated (Figure 3.2), with the 18:0-CoA species' specific activity reaching 25%, while 16:1-CoA and 18:1-CoA specific activities were 39 and 13 percent respectively, at 6 h.

Thus assuming this is a single precursor pool, the simplest prediction would be that in addition to the incorporation of U-^{13}C-palmitate that is being synthesized into C16:0 Cer, there will also be incorporation of unlabelled precursor (^{12}C-16:0-CoA). Therefore, for the first 3 hours, the total *de novo* incorporation of U-^{13}C-palmitate in the backbone would be ~ 150 + 70 pmol/ mg protein or 220 pmol/ mg protein [dual (^{13}C-d18:1/^{13}C-16:0) + base (^{13}C-d18:1/^{12}C-16:0) labeled C16:0 Cer]. If the U-^{13}C-palmitoyl-CoA specific activity during this period is roughly estimated to be 30% (Figure 3.2), one would predict that Cer made *de novo* with ^{12}C backbone could be (220/30)*100, or 733 pmol/mg protein. However, the change in ^{12}C-C16:0 Cer from 0 until 3 h is only 130 + 50 pmol/mg protein (^{12}C-C16:0 Cer and fatty acid labeled C16:0 Cer).

One cause of this could be the incorporation of Cer into the downstream products GlcCer and SM. The incorporation of U-^{13}C-palmitate in C16:0 GlcCer at 3 h is 90 pmol/mg protein [dual (^{13}C-d18:1/^{13}C-16:0) + base (^{13}C-d18:1/^{12}C-16:0)]. If the U-^{13}C-palmitoyl-CoA specific activity during this period is roughly estimated to be 30%, a prediction of the amount of *de novo* ^{12}C C16:0 GlcCer would be 210 pmol/mg protein.

However, the change in ^{12}C-C16:0 GlcCer from 0 until 3 h is 330 + 100 pmol/mg protein (^{12}C-C16:0 GlcCer and fatty acid labeled C16:0 GlcCer).

The incorporation of U-^{13}C-palmitate in C16:0 SM at 3 h is 320 pmol/mg protein [dual (^{13}C-d18:1/^{13}C-16:0) + base (^{13}C-d18:1/^{12}C-16:0)]. If the U-^{13}C-palmitoyl-CoA specific activity during this period is roughly estimated to be 30%, a prediction of the amount of *de novo* ^{12}C C16:0 SM would be 747 pmol/mg protein. However, the change in ^{12}C-C16:0 SM from 0 until 3 h is 130- 40 pmol/mg protein (^{12}C-C16:0 SM and fatty acid labeled C16:0 SM).

Incorporation of label into RAW264.7 cells

The sphingolipid profile in extracts of RAW264.7 cells treated with 0.1 mM U-^{13}C-palmitate was first explored by precursor ion scans and the predominant N-acyl chain lengths for Cer, HexCer, SM, and Cer1P were identified as 16:0, 18:0, 20:0, 22:0, 24:1, 24:0, 26:1, and 26:0. The presence of elongated U-^{13}C-palmitate in N-acyl chains was also detected.

Time points were taken from 0 h to 24 h intervals with and without KDO_2 lipid A treatment. A distribution of chain lengths is observed in [^{12}C]-Cer (Figure 3.10). In control cells one major Cer, d18:1/16:0 Cer, increases from 0 h to 24 h at 3.9 ± 0.3 to 5.5 ± 0.1 pmol/µg DNA. In treated cells one major Cer, d18:1/16:0 Cer, decreases from 8.5 ± 0.1 to 3.2 ± 0.1 pmol/µg DNA from t=0 to 2 h, then increases to 26.4 ± 0.2 pmol/µg DNA at 24 h. In control cells a decrease in d18:0/24:1 Cer was observed from 13.1 ± 0.4 to 4.3 ± 0.1 pmol/µg DNA from 0.5 to 24 h. Treated cells followed a similar decrease until 8 h; however, an increase in d18:0/24:1 Cer was observed from 8.8 ± 0.3 to 15.0 ± 1.5 pmol/µg DNA from 8 to 24 h.

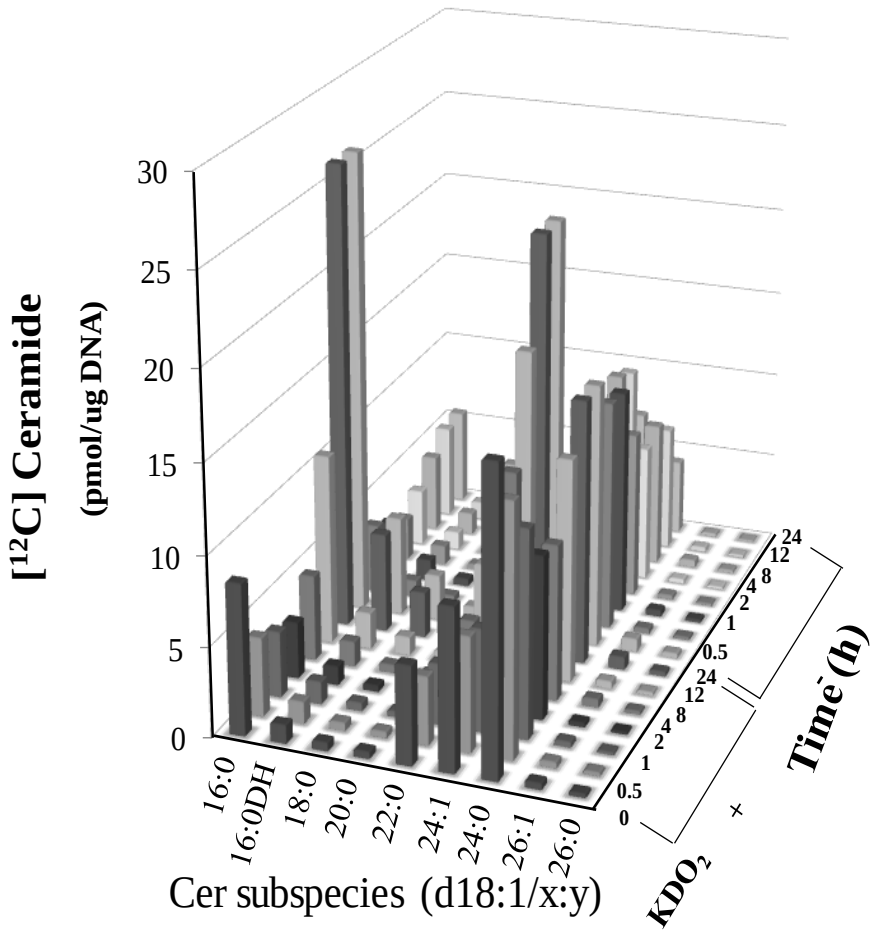

Figure 3.10. [^{12}C] ceramides from extracts of RAW264.7 cells treated with ± KDO_2 Lipid A and 0.1mM [^{13}C]-palmitate for 0-24 h.

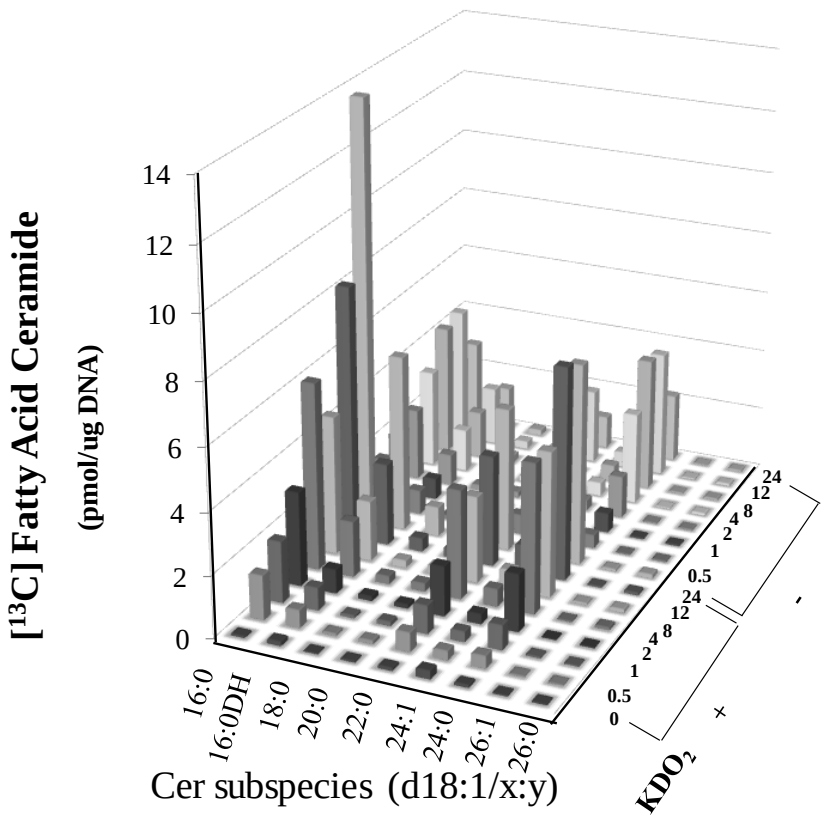

Figure 3.11. Fatty acid labeled ceramides from extracts of RAW264.7 cells treated with ± KDO_2 Lipid A and 0.1mM [^{13}C]-palmitate for 0-24 h.

U-[^{13}C]-palmitate was shown to be readily incorporated into sphingolipids in RAW264.7 cells. Incorporation into the N-acyl chains was examined and designated as the fatty acid labeled complex species in Cer (Figure 3.11), GlcCer, and SM. Appreciable incorporation was seen in ^{12}C-d18:1/[^{13}C]-16:0, ^{12}C-d18:1/[^{13}C]-22:0, and ^{12}C-d18:1/[^{13}C]24:0 Cer in both treated and untreated cells. Total fatty acid labeled Cer in treated cells continued to increase from 12 h to 24 h, while control decreased by 40 % between 12 h and 24 h. This trend was consistent for all chain lengths. In treated cells one major Cer, d18:1/16:0 Cer, increases from 1.2 ± 0.1 to 13.7 ± 0.1 pmol/µg DNA from t=0.5 to 24 h. An increase in treated cells was observed for d18:0/24:0 Cer from 0.8

± 0.2 to 7.7 ± 0.3 pmol/µg DNA from 0.5 to 24 h. Likewise, in treated cells, d18:1/22:0 Cer increases from 0.4 ± 0.1 to 6.3 ± 0.1 pmol/µg DNA from 0.5 to 24 h.

Cer having incorporated label into both the fatty acid and sphingoid base were quantitatively the predominantly labeled species in treated cells. [^{13}C]-d18:1/[^{13}C]-16:0 , [^{13}C]-d18:1/[^{13}C]-22:0, and [^{13}C]-d18:1/[^{13}C]-24:0 Cer were the major labeled species (Figure 3.12). Treated cells showed a marked increase in [^{13}C]-d18:1/[^{13}C]-16:0 Cer increased from an initial quantity of 4.4 ± 0.2 pmol/µg DNA at 0.5 h to 41.3 ± 1.3 pmol/µg DNA at 24 h.

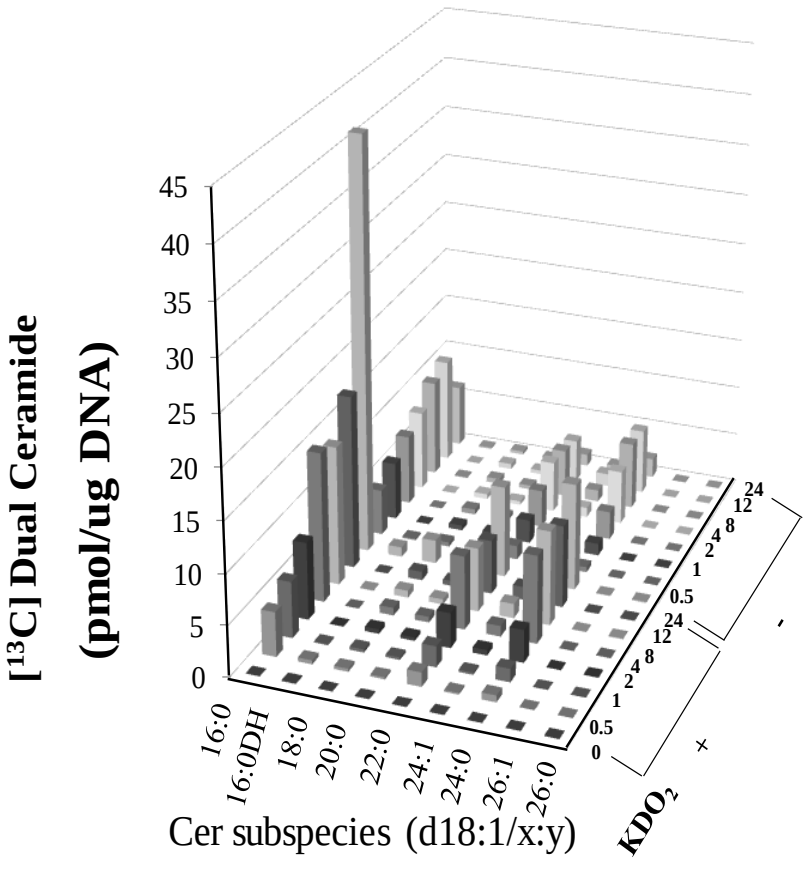

Figure 3.12. Dual labeled ceramides from extracts of RAW264.7 cells treated with ± KDO_2 Lipid A and 0.1mM [^{13}C]-palmitate for 0-24 h.

In treated cells one major Cer, d18:1/16:0 Cer, increases from 1.2 ± 0.1 to 13.7 ± 0.1 pmol/µg DNA from t=0.5 to 24 h. An increase in treated cells was observed for d18:0/24:0 Cer from 0.8 ± 0.2 to 7.7 ± 0.3 pmol/µg DNA from 0.5 to 24 h. Likewise, in treated cells, d18:1/22:0 Cer increases from 0.4 ± 0.1 to 6.3 ± 0.1 pmol/µg DNA from 0.5 to 24 h. Control cells showed an increase until 12 h, but then a decrease between 12 h and 24 h was observed.

Incorporation of U-[^{13}C]-palmitate into the sphingoid base, but not the fatty acid, in Cer showed a different chain length distribution than other labeled species. (Figure 3.13). Also quantities between treated and control cells were similar.

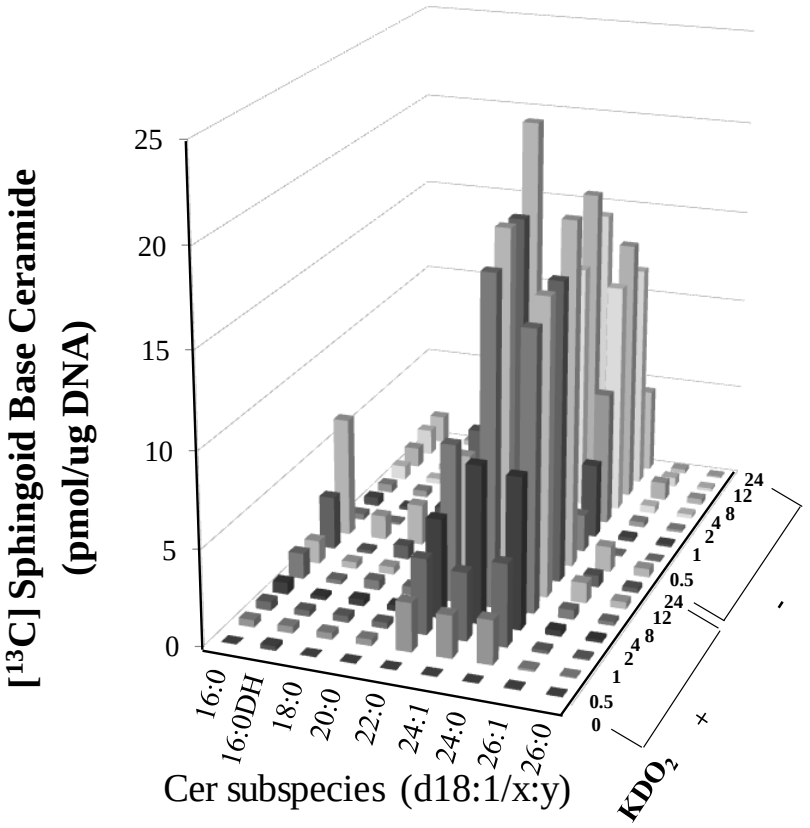

Figure 3.13. Sphingoid Base labeled ceramides from extracts of RAW264.7 cells treated with ± KDO_2 Lipid A and 0.1mM [^{13}C]-palmitate for 0-24 h.

Discussion

Described here is a sensitive and selective LC-MS/MS method utilizing a uniformly labeled [^{13}C]-palmitate tracer for determination of the *de novo* biosynthesis of sphingolipids. Utilizing an isotopic precursor was first addressed by Tserng et al., but this uniformly labeled precursor method has several distinct advantages over Tserng et al. use of a non-uniformly labeled precursor [188]. First, HPLC separation prior to introduction in the mass spectrometer allows the resolution of all N-acyl chain lengths of sphingolipids; whereas, the resolution of chain lengths longer than C16 by reverse phase GC is poor and could lead to miscalculation of chain length distribution [188]. Also Tserng et al. used repetitive scans as opposed to selected monitoring of precursor-product pairs with the explanation that other peaks of interest could be examined later. If proper prescreening with SM or Cer precursors scans is performed as described previously, then no scan time and resolution need to be lost to wide *m/z* windows.

Fatty acid β-oxidation coupled with resynthesis could produce non-uniformly labeled [^{13}C]-palmitate, and thereby skew data, as previously stated [188]. To examine this issue, precursor scans for *m/z* 184.4 and *m/z* 264.4 in treated HEK293 cells were performed. The resulting data did not show significant quantities of labeled sphingolipids containing less than 16 amu shifts due to these β-oxidation pathways.

Cer and GlcCer fragment to produce the same sphingoid base fragment ion of *m/z* 264.4 as the sphingoid bases. SM fragments differently by keeping the charge on their phosphocholine moiety after dissociation. Therefore, no charge is left on the Cer moiety to determine label position if the SM is singly-labeled. In order to determine the label position in these singly-labeled SM, each extract is treated with PLaseD to convert the

SM to Cer1P. The Cer1P will then fragment along the same pathways as Cer. In a similar manner Tserng et al. used a sphingomyelinase to produce Cer from SM in HL60 cells [188, 189].

The immediate product of SPT is 3-keto-sphinganine; however, no labeled 3-keto-sphinganine (< 10 pmol) was detected. HEK 293 cells have been screened for 3-keto-sphinganine, and these values are consistently low (less than 5% the signal from Sa). This implies that 3-keto-sphinganine is rapidly reduced to Sa and does not accumulate under normal circumstances.

It has been previously shown that when cells are treated with FB_1, production of Cer is blocked and Sa accumulates [194-197]. U-[^{13}C]-palmitate experiments independently confirm this conclusion and provide additional details regarding the fate of labeled Sa demonstrated by the accumulation of labeled Sa1P.

Differences were observed in the relative quantities of the three types of labeled complex sphingolipids. The dual-labeled species were the predominant species, and had a similar distribution of fatty acid chain lengths to that of the fatty acid only labled species with [^{13}C]-d18:1/[^{13}C]-C16:0 Cer being the most abundant. Singly-labeled Cer, however, were significantly different. In the sphingoid base labeled Cer, [^{13}C]-d18:1/16:0 was no longer the major species. This is most likely attributable to the dilution of [^{12}C]-palmitate by U-[^{13}C]-palmitate, which lowers the access of ceramide synthase to non-labeled fatty acids. Conversely, fatty acid only labeled Cer had the opposite pattern, as d18:1/[^{13}C]-16:0 was elevated. GlcCer exhibited similar patterns to the Cer, but at lower concentrations. SM was the major complex sphingolipid species observed. However, fatty acidonly labeled and SM and sphingoid base labed SM initially

could not be distinguished from the MS/MS of the intact species, for previously mentioned reasons. Furthermore, it is conclusively shown that *de novo* Cer biosynthesis is reduced by FB1 treatment due to the absence of U-[^{13}C] labeled Cer. The major increase in Cer population in FB1 treated cells was seen in the [^{12}C] Cer species. This increase is likely due to turnover of GlcCer and SM back to Cer.

FB1 treatment induced a decrease in all labeled complex sphingolipids. To explore the fate of the [^{13}C]-palmitate in these samples, long chain base species were analyzed as well (Figure 3.9). Treatment with FB1 induced an accumulation of *de novo* Sa; however, most of this [^{13}C]-Sa is converted to [^{13}C]-Sa1P. This data suggests that HEK293 cells rapidly phosphorylate the accumulating *de novo* Sa, possibly to prevent apoptosis (30). Conversion to Sa1P provides a mechanism not examined or discussed by Tserng et al (24) as a role of metabolism of pro-apoptotic So/Sa.

Labeled Cer1P is produced in very low amounts in HEK293. These values (typically fewer than 50 pmol/1x10^6 cells) are subtracted from Cer1P amounts measured after PLaseD treatment, resulting in signal originating only from singly labeled SM (i.e. 7 pmol/mg protein d18:1/[^{13}C]-16:0 Cer1P prior to PLaseD treatment vs. 306 pmol/mg protein d18:1/[^{13}C]-16:0 Cer1P after PLaseD treatment). The derived individual amounts of sphingoid base and fatty acid only labeled sum to approximately 90% of the original SM, supporting the accuracy of this method's estimation of SM label position. PLaseD readily converts the C12:0 SM internal standard to C12:0 Cer1P also at a rate of ~90%, which can then be used to quantify the other Cer1P produced. This fact coupled with SM being observed in amounts significantly over detection limits (nmol range in 1 x 10^6 cells) allow for an accurate recapitulation of singly-labeled SM.

PLaseD treatment was able to distinguish labeled species in cells only treated for 3 h with U-[^{13}C]-palmitate (Table 3.1-3.3). Here the data show incorporation of label and when many of these tables from differing time points are examined together, a very detailed view of the pathway is observed.

Use of U-[^{13}C]-palmitate treatment aided in the identification of biosynthetic differences in RAW264.7 cells. Most notably the increase in dual labeled Cer in treated cells. The incorporation of label at two points demonstrates that this compound is indeed newly synthesized, and one can begin to hypothesize about KDO2 lipid A stimulated enzymes that would selectively produce the cual labled Cer in abundance.

U-[^{13}C]-palmitate treatment in conjunction with ESI LC-MS/MS analyses yields highly informative data regarding sphingolipid mass. It is also important to note that the biosynthetic pathways can be observed as seen with FB1 treatment with newly synthesized [^{13}C]-Sa piling up into amounts 5 fold their [^{13}C]-So and [^{13}C]-So1P counterparts in control cells. The observations would be less definitive without the distinctive positional labeling of complex sphingolipids produced by U-[^{13}C]-palmitate, and provides a model for further exploration of modulators of the sphingolipid pathway.

CHAPTER 4

Development of additional mass spectrometric methods for specific applications

In the course of collaborations with other researchers, existing methods were adapted to analyze samples the use of existing methods with minor changes, such as the identification of a methylated species[198], or significant changes, such as resolution of isomeric drug candidates and their metabolites[41] have allowed for application-based discoveries. Following are examples of successful collaborations and the methodological modifications that made them possible.

A. Safingol Toxicology After Oral Administration to TRAMP Mice: Demonstration of Safingol Uptake and Metabolism by N-Acylation and N-Methylation

Pablo R. Morales; Dirck L. Dillehay; Steven J. Moody; David C. Pallas; Sarah Pruett, Jeremy C. Allegood; Holly Symolon; Alfred H. Merrill Jr.
Drug and Chemical Toxicology, Volume 30, Issue 3 July 2007 , pages 197 – 216

Abstract

Safingol (L-*threo*-dihydrosphingosine) is an unnatural stereoisomer of sphinganine (D-*Erythro*-dihydrosphingosine) that is being tested as an anti-cancer agent. To learn how safingol affects a mouse strain that is often used in prostate cancer studies (Transgenic Adenocarcinoma of Mouse Prostate, TRAMP) mice, safingol was administered orally via supplementation of the diet at 0.0125, 0.025, 0.05 and 0.1% (w/w). Significant hepatotoxicity was found after 2 weeks at all dosages by analysis of liver alanine-aminotransferase (ALT); renal toxicity was only noted in mice administered 0.1% safingol, based on moderate elevation of blood urea nitrogen (BUN). Bilirubin, serum proteins, electrolytes and urinalysis were within normal limits. Hematology revealed a significant decrease in the packed cell

volume for the group fed at the higher dosage of safingol. Mice fed the 0.0125% diet, maintained a normal weight during the experiment, but a significant weight loss (>30%) was observed in mice given the highest dosage of safingol. Tissues examined by histology showed moderate changes in liver for the 0.1% safingol group. Safingol added in the diet at these concentrations did not inhibit the production of prostate intraepithelial neoplasia (PIN), a common naturally occurring pre-neoplastic lesion in this strain of mice as they age. Analysis of safingol and metabolites in blood and tissues by liquid chromatography electrospray tandem mass spectrometry revealed extensive conversion of safingol to N-acyl-species (analogous to the "ceramides" found in naturally occurring sphingolipids) and N-mono-, di-and tri-methyl metabolites. The latter are particularly intriguing because N, N-dimethylsphingosine is a highly toxic metabolite of sphingosine, therefore, some of these safingol metabolites may contribute its toxicity.

Synthesis of methylated safingols

Internal standards were synthesized for mass spectrometric characterization and evaluation of LC mobility because a range of methylated sphingoid base standards were not available. Methylsafingols were synthesized by methyl iodide addition to safingol as follows: 1.23 g of safingol (4.08 mmol) was placed in an Erlenmeyer flask, and the safingol was dissolved in 100 mL of ethanol. With the addition of 3.4 mL of CH_3I (54.90 mmol) to the flask, the mixture was stirred at room temperature for three days. Excess CH_3I was precipitated by the addition of 500 mL ether. The solvent was decanted to a round bottom flask and solvent was removed using a Heidolph Labrotora 4001 rotovap. Because the individual methylated species were difficult to separate from each other, the

mixture was evaluated by NMR and LC-MS/MS to determine the molar ratio between species and used as a mixture in experiments.

The presence of three separate methyl species was verified by LC-MS/MS, which yielded 3 individual peaks corresponding to the MRM transitions for N-methylsafingol, N,N-dimethylsafingol, and N,N,N-trimethylsafingol. ^{13}C NMR was performed using a Varian Mercury Vx 300 MHz instrument. A mixture of the methylated safingol was examined relative to TMS. Three separate shifts were observed for the ^{13}C from the N-methyl carbons. N-methylsafingol, N,N-dimethylsafingol, and N,N,N-trimethylsafingol were identified by signal at 34.5, 44.2, 52.8 ppm, respectively. Integration of the signals for each of these subspecies allowed for determination of the molar ratios, which were approximately 1:0.5:0.1 for N-methylsafingol:N,N-dimethylsafingol:N,N,N-trimethylsafingol, respectively.

Liquid Chromatography Electrospray Tandem Mass Spectrometry of Sphingoid Bases and Safingol

Free sphingoid bases (sphingosine, sphinganine, and safingol) as well as methylated, and acylated metabolites were separated by reverse phase HPLC using a binary system and a Supelco 2.1mm x 25 cm Discovery C18 column. Mobile phase A and B were the same as previously described for the sphingoid bases. All runs were maintained at 0.5 mL/min flow rate. Before each run, the column was equilibrated for 1.5 min. at 60:40 (A:B). After sample injection (50 μL by a Perkin Elmer Series 200 Autosampler), the system was held at 60:40 (A:B) for 6.5 min, followed by a 9.0 min linear gradient to 100% B, which was held for 44.5 min and followed by a 1.5 min re-equilibration at initial conditions.

Liquid chromatographic separation of safingol and sphinganine allowed distinction of these two species and their metabolites (Figure 4.1). Safingol eluted with greater than 1 minute separation in standards and in biological samples

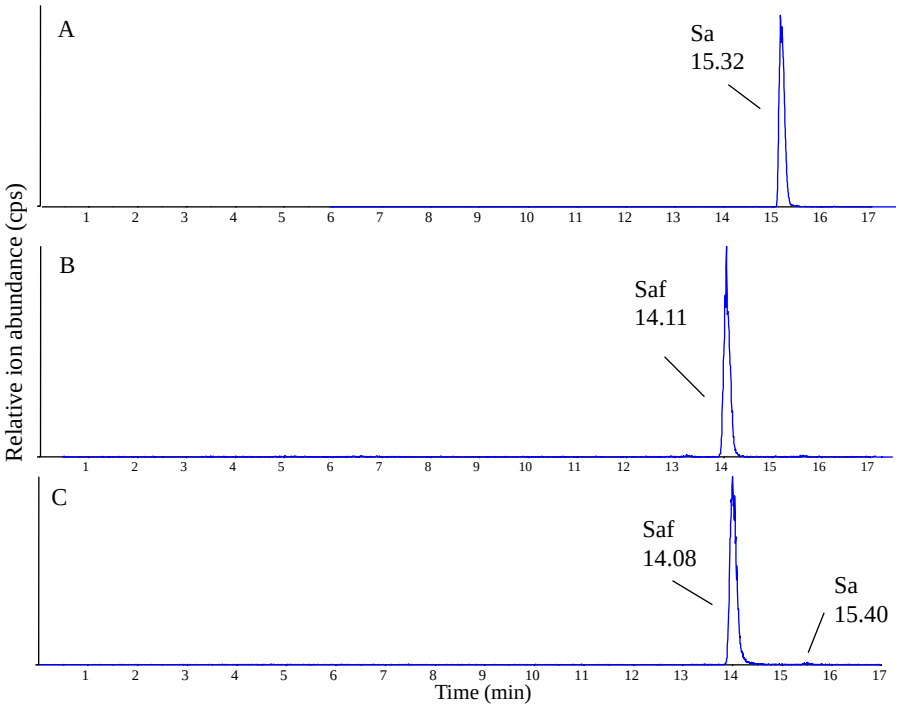

Figure 4.1. Reverse phase LC-MS/MS analysis of A) sphinganine, B) safingol, C) sphinganine and safingol in TRAMP mouse liver.

As expected, safingol was N-acylated; however, there was also a significant amount of N-methylated species (mono-, di-, and tri-). Both mono (Figure 4.2) and N,N-dimethylsafingol (Figure 4.3) fragment via loss of the N-methyl groups and double dehydration to yield *m/z* 280 and 294. Similar fragmentations were observed in pure mono and N,N-dimethylsphingosine purchased from Avanti Polar Lipids.

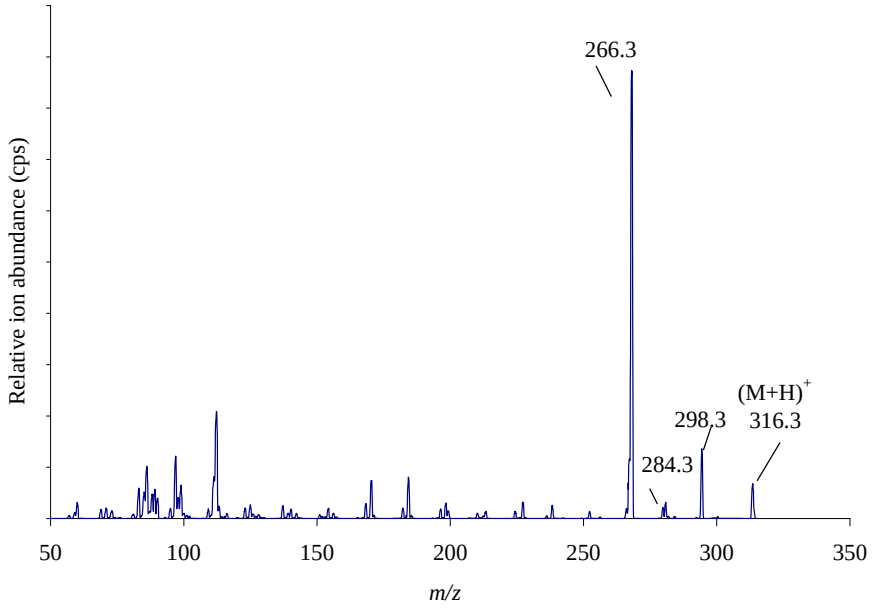

Figure 4.2. Product ion spectrum of N-methylsafingol (*m/z* 316.3).

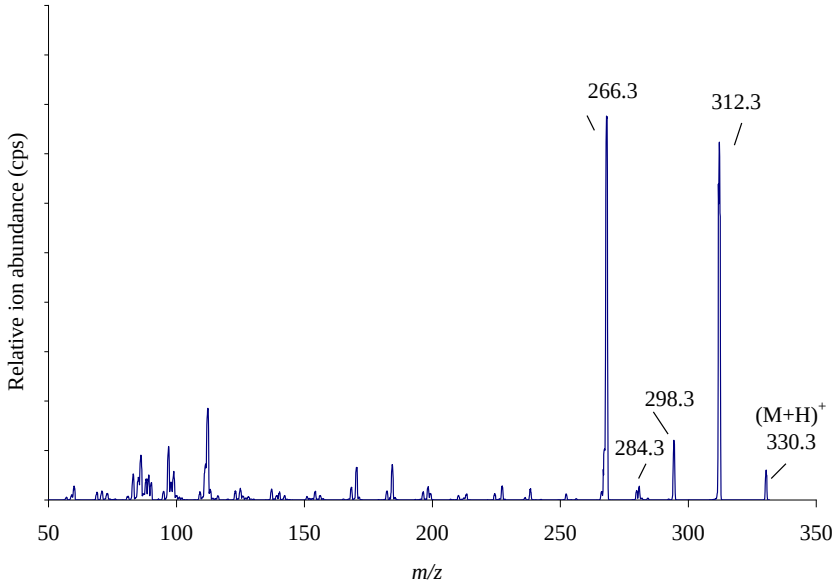

Figure 4.3. Product ion spectrum of N,N-dimethylsafingol(*m/z* 330.3).

Trimethyl species (Figure 4.4) retain charge of the nitrogen and preferentially fragment to $NH(CH_3)_3^+$ (*m/z* 60.1). Methylated species eluted in identical order to sphingoid bases, which allowed for ease in peak assignment.

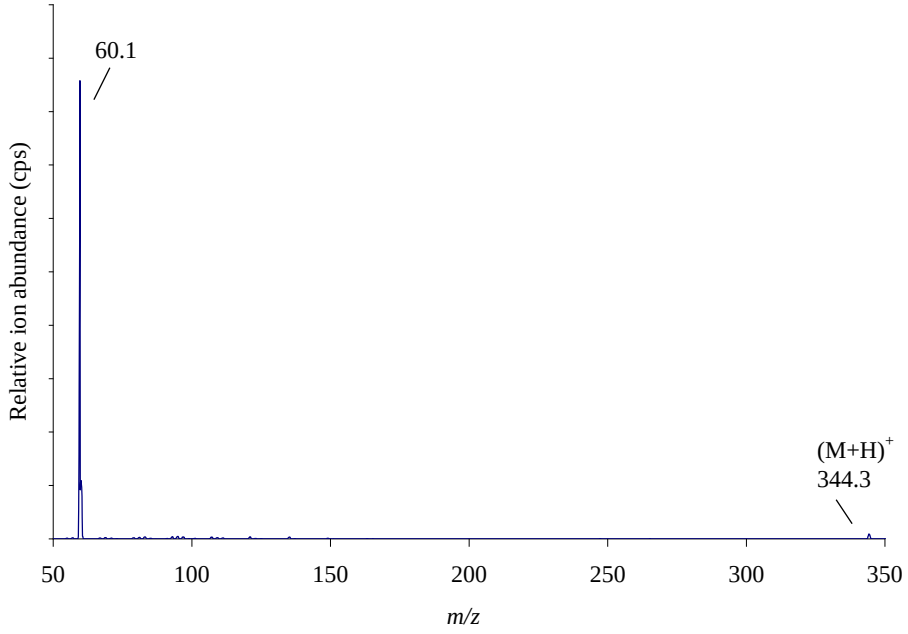

Figure 4.4. Product ion spectrum of N,N,N-trimethylsafingol.

B. Upstream of growth and differentiation factor 1 (uog1), a mammalian homolog of the yeast longevity assurance gene 1 (LAG1), regulates N-stearoyl-sphinganine (C18-(dihydro)ceramide) synthesis in a fumonisin B1-independent manner in mammalian cells.

Venkataraman K, Riebeling C, Bodennec J, Riezman H, Allegood JC, Sullards MC, Merrill AH Jr., Futerman AH.

J Biol Chem. 2002 Sep 20;277(38):35642-9. Epub 2002 Jun 24

Abstract

The longevity assurance gene (LAG1) and its homolog (LAC1) are required for acyl-CoA-dependent synthesis of ceramides containing very long acyl chain (e.g. C26) fatty

acids in yeast, and a homolog of LAG1, ASC1, confers resistance in plants to fumonisin B(1), an inhibitor of ceramide synthesis. To understand further the mechanism of regulation of ceramide synthesis, we now characterize a mammalian homolog of LAG1, upstream of growth and differentiation factor-1 (uog1). cDNA clones of uog1 were obtained from expression sequence-tagged clones and sub-cloned into a mammalian expression vector. Transient transfection of human embryonic kidney 293T cells with uog1 followed by metabolic labeling with [4,5-(3)H]sphinganine or L-3-[(3)H]serine demonstrated that uog1 conferred fumonisin B(1) resistance with respect to the ability of the cells to continue to produce ceramide. Surprisingly, this ceramide was channeled into neutral glycosphingolipids but not into gangliosides. Electrospray tandem mass spectrometry confirmed the elevation in sphingolipids and revealed that the ceramides and neutral glycosphingolipids of uog1-transfected cells contain primarily stearic acid (C18), that this enrichment was further increased by FB(1), and that the amount of stearic acid in sphingomyelin was also increased. UOG1 was localized to the endoplasmic reticulum, demonstrating that the fatty acid selectivity and the fumonisin B(1) resistance are not due to a subcellular localization different from that found previously for ceramide synthase activity. Furthermore, in vitro assays of uog1-transfected cells demonstrated elevated ceramide synthase activity when stearoyl-CoA but not palmitoyl-CoA was used as substrate. We propose a role for UOG1 in regulating C18-ceramide (N-stearoyl-sphinganine) synthesis, and we note that not only is this the first case of ceramide formation in mammalian cells with such a high degree of fatty acid specificity, but also that the N-stearoyl-sphinganine produced by UOG1 most significantly impacts neutral glycosphingolipid synthesis.

C. Two mammalian longevity assurance gene (LAG1) family members, trh1 and trh4, regulate dihydroceramide synthesis using different fatty acyl-CoA donors.

Riebeling C, Allegood JC, Wang E, Merrill AH Jr., Futerman AH.
J Biol Chem. 2003 Oct 31;278(44):43452-9.

Abstract

Overexpression of upstream of growth and differentiation factor 1 (uog1), a mammalian homolog of the yeast longevity assurance gene (LAG1), selectively induces the synthesis of stearoyl-containing sphingolipids in mammalian cells (Venkataraman, K., Riebeling, C., Bodennec, J., Riezman, H., Allegood, J. C., Sullards, M. C., Merrill, A. H. Jr., and Futerman, A. H. (2002) J. Biol. Chem. 277, 35642-35649). Gene data base analysis subsequently revealed a new subfamily of proteins containing the Lag1p motif, previously characterized as translocating chain-associating membrane (TRAM) protein homologs (TRH). We now report that two additional members of this family regulate the synthesis of (dihydro)ceramides with specific fatty acid(s) when overexpressed in human embryonic kidney 293T cells. TRH1 or TRH4-overexpression elevated [3H](dihydro)ceramide synthesis from l-[3-3H]serine and the increase was not blocked by the (dihydro)ceramide synthase inhibitor, fumonisin B1 (FB1). Analysis of sphingolipids by liquid chromatography-electrospray tandem mass spectrometry revealed that TRH4 overexpression elevated mainly palmitic acid-containing sphingolipids whereas TRH1 overexpression increased mainly stearic acid and arachidic acid, which in both cases were further elevated upon incubation with FB1. A similar fatty acid specificity was obtained upon analysis of (dihydro)ceramide synthase activity in vitro using various fatty acyl-CoA substrates, although in a FB1-sensitive manner. Moreover, in homogenates from TRH4-overexpressing cells, sphinganine, rather than sphingosine

was the preferred substrate, whereas no preference was seen in homogenates from TRH1-overexpressing cells. These findings lend support to our hypothesis (Venkataraman, K., and Futerman, A. H. (2002) FEBS Lett. 528, 3-4) that Lag1p family members regulate (dihydro)ceramide synthases responsible for production of sphingolipids containing different fatty acids.

Ceramide Synthase

Sphingolipidomic analyses are important in that they reveal the pathways of metabolic flux of lipids from either biosynthesis or turnover in a biological system. For example, a family of genes has recently been linked to the biosynthesis of ceramides and dihydroceramides in mammalian cells, and different gene products preferentially utilize different fatty acyl-CoA substrates [58, 199, 200]. Initially LASS1 (formerly named UOG-1) was investigated as a mammalian homolog to the yeast Longevity Assurance Gene 1 (LAG-1) [199]. Detailed analysis of the full spectrum of N-acyl chain lengths for ceramides in HEK-293T transiently over-expressing *LASS1* and monohexosylceramides revealed a marked increase in C18:0 Cer. This matched *in vitro* assays which showed a preference for stearoyl-CoA (Figure 4.5), which in turn showed resistance to inhibition by fumonisin B1 (FB1), a known inhibitor of DHCerS.

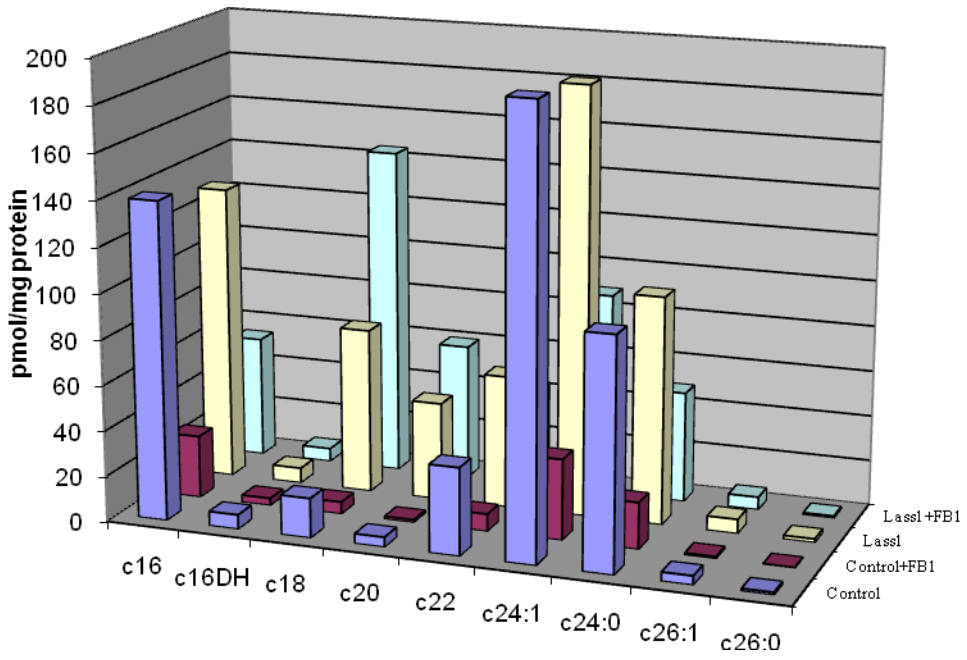

Figure 4.5. Ceramides in HEK-293T cells and HEK-293T cells transiently over-expressing *LASS1*.

While radiolabeling experiments were also performed, the structure-specific data from LC-MS/MS analysis provided the necessary specificity to determine chain length preference for this protein.

LASS4 and *LASS5* (formerly trh1 and trh4) were subsequently shown also to determine chain length preference of DHCerS [58]. Analysis of N-acyl chain lengths from HEK-293T transiently over-expressing *LASS4* or *LASS5* is shown for C16:0 to C26:0 for ceramides (Figure 4.6), monohexosylceramides, sphingomyelin, and their dihydro-

counterparts. LASS5 greatly influenced synthesis of C16:0 dihydroceramides, while LASS4 showed a more general preference for C18:0 and C20:0 species.

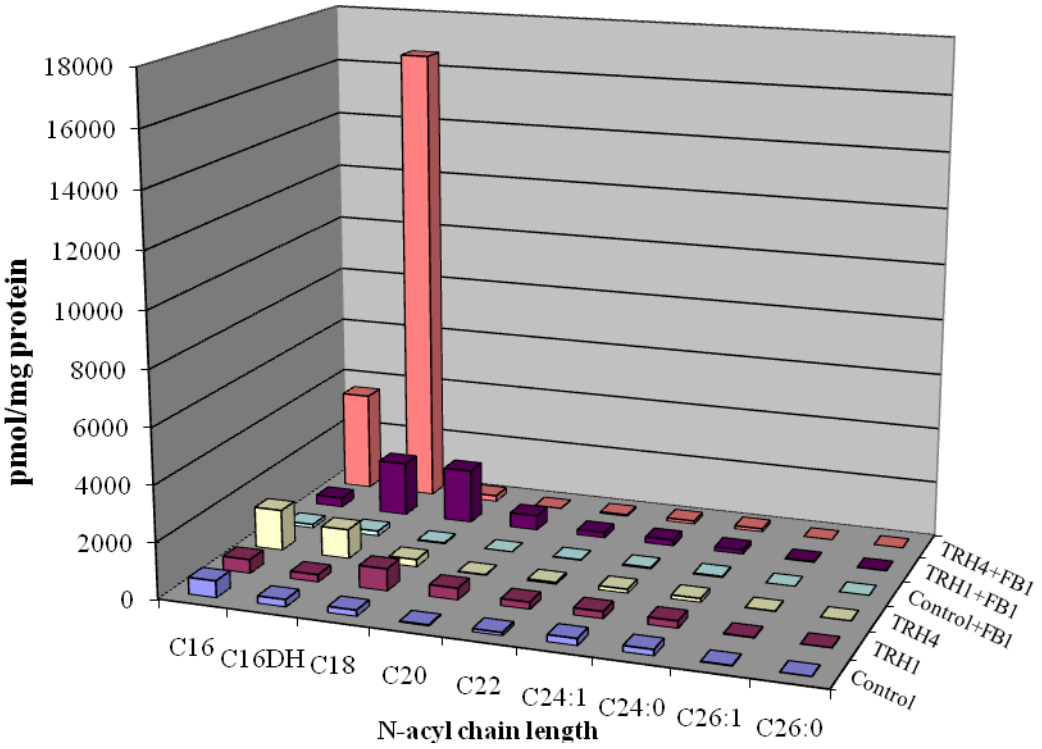

Figure 4.6. Ceramides in HEK-293T cells and HEK-293T cells transiently over-expressing *LASS4* and *LASS5*.

Further work demonstrated LASS5 to be an actual DHCerS [59]. HA-tagged LASS5 was immuno-purified and assayed for activity with palmitoyl-CoA and stearoyl-CoA. The purified LASS5 was shown to have a higher preference for palmitoyl-CoA. Thus, combinatory studies between "sphingolipidomics" and more traditional biochemical methodologies were able to identify a family of genes through homology, characterize the sphingolipids they influenced, determine their susceptibility to an inhibitor, and lend direction to enzymatic classification.

D. Hydrolyzed fumonisins HFB1 and HFB2 are acylated in vitro and in vivo by ceramide synthase to form cytotoxic N-acyl-metabolites.

Seiferlein M, Humpf HU, Voss KA, Sullards MC, Allegood JC, Wang E, Merrill AH Jr.
Mol Nutr Food Res. 2007 Sep;51(9):1120-30.

Abstract

Fumonisins B1 and B2 (FB1 and FB2) are the most abundant members of the fumonisins--mycotoxins that are produced by Fusarium verticillioides and are natural inhibitors of ceramide synthase. Their hydrolyzed forms, HFB1 and HFB2 (also called AP1 and AP2) are found in some foods, and they are not only inhibitors of ceramide synthase but also undergo acylation by this enzyme. This study characterized the conversion of HFB1 and HFB2 by ceramide synthase to their respective N-acylated metabolites using rat liver microsomes and palmitoyl-CoA or nervonoyl-CoA as cosubstrates, and examined animals that had been dosed with hydrolyzed fumonisins to ascertain if acylation occurs in vivo. Using an HPLC-MS/MS method that allowed the sensitive and selective detection of the acylation products, both HFB1 and HFB2 were found to be metabolized in vitro to nervonoyl- or palmitoyl-HFB1 and -HFB2 (i.e. C24:1-HFB1/2 and C16-HFB1/2, respectively). The apparent vmax was considerably higher for formation of C24:1HFB1 (157 pmol/min/mg protein) than for formation of C16HFB1 (8.7 pmol/min/mg protein). The acylation products also inhibited ceramide synthase and significantly reduced the number of viable cells in an in vitro [3-(4,5-dimethylthiazol-2-yl)-2,5-diphenyltetrazolium bromide (MTT)] assay using a human colonic cell line (HT29). Furthermore, HPLC-MS/MS analysis of tissues from rats given intraperitoneal doses of HFB1 confirmed that formation of N-acyl-HFB1 occurs in vivo to produce metabolites with fatty acids of various chain lengths. The contribution of

acylated HFB1 and HFB2 metabolites to fumonisin toxicity in vivo warrants further investigation.

n	R1	R2
1	OH	OH
2	OH	H
3	H	OH

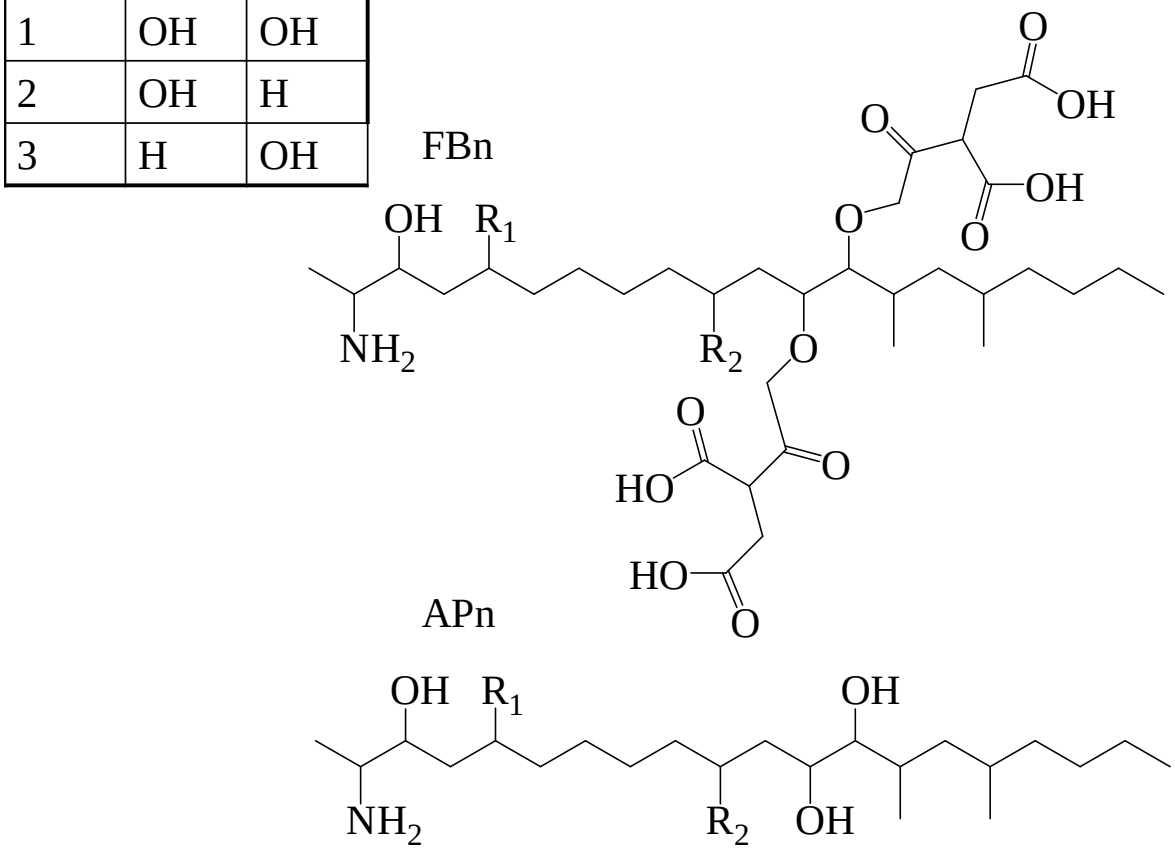

Figure 4.7. Structures of fumonisins (FBn) and aminopentols (APn).

Liquid Chromatography Electrospray Tandem Mass Spectrometry of FBn and APn

All samples were analyzed by a Perkin-Elmer API3000 Triple Quadrupole Mass Spectrometer with a Perkin-Elmer Series 200 autosampler and binary HPLC system attached to the ESI source.

Fragmentation of fumonisins and their aminopentol (AP) derivatives are dependent on dehydration and cleavage of the tricarballylic acid (TCA) moieties. In all cases all TCA are cleaved and (n-1) dehydrations occur (i.e. FB1 loses both TCA and 2 of 3 hydroxyls) (Figure 4.8).

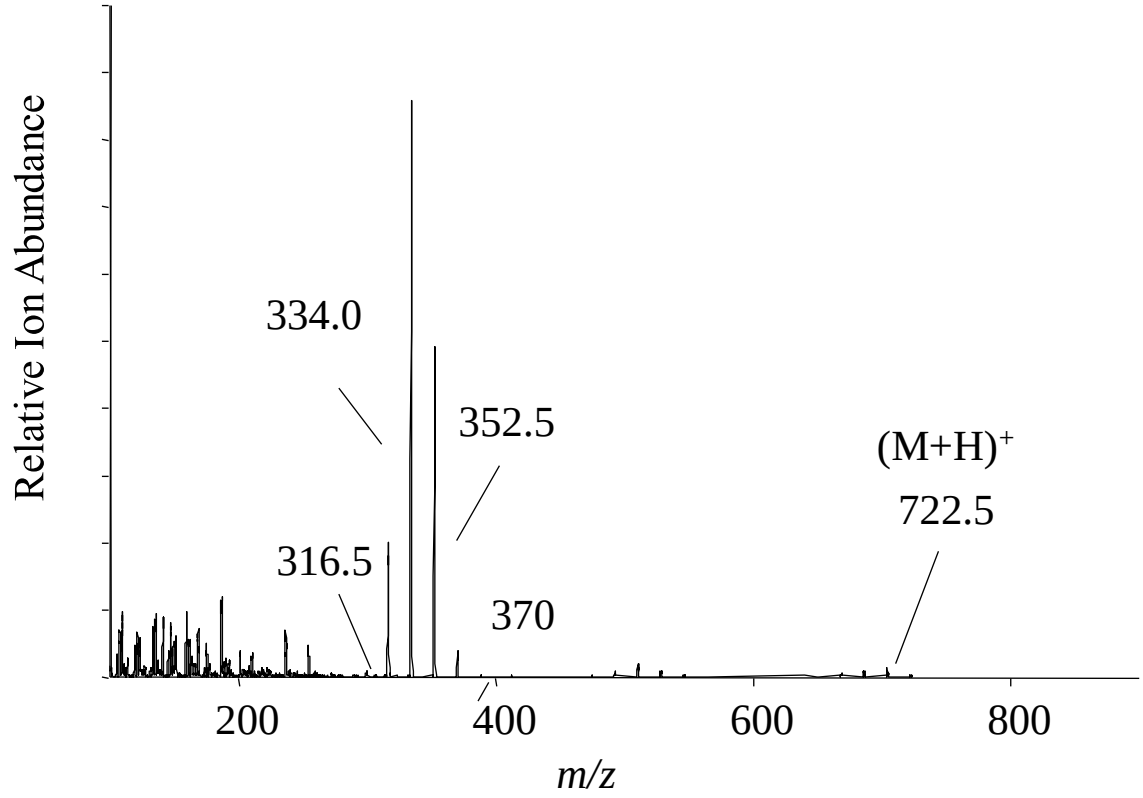

Figure 4.8. Product ion scan of FB1 (*m/z* 722.6) at 60 eV.

Table 4.1 Ion source and CID settings for FB1-3 and AP1-3 API 3000.

Compound	Precursor ion *m/z*	Product ion *m/z*	Declustering Potential (eV)	Focusing Potential (eV)	Collision Energy (eV)
FB1	722.4	334.3	70	300	45
FB2	706.4	336.2	70	300	45
FB3	706.4	336.2	70	300	45
AP1	406.4	334.3	45	100	32.5
AP2	390.2	336.2	45	100	32.5
AP3	390.2	336.2	45	100	32.5

LC separation

FBn/APn compounds were separated on a binary LC system Mobile Phase A (69:30:1) (v/v/v) Water:Methanol:Acetic Acid with 5mM Ammonium Acetate, and Mobile Phase B (99:1) (v/v) Methanol:Acetic Acid with 5mM Ammonium Acetate (Figure 4.11). The column used was a Supelco 2.1 x 50 mm (5 micron particles) C18 column with an initial solvent system of 80:20 (A:B). This was held for 1.0 min, followed by a gradient to 60% B over 3.0 min, followed by a 0.5 min linear gradient to 100 % B. This 100% condition was held for 0.5 minutes. Ion source temperature was set to 350°C

because of partial decomposition of FB to AP species in the source at higher temperatures.

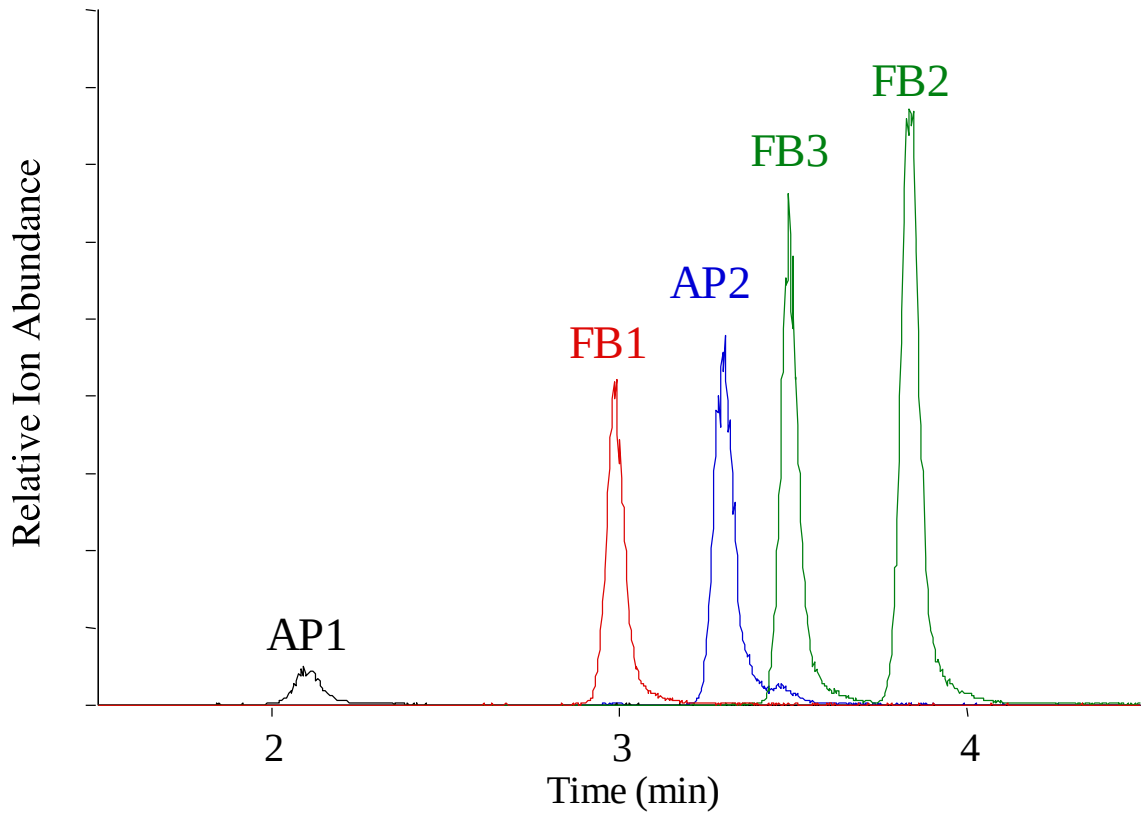

Figure 4.9. Reverse phase LC-MS/MS of FB1-3/AP1-2 standards.

The amino-acyl AP1 derivatives were analyzed using a Supelco 5μm id C-16 Amide column (Figure 4.10). The initial condition of 100% A is held for 2 minutes, and then followed by a 5 minute gradient to 100 % B. The 100 % B condition was held for 8 minutes prior to a 2 min re-equilibration at initial conditions.

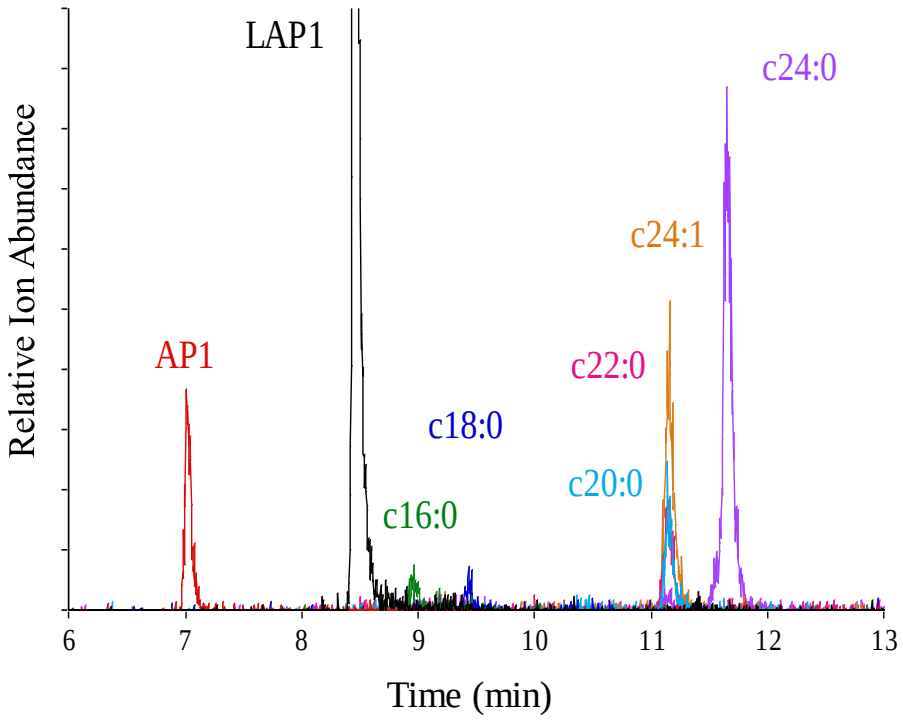

Figure 4.10. Reverse phase LC separation of N-acyl AP1.

Rat injection experiments

Rats were given intraperitoneal injections by collaborators with 0, 52, 115, and 230 µg/day of AP1 (control, low, medium, and high dose respectively). Liver tissue had a high affinity for C24:1 and C24:0 N-acylations, although C16:0, C18:0, C20, and C22:0 species were also observed (Figure 4.11). Samples were extracted using the extraction method from chapter 2 after homogenizing the tissues in PBS. Samples were used as a dry weight of 50-200 mg and extacted to a 10% homogenate solution.

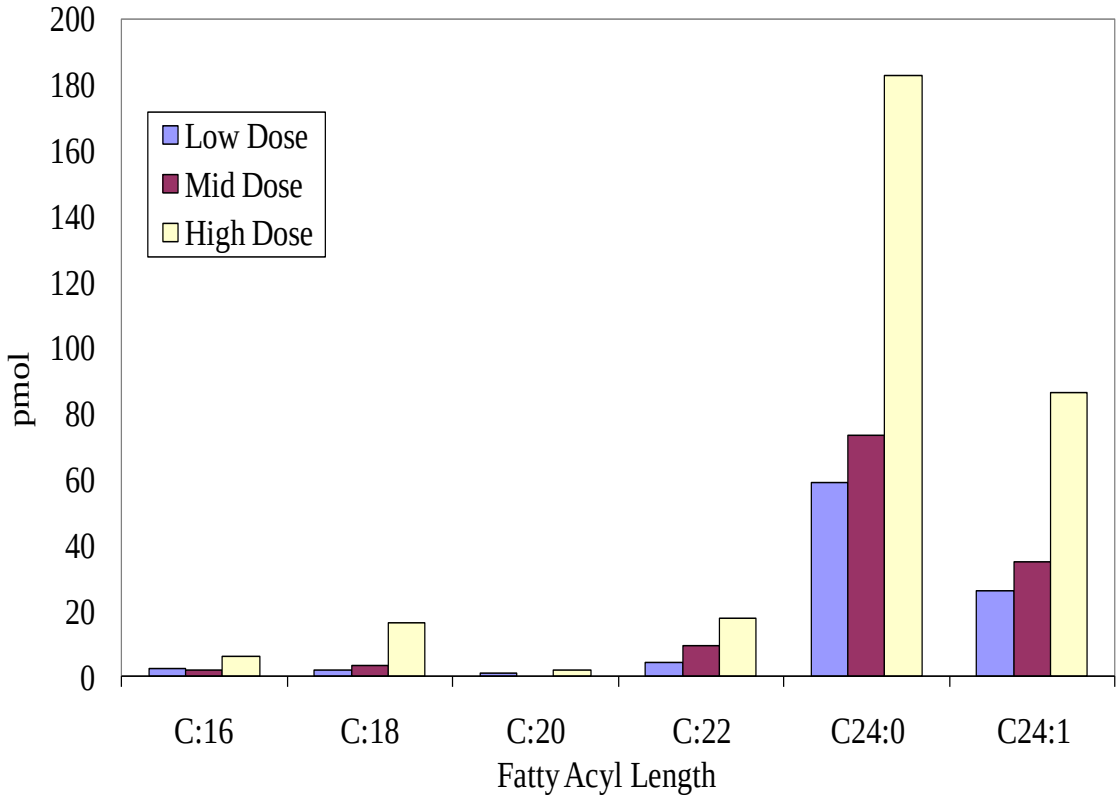

Figure 4.11 N-acyl AP1 composition in rat liver. Rats were injected over 5 days with 0, 52, 115, or 230 µg/day.

E. **Imaging MALDI Mass Spectrometry Using an Oscillating Capillary Nebulizer Matrix Coating System and Its Application to Analysis of Lipids in Brain from a Mouse Model of Tay-Sachs/Sandhoff Disease**
Chen, Y.; Allegood, J.; Liu, Y.; Wang, E.; Cachon-Gonzalez, B.; Cox, T. M.; Merrill, A. H., Jr.; Sullards, M. C. Anal. Chem.; 2008; ASAP Article

Abstract

The quality of tissue imaging by matrix-assisted laser desorption/ionization mass spectrometry (MALDI-MS) depends on the effectiveness of the matrix deposition, especially for lipids that may dissolve in the solvent used for the matrix application. This

article describes the use of an oscillating capillary nebulizer (OCN) to spray small droplets of matrix aerosol onto the sample surface for improved matrix homogeneity, reduced crystal size, and controlled solvent effects. This system was then applied to the analysis of histological slices of brains from mice with homozygous disruption of the hexb gene ($hexb^{-/-}$), a model of Tay-Sachs and Sandhoff disease, versus the functionally normal heterozygote ($hexb^{+/-}$) by imaging MALDI-MS. This allowed profiling and localization of many different lipid species, and of particular interest, ganglioside GM2, asialo-GM2 (GA2), and sulfatides (ST). The presence of these compounds was confirmed by analysis of brain extracts using electrospray ionization in conjunction with tandem mass spectrometry (MS/MS). The major fatty acid of the ceramide backbone of both GM2 and GA2 was identified as stearic acid (18:0) versus nervonic acid (24:1) for ST by both tissue-imaging MS and ESI-MS/MS. GM2 and GA2 were highly elevated in $hexb^{-/-}$ and were both localized in the granular cell region of the cerebellum. ST, however, was localized mainly in myelinated fiber (white matter) region of the cerebellum as well as in the brain stem with a relatively uniform distribution and had similar relative signal intensity for both $hexb^{+/-}$ and $hexb^{-/-}$ brain. It was also observed that there were distinct localizations for numerous other lipid subclasses; hence, imaging MALDI-MS could be used for "lipidomic" studies. These results illustrate the usefulness of tissue-imaging MALDI-MS with matrix deposition by OCN for histologic comparison of lipids in tissues such as brains from this mouse model of Tay-Sachs and Sandhoff disease.

MS, MS/MS, and MS/MS/MS

Mouse brains were homogenized (10 mg/ml) in 10 mM potassium phosphate buffer (pH 7.4) on ice. The homogenate was extracted via established methods[201]. The

acidic glycolipids recovered by batch elution from a DEAE-column, then analyzed by ESI-MS/MS or ESI-MS^3.

The samples were re-suspended in 1.0 ml of MeOH and analyzed by syringe infusion (0.6 mL/h) into an API 4000 QTrap mass spectrometer. Acidic gangliosides and sulfatides were examined in negative ion mode, while neutral glycosphingolipids were examined in positive ion mode.

Sulfatides fragment via cleavage and charge retention by their sulfate to yield a primary product ion of *m/z* 96.9. Precursor ion scans for *m/z* 96.9 were used to determine the potential N-acyl chain length subspecies in each sample. These scans were performed with declustering potential (DP) set to -220 eV and collision energies ranging from -100-120 eV. Once individual sulfatide subspecies were identified, ionization conditions were optimized for each and enhanced product ion (EPI) scans were performed (fragmentation was performed by excitation ion trap as opposed to collisionally induced dissociation in Q2). EPI scans were performed with Q0 trapping set to "on", a linear ion trap fill time of 100 ms, and a scan rate of 1000 amu/s. (Figure 4.12).

Acidic gangliosides fragment via cleavage of their sialic acids as well as other glycan-constituents. Collisionally induced fragmentation yields a product ion of *m/z* 290.1, which is representative of the sialic acid moiety. Precursor ion scans for *m/z* 290.1 were used to identify the potential N-acyl chain length subspecies within each family of acidic gangliosides (i.e. GM1, GD1, GT1). These scans were performed with declustering potential set to -70-100 eV. The lower DP was required to reduce in-source fragmentation of species having multiple sialic acid residues. Collision energies ranged from -55-75 eV with lower collision energies used for species having increasing numbers

of sialic acid residues because of the lability of these molecules toward fragmentation. Once individual ganglioside subspecies were identified, ionization conditions were optimized for each and EPI scans were performed. EPI scans were performed with Q0 trapping set to "on", a linear ion trap fill time of 100 ms, and a scan rate of 1000 amu/s. These scans were used to structurally identify the ganglioside species by analyzing the carbohydrate cleavages for each species (Figure 4.13A). MS^3 scans were also performed with Q1 resolution set to "open", Q0 trapping set to "on", a linear ion trap fill time of 100 ms, and a scan rate of 1000 amu/s. The MS^2 product ion picked in all cases corresponded to the ceramide portion of each ganglioside. These were then analyzed for sphingoid base and fatty acid composition(Figure 4.13B).

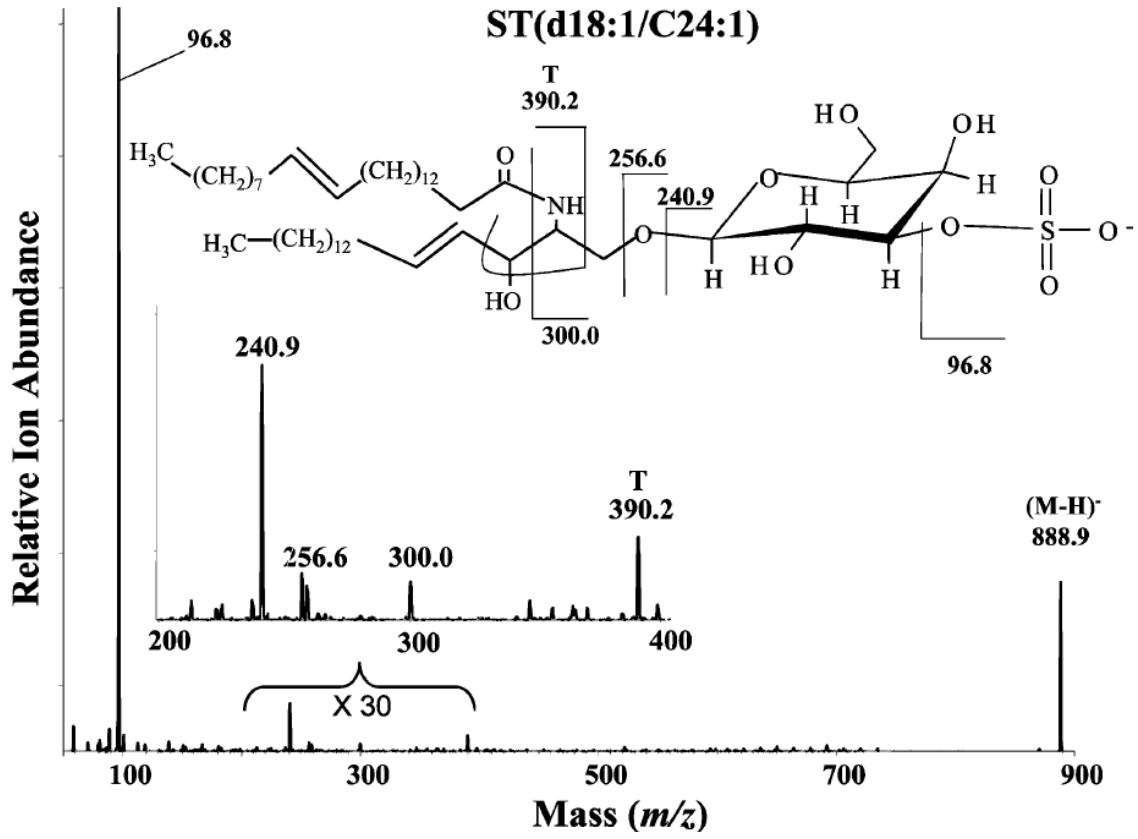

Figure 4.12 ESI-MS/MS of d18:1/C24:1 Sulfatide.

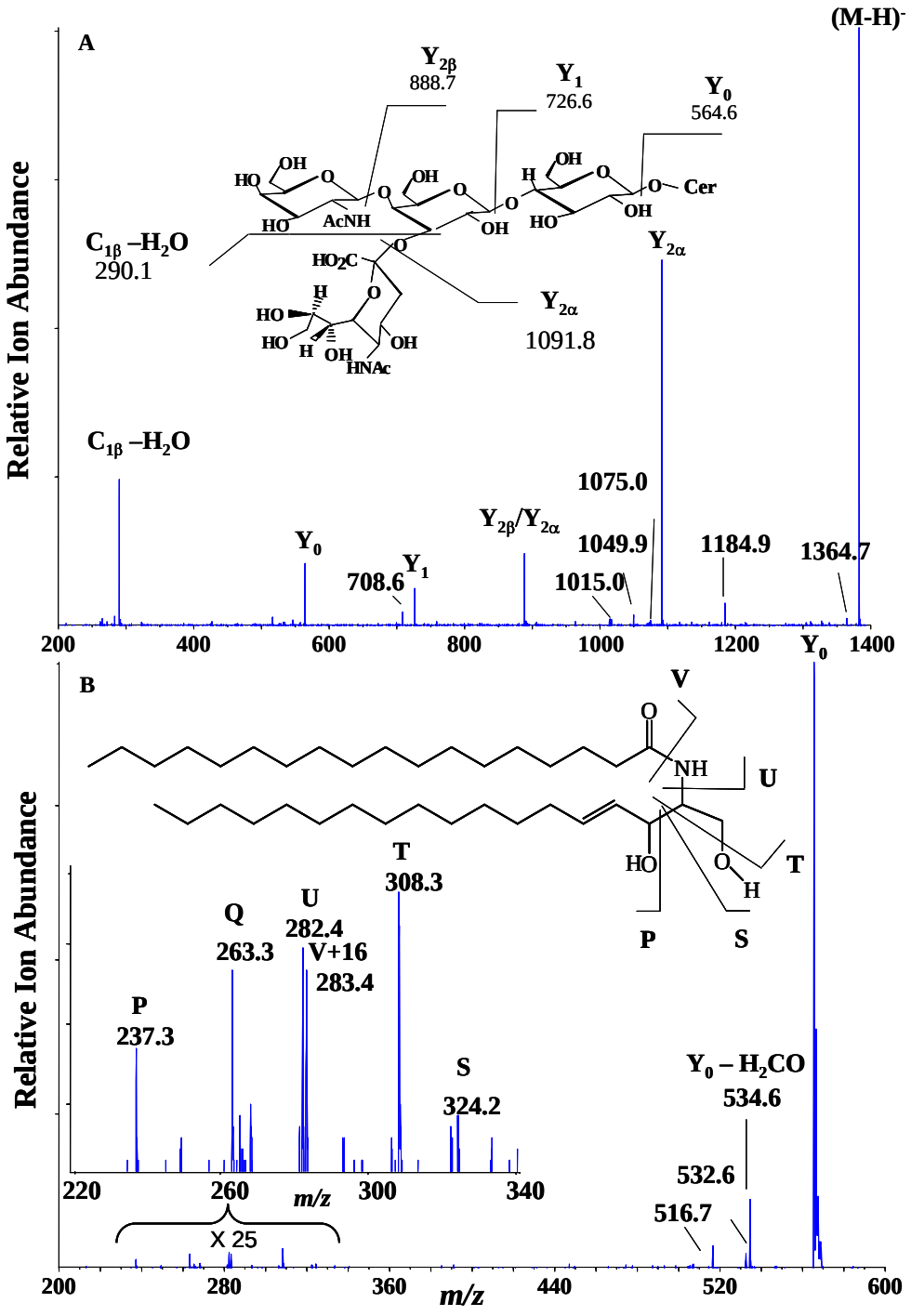

Figure 4.13 (A) ESI-MS/MS spectrum of m/z 1383 and (B) ESI-MS3 spectrum of the 1383/564 transition.

Neutral glycosphingolipids were analyzed in positive ion mode as both $(M+H)^+$ and $(M+Na)^+$ species (Figure 4.14). Neutral gangliosides fragment via cleavage of carbohydrate groups. Due to these groups mainly consisting of hexose and N-acetyl-hexosamine in these samples, potential subspecies were identified via neutral loss scans for hexose and N-acetyl-hexosamine loss (*m/z* 162 and 203 respectively). EPI scans were performed with Q0 trapping set to "on", a linear ion trap fill time of 100 ms, and a scan rate of 1000 amu/s. These scans were used to structurally identify the ganglioside species by analyzing the carbohydrate cleavages for each species. MS^3 scans were also performed with Q1 resolution set to "open", Q0 trapping set to "on", a linear ion trap fill time of 100 ms, and a scan rate of 1000 amu/s. The MS^2 product ion picked in all cases corresponded to the ceramide portion of each ganglioside. These were then analyzed for sphingoid base and fatty acid composition.

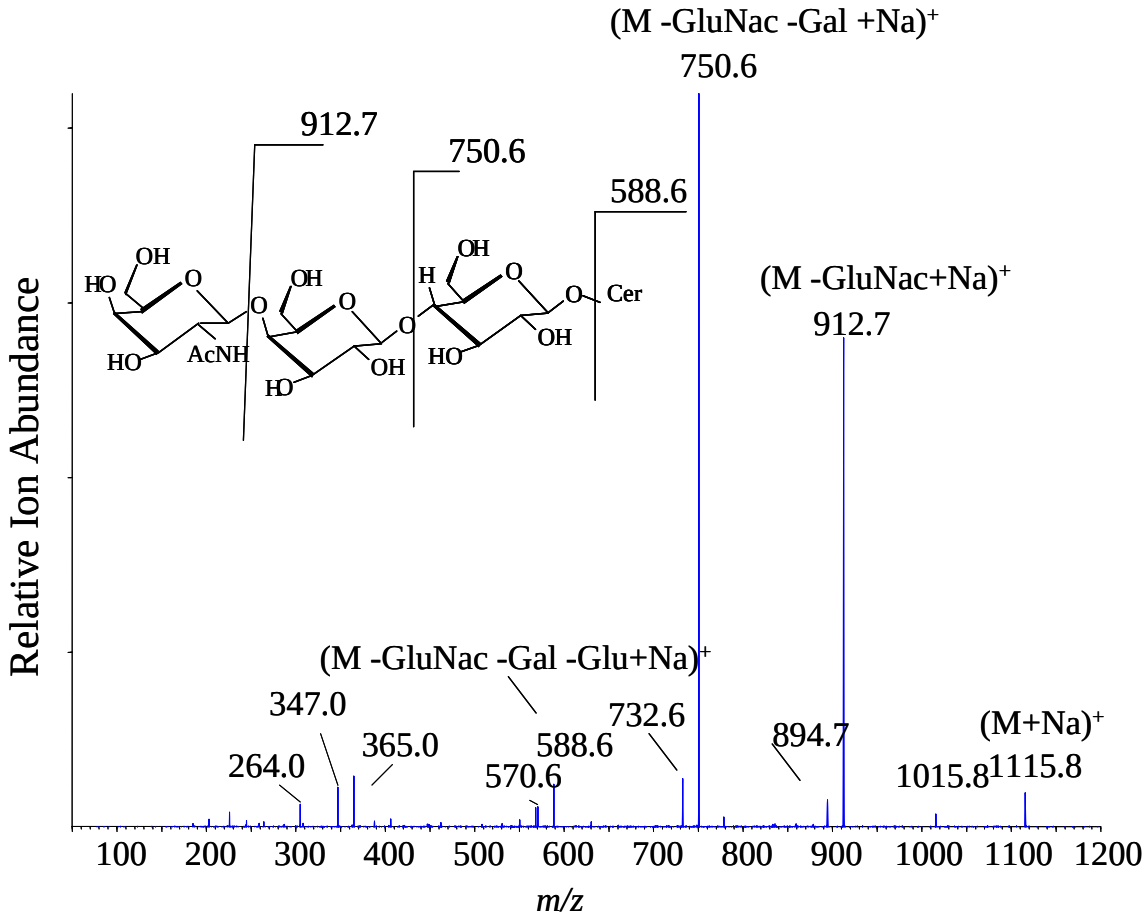

Figure 4.14. ESI-MS/MS spectrum of GA2 (*m/z* 1115.8).

CHAPTER 5

Perspectives for the future

Initially described and named in 1884 by J.L.W. Thudichum[1], sphingolipids are now known to mediate many important cellular processes, such as apoptosis, differentiation, and chemotaxis[202-204]. The structural diversity of SL has been established by numerous chromatographic separation techniques, including TLC and HPLC. Mass spectrometry provides many advantages in the detection of SL, these include: sensitivity, specificity, and structural information (MS/MS). An additional advantage of MS and MS/MS is the ability to detect or quantitate multiple analytes in a single sample. This allows multi-component analysis and the extensive metabolic interconversion of SL can be monitored. Resolution with TLC and HPLC before MS or MS/MS analysis provides an additional criterion (relative mobility or retention time) for identification. It also allows differentiation of isobaric and isomeric species while reducing ionization suppression, which may dramatically effect subsequent quantitation.

Methodologies which employ the strictest analytical standards for detection and quantitation will continue to be explored as newer instrumentation and techniques becomes available. Comparisons of pre-existing ionization and fragmentation techniques, such as evaluating the behavior of SL in triple quadrupole and quadrupole linear ion trap mass spectrometers will be required. Developing methodologies such as ion mobility, tissue imaging, and nano-scale separations hold promise for further gains in separations, localizations, and sensitivity in the analysis of sphingolipids.

Stable isotopic labeling will remain a valuable technique for tracking metabolomic changes within biological samples; however, the field must explore localization of sphingolipids because macromolecular complexes and substrate availability will elucidate cellular behavior and aid in the explanation of variance in cellular SL composition. To accomplish these goals continued expanse in the interaction between mass spectrometrists and biologists will further the understanding of the sphingolipidome.

In spite of the last century's advances in the detection, structural elucidation, and quantitation of SL, important challenges remain unsolved. The numerous roles of GSL, the most structurally elaborate sphingolipids, are being uncovered by many groups. Stable isotopes are being used to trace SL metabolic flux, and at least one mathematical model of this flux has also been developed [205]. Connections between SL and non-SL signal transduction cascades are being reported[206]. However, the location, timing, and regulation of changes in SL metabolic flux (the status of the sphingolipidome) remain among the fields of study wherein the analytical tools described by this thesis are indispensable.

APPENDIX A

IONIZATION AND FRAGMENTATION CONDITIONS FOR SPHINGOLIPIDS

Table A.1. API 3000 Mass Spectrometer Settings for Long Chain Bases and Phosphates and Linear Regressions for 0.5 pmol to 1 nmol

	Precursor ion *m/z*	Product ion *m/z*	DP (V)	FP(V)	CE (V)	R^2
d17:1 So	286.4	250.3	30	180	28	0.996
d17:0 Sa	288.4	252.4	30	180	28	0.993
d18:1 So	300.4	264.4	30	180	35	0.997
d18:0 Sa	302.4	266.4	30	180	35	0.997
d17:1 S1P	366.4	250.3	30	180	30	0.999
d17:0 Sa1P	368.4	252.4	30	180	30	0.992
d18:1 S1P	380.4	264.4	30	180	35	0.994
d18:0 Sa1P	382.4	266.4	30	180	35	0.991

Table A.2. ABI 4000 Mass Spectrometer Settings for Long Chain Bases and Phosphates and Linear Regressions for 0.5 pmol to 1 nmol

	Precursor ion *m/z*	Product ion *m/z*	DP (V)	CE(V)	CXP (V)	R^2
d17:1 So	286.4	268.3	40	15	15	0.999
d17:0 Sa	288.4	60.0	50	45	9	0.995
d18:1 So	300.4	282.4	40	21	16	0.996
d18:0 Sa	302.4	60.0	50	50	10	0.994
d17:1 S1P	366.4	250.3	50	23	16	0.994
d17:0 Sa1P	368.4	252.2	50	25	16	0.997
d18:1 S1P	380.4	264.4	50	25	16	0.993
d18:0 Sa1P	382.4	266.4	50	25	16	0.998

Table A.3. API 3000 Mass Spectrometer Settings for Complex Sphingolipids and Linear Regressions for 0.5 pmol to 1 nmol

	N-Acyl	Precursor ion *m/z*	Product ion *m/z*	DP (V)	FP(V)	CE (V)	R^2
Cer (d18:1)							
	C12:0	486.6	264.4	40	220	35	0.996
	C16:0	538.7	264.4	40	220	40	0.997
	C18:0	566.7	264.4	40	220	42.5	0.999
	C24:1	648.9	264.4	40	220	45	0.998
	C24:0	650.9	264.4	40	220	45	0.997
	C25:0	664.9	264.4	40	220	47.5	0.999
DHCer (d18:0)							
	C16:0	540.7	266.4	40	220	40	0.996
	C18:0	568.7	266.4	40	220	42.5	0.992
	C24:1	650.9	266.4	40	220	45	0.997
	C24:0	652.9	266.4	40	220	45	0.996
GlcCer (d18:1)							
	C12:0	644.6	264.4	50	300	45	0.991
	C16:0	700.7	264.4	50	300	50	0.994
	C18:0	728.7	264.4	50	300	52.5	0.996
	C24:1	810.9	264.4	50	300	60	0.990
DHGlcCer (d18:0)							
	C12:0	646.6	266.4	50	300	45	0.992
	C16:0	702.7	266.4	50	300	50	0.993
	C18:0	730.7	266.4	50	300	52.5	0.997
	C24:0	814.9	266.4	50	300	60	0.994
SM (d18:1)							
	C12:0	647.7	184.4	20	200	40	0.999
	C18:0	731.8	184.4	20	200	45	0.999
	C24:0	815.9	184.4	20	200	50	0.998
DHSM (d18:0)							
	C12:0	649.7	184.4	20	200	40	0.998
	C18:0	733.8	184.4	20	200	45	0.997

	C24:0	817.9	184.4	20	200	50	0.998
Cer1P (d18:1) (pos)							
	C12:0	562.6	264.4	40	220	45	0.992
	C16:0	618.7	264.4	40	220	50	0.990
	C24:0	730.9	264.4	40	220	55	0.997
DHCer1P (d18:0) (pos)							
	C16:0	564.6	266.4	40	220	50	0.994
	C24:0	732.9	266.4	40	220	55	0.996
Cer1P (d18:1) (neg)							
	C12:0	560.6	78.9	-35	-180	70	0.993
	C16:0	616.7	78.9	-35	-180	75	0.991
	C24:0	728.9	78.9	-35	-180	80	0.995
DHCer1P (d18:0) (neg)							
	C16:0	562.6	78.9	-35	-180	75	0.999
	C24:0	730.9	78.9	-35	-180	80	0.992
Sulfatide (d18:1)							
	C12:0	722.4	96.9	-55	-140	110	0.999
	C16:0	778.6	96.6	-55	-140	115	0.993
	C24:0	890.9	96.9	-55	-140	120	0.995
LacCer (d18:1)							
	C12:0	806.6	264.4	40	220	50	0.991
	C16:0	862.7	264.4	40	220	55	0.995
	C24:0	974.9	264.4	40	220	60	0.989

Table A.4. ABI 4000 Mass Spectrometer Settings for Complex Sphingolipids and Linear Regressions for 0.5 pmol to 1 nmol

	N-Acyl	Q1 *m/z*	Q3 *m/z*	DP (V)	CE(V)	CXP (V)	R^2
Cer (d18:1)							
	C12:0	486.6	264.4	55	35	15	0.994
	C16:0	538.7	264.4	55	37.5	15	0.997
	C18:0	566.7	264.4	55	37.5	15	0.992
	C24:1	648.9	264.4	55	42.5	15	0.996
	C24:0	650.9	264.4	55	42.5	15	0.997
	C25:0	664.9	264.4	55	45	15	0.997
DHCer (d18:0)							
	C16:0	540.7	266.4	55	37.5	15	0.990
	C18:0	568.7	266.4	55	37.5	15	0.995
	C24:1	650.9	266.4	55	42.5	15	0.989
	C24:0	652.9	266.4	55	42.5	15	0.992
GlcCer (d18:1)							
	C12:0	644.6	264.4	35	42.5	15	0.996
	C16:0	700.7	264.4	35	45	15	0.995
	C18:0	728.7	264.4	35	47.5	15	0.995
	C24:1	810.9	264.4	35	55	15	0.987
DHGlcCer (d18:0)							
	C12:0	646.6	266.4	35	42.5	15	0.995
	C16:0	702.7	266.4	35	45	15	0.990
	C18:0	730.7	266.4	35	47.5	15	0.998
	C24:0	814.9	266.4	35	55	15	0.986
SM (d18:1)							
	C12:0	647.7	184.4	45	40	10	0.997
	C18:0	731.8	184.4	45	45	10	0.996
	C24:0	815.9	184.4	45	50	10	0.999
DHSM (d18:0)							
	C12:0	649.7	184.4	45	40	10	0.999
	C18:0	733.8	184.4	45	45	10	0.994
	C24:0	817.9	184.4	45	50	10	0.999

Cer1P (d18:1) (pos)							
	C12:0	562.6	264.4	40	45	15	0.996
	C16:0	618.7	264.4	40	47.5	15	0.993
	C24:0	730.9	264.4	40	52.5	15	0.995
DHCer1P (d18:0) (pos)							
	C16:0	564.6	266.4	40	47.5	15	0.992
	C24:0	732.9	266.4	40	52.5	15	0.985
Cer1P (d18:1) (neg)							
	C12:0	560.6	78.9	-120	-60	-15	0.996
	C16:0	616.7	78.9	-120	-65	-15	0.993
	C24:0	728.9	78.9	-120	-72.5	-15	0.997
DHCer1P (d18:0) (neg)							
	C16:0	562.6	78.9	-120	-65	-15	0.998
	C24:0	730.9	78.9	-120	-72.5	-15	0.995
Sulfatide (d18:1)							
	C12:0	722.4	96.9	-220	-100	-15	0.994
	C16:0	778.6	96.6	-220	-110	-15	0.999
	C24:0	890.9	96.9	-220	-125	-15	0.995
LacCer (d18:1)							
	C12:0	806.6	264.4	45	55	15	0.990
	C16:0	862.7	264.4	45	60	15	0.987
	C24:0	974.9	264.4	45	70	15	0.986

APPENDIX B

FRAGMENTATION MECHANISM FOR SPHINGOLIPIDS

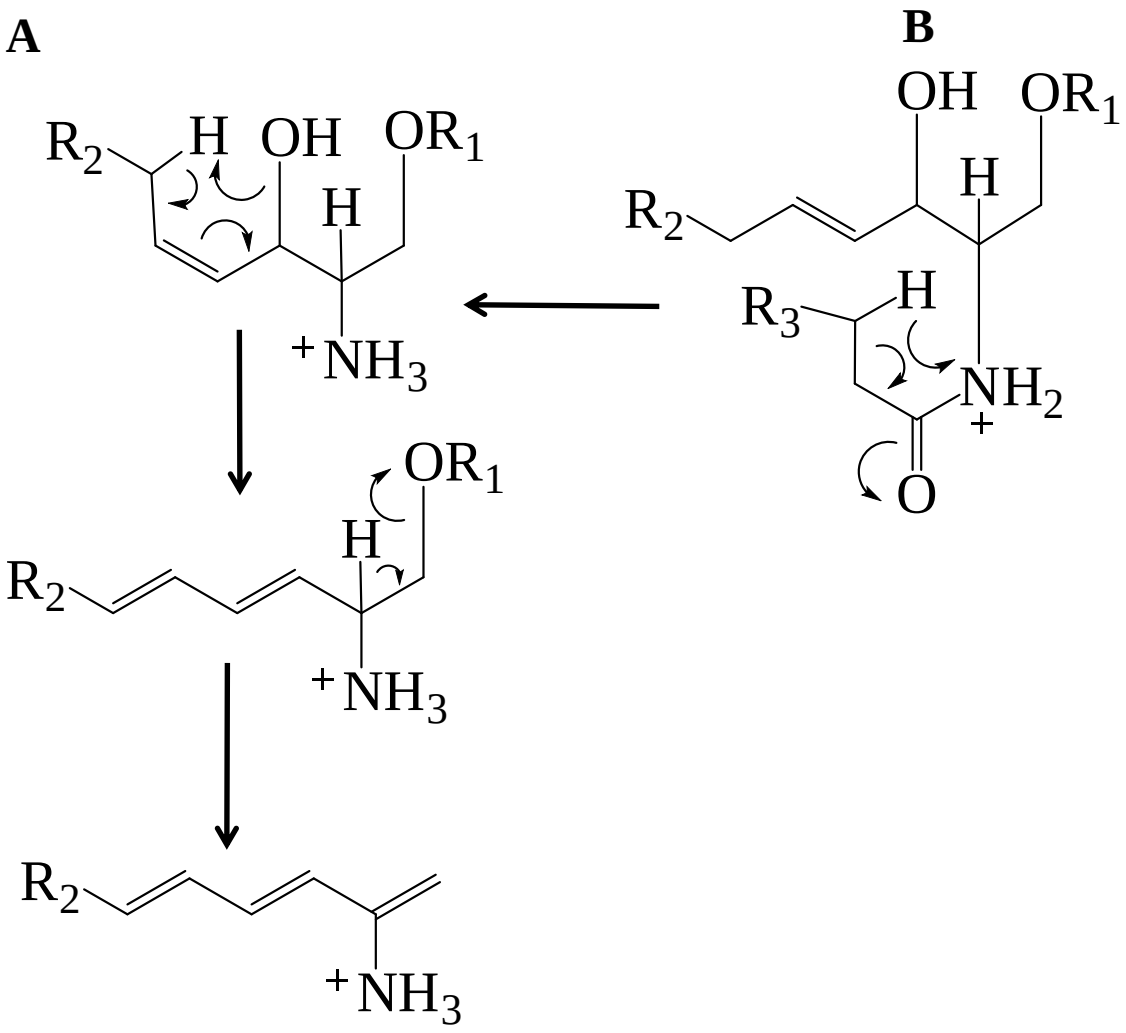

Figure A2.1 Fragmentation Mechanism for A) sphingoid bases and lysosphingolipids and B) for N-acylated species.

REFERENCES

1. Thudichum, J. L. W., *A Treatise on the Chemical Constitution of Brain*. Bailliere, Tindall, and Cox: London, 1884.

2. Zheng, W.; Kollmeyer, J.; Symolon, H.; Momin, A.; Munter, E.; Wang, E.; Kelly, S.; Allegood, J. C.; Liu, Y.; Peng, Q.; Ramaraju, H.; Sullards, M. C.; Cabot, M.; Merrill, A. H., Jr., Ceramides and other bioactive sphingolipid backbones in health and disease: lipidomic analysis, metabolism and roles in membrane structure, dynamics, signaling and autophagy. *Biochim Biophys Acta* **2006,** 1758, (12), 1864-84.

3. Milstien, S.; Gude, D.; Spiegel, S., Sphingosine 1-phosphate in neural signalling and function. *Acta Paediatr Suppl* **2007,** 96, (455), 40-3.

4. Hakomori, S. I., Structure and function of glycosphingolipids and sphingolipids: Recollections and future trends. *Biochim Biophys Acta* **2007**.

5. Donati, C.; Cencetti, F.; Nincheri, P.; Bernacchioni, C.; Brunelli, S.; Clementi, E.; Cossu, G.; Bruni, P., Sphingosine 1-phosphate mediates proliferation and survival of mesoangioblasts. *Stem Cells* **2007,** 25, (7), 1713-9.

6. Toman, R. E.; Spiegel, S.; Faden, A. I., Role of ceramide in neuronal cell death and differentiation. *J Neurotrauma* **2000,** 17, (10), 891-8.

7. Sun, W.; Xu, R.; Hu, W.; Jin, J.; Crellin, H. A.; Bielawski, J.; Szulc, Z. M.; Thiers, B. H.; Obeid, L. M.; Mao, C., Upregulation of the human alkaline ceramidase 1 and acid ceramidase mediates calcium-induced differentiation of epidermal keratinocytes. *J Invest Dermatol* **2008,** 128, (2), 389-97.

8. Hait, N. C.; Oskeritzian, C. A.; Paugh, S. W.; Milstien, S.; Spiegel, S., Sphingosine kinases, sphingosine 1-phosphate, apoptosis and diseases. *Biochim Biophys Acta* **2006,** 1758, (12), 2016-26.

9. Morales, A.; Lee, H.; Goni, F. M.; Kolesnick, R.; Fernandez-Checa, J. C., Sphingolipids and cell death. *Apoptosis* **2007,** 12, (5), 923-39.

10. Ichi, I.; Nakahara, K.; Miyashita, Y.; Hidaka, A.; Kutsukake, S.; Inoue, K.; Maruyama, T.; Miwa, Y.; Harada-Shiba, M.; Tsushima, M.; Kojo, S., Association of ceramides in human plasma with risk factors of atherosclerosis. *Lipids* **2006,** 41, (9), 859-63.

11. Glaros, E. N.; Kim, W. S.; Wu, B. J.; Suarna, C.; Quinn, C. M.; Rye, K. A.; Stocker, R.; Jessup, W.; Garner, B., Inhibition of atherosclerosis by the serine palmitoyl

transferase inhibitor myriocin is associated with reduced plasma glycosphingolipid concentration. *Biochem Pharmacol* **2007,** 73, (9), 1340-6.

12. Bismuth, J.; Lin, P.; Yao, Q.; Chen, C., Ceramide: a common pathway for atherosclerosis? *Atherosclerosis* **2008,** 196, (2), 497-504.

13. Liu, Y.; McCarthy, J.; Ladisch, S., Membrane ganglioside enrichment lowers the threshold for vascular endothelial cell angiogenic signaling. *Cancer Res* **2006,** 66, (21), 10408-14.

14. Dyatlovitskaya, E. V.; Kandyba, A. G., Sphingolipids in tumor metastases and angiogenesis. *Biochemistry (Mosc)* **2006,** 71, (4), 347-53.

15. Delves, G. H.; Stewart, A. B.; Cooper, A. J.; Lwaleed, B. A., Prostasomes, angiogenesis, and tissue factor. *Semin Thromb Hemost* **2007,** 33, (1), 75-9.

16. Summers, S. A., Ceramides in insulin resistance and lipotoxicity. *Prog Lipid Res* **2006,** 45, (1), 42-72.

17. Kabayama, K.; Sato, T.; Saito, K.; Loberto, N.; Prinetti, A.; Sonnino, S.; Kinjo, M.; Igarashi, Y.; Inokuchi, J., Dissociation of the insulin receptor and caveolin-1 complex by ganglioside GM3 in the state of insulin resistance. *Proc Natl Acad Sci U S A* **2007,** 104, (34), 13678-83.

18. Holland, W. L.; Brozinick, J. T.; Wang, L. P.; Hawkins, E. D.; Sargent, K. M.; Liu, Y.; Narra, K.; Hoehn, K. L.; Knotts, T. A.; Siesky, A.; Nelson, D. H.; Karathanasis, S. K.; Fontenot, G. K.; Birnbaum, M. J.; Summers, S. A., Inhibition of ceramide synthesis ameliorates glucocorticoid-, saturated-fat-, and obesity-induced insulin resistance. *Cell Metab* **2007,** 5, (3), 167-79.

19. Pickersgill, L.; Litherland, G. J.; Greenberg, A. S.; Walker, M.; Yeaman, S. J., Key role for ceramides in mediating insulin resistance in human muscle cells. *J Biol Chem* **2007,** 282, (17), 12583-9.

20. Lamour, N. F.; Chalfant, C. E., Ceramide-1-phosphate: the "missing" link in eicosanoid biosynthesis and inflammation. *Mol Interv* **2005,** 5, (6), 358-67.

21. El Alwani, M.; Wu, B. X.; Obeid, L. M.; Hannun, Y. A., Bioactive sphingolipids in the modulation of the inflammatory response. *Pharmacol Ther* **2006,** 112, (1), 171-83.

22. Won, J. S.; Singh, A. K.; Singh, I., Lactosylceramide: a lipid second messenger in neuroinflammatory disease. *J Neurochem* **2007,** 103 Suppl 1, 180-91.

23. Masini, E.; Giannini, L.; Nistri, S.; Cinci, L.; Mastroianni, R.; Xu, W.; Comhair, S. A.; Li, D.; Cuzzocrea, S.; Matuschak, G. M.; Salvemini, D., Ceramide: a key signaling

molecule in a Guinea pig model of allergic asthmatic response and airway inflammation. *J Pharmacol Exp Ther* **2008,** 324, (2), 548-57.

24. Bieberich, E., Smart Drugs for Smarter Stem Cells: Making SENSe (Sphingolipid-Enhanced Neural Stem Cells) of Ceramide. *Neurosignals* **2008,** 16, (2-3), 124-39.

25. McCampbell, A.; Truong, D.; Broom, D. C.; Allchorne, A.; Gable, K.; Cutler, R. G.; Mattson, M. P.; Woolf, C. J.; Frosch, M. P.; Harmon, J. M.; Dunn, T. M.; Brown, R. H., Jr., Mutant SPTLC1 dominantly inhibits serine palmitoyltransferase activity in vivo and confers an age-dependent neuropathy. *Hum Mol Genet* **2005,** 14, (22), 3507-21.

26. Teng, C.; Dong, H.; Shi, L.; Deng, Y.; Mu, J.; Zhang, J.; Yang, X.; Zuo, J., Serine palmitoyltransferase, a key enzyme for de novo synthesis of sphingolipids, is essential for male gametophyte development in Arabidopsis. *Plant Physiol* **2008**.

27. Dietrich, C. R.; Han, G.; Chen, M.; Berg, R. H.; Dunn, T. M.; Cahoon, E. B., Loss-of-Function Mutations and Inducible RNAi Suppression of Arabidopsis LCB2 Genes Reveal the Critical Role of Sphingolipids in Gametophytic and Sporophytic Cell Viability. *Plant J* **2008**.

28. Hanada, K.; Nishijima, M.; Fujita, T.; Kobayashi, S., Specificity of inhibitors of serine palmitoyltransferase (SPT), a key enzyme in sphingolipid biosynthesis, in intact cells. A novel evaluation system using an SPT-defective mammalian cell mutant. *Biochem Pharmacol* **2000,** 59, (10), 1211-6.

29. Blank, N.; Schiller, M.; Gabler, C.; Kalden, J. R.; Lorenz, H. M., Inhibition of sphingolipid synthesis impairs cellular activation, cytokine production and proliferation in human lymphocytes. *Biochem Pharmacol* **2005,** 71, (1-2), 126-35.

30. Vesper, H.; Schmelz, E. M.; Nikolova-Karakashian, M. N.; Dillehay, D. L.; Lynch, D. V.; Merrill, A. H., Jr., Sphingolipids in food and the emerging importance of sphingolipids to nutrition. *J Nutr* **1999,** 129, (7), 1239-50.

31. Sugawara, T.; Kinoshita, M.; Ohnishi, M.; Nagata, J.; Saito, M., Digestion of maize sphingolipids in rats and uptake of sphingadienine by Caco-2 cells. *J Nutr* **2003,** 133, (9), 2777-82.

32. Le Stunff, H.; Galve-Roperh, I.; Peterson, C.; Milstien, S.; Spiegel, S., Sphingosine-1-phosphate phosphohydrolase in regulation of sphingolipid metabolism and apoptosis. *J Cell Biol* **2002,** 158, (6), 1039-49.

33. Sigal, Y. J.; McDermott, M. I.; Morris, A. J., Integral membrane lipid phosphatases/phosphotransferases: common structure and diverse functions. *Biochem J* **2005,** 387, (Pt 2), 281-93.

34. Hung, W. C.; Chang, H. C.; Chuang, L. Y., Activation of caspase-3-like proteases in apoptosis induced by sphingosine and other long-chain bases in Hep3B hepatoma cells. *Biochem J* **1999,** 338 (Pt 1), 161-6.

35. Osawa, Y.; Banno, Y.; Nagaki, M.; Brenner, D. A.; Naiki, T.; Nozawa, Y.; Nakashima, S.; Moriwaki, H., TNF-alpha-induced sphingosine 1-phosphate inhibits apoptosis through a phosphatidylinositol 3-kinase/Akt pathway in human hepatocytes. *J Immunol* **2001,** 167, (1), 173-80.

36. Alemany, R.; van Koppen, C. J.; Danneberg, K.; Ter Braak, M.; Meyer Zu Heringdorf, D., Regulation and functional roles of sphingosine kinases. *Naunyn Schmiedebergs Arch Pharmacol* **2007,** 374, (5-6), 413-28.

37. Maceyka, M.; Sankala, H.; Hait, N. C.; Le Stunff, H.; Liu, H.; Toman, R.; Collier, C.; Zhang, M.; Satin, L. S.; Merrill, A. H., Jr.; Milstien, S.; Spiegel, S., SphK1 and SphK2, sphingosine kinase isoenzymes with opposing functions in sphingolipid metabolism. *J Biol Chem* **2005,** 280, (44), 37118-29.

38. van Echten-Deckert, G.; Herget, T., Sphingolipid metabolism in neural cells. *Biochim Biophys Acta* **2006**.

39. Hannun, Y. A.; Luberto, C.; Argraves, K. M., Enzymes of sphingolipid metabolism: from modular to integrative signaling. *Biochemistry* **2001,** 40, (16), 4893-903.

40. Smith, W. L.; Merrill, A. H., Jr., Sphingolipid metabolism and signaling minireview series. *J Biol Chem* **2002,** 277, (29), 25841-2.

41. Menaldino, D. S.; Bushnev, A.; Sun, A.; Liotta, D. C.; Symolon, H.; Desai, K.; Dillehay, D. L.; Peng, Q.; Wang, E.; Allegood, J.; Trotman-Pruett, S.; Sullards, M. C.; Merrill, A. H., Jr., Sphingoid bases and de novo ceramide synthesis: enzymes involved, pharmacology and mechanisms of action. *Pharmacol Res* **2003,** 47, (5), 373-81.

42. Chalfant, C. E.; Spiegel, S., Sphingosine 1-phosphate and ceramide 1-phosphate: expanding roles in cell signaling. *J Cell Sci* **2005,** 118, (Pt 20), 4605-12.

43. Futerman, A. H.; Hannun, Y. A., The complex life of simple sphingolipids. *EMBO Rep* **2004,** 5, (8), 777-82.

44. Sonnino, S.; Prinetti, A.; Mauri, L.; Chigorno, V.; Tettamanti, G., Dynamic and structural properties of sphingolipids as driving forces for the formation of membrane domains. *Chem Rev* **2006,** 106, (6), 2111-25.

45. Sperling, P.; Heinz, E., Plant sphingolipids: structural diversity, biosynthesis, first genes and functions. *Biochim Biophys Acta* **2003,** 1632, (1-3), 1-15.

46. Omae, F.; Miyazaki, M.; Enomoto, A.; Suzuki, M.; Suzuki, Y.; Suzuki, A., DES2 protein is responsible for phytoceramide biosynthesis in the mouse small intestine. *Biochem J* **2004,** 379, (Pt 3), 687-95.

47. Stewart, M. E.; Downing, D. T., Free sphingosines of human skin include 6-hydroxysphingosine and unusually long-chain dihydrosphingosines. *J Invest Dermatol* **1995,** 105, (4), 613-8.

48. Kyogashima, M.; Tamiya-Koizumi, K.; Ehara, T.; Li, G.; Hu, R.; Hara, A.; Aoyama, T.; Kannagi, R., Rapid demonstration of diversity of sulfatide molecular species from biological materials by MALDI-TOF MS. *Glycobiology* **2006,** 16, (8), 719-28.

49. Fyrst, H.; Herr, D. R.; Harris, G. L.; Saba, J. D., Characterization of free endogenous C14 and C16 sphingoid bases from Drosophila melanogaster. *J Lipid Res* **2004,** 45, (1), 54-62.

50. Merrill, A. H., Jr.; Hannun, Y. A.; Bell, R. M., Introduction: sphingolipids and their metabolites in cell regulation. *Adv Lipid Res* **1993,** 25, 1-24.

51. Ternes, P.; Franke, S.; Zahringer, U.; Sperling, P.; Heinz, E., Identification and characterization of a sphingolipid delta 4-desaturase family. *J Biol Chem* **2002,** 277, (28), 25512-8.

52. Sullards, M. C.; Wang, E.; Peng, Q.; Merrill, A. H., Jr., Metabolomic profiling of sphingolipids in human glioma cell lines by liquid chromatography tandem mass spectrometry. *Cell Mol Biol (Noisy-le-grand)* **2003,** 49, (5), 789-97.

53. Tani, M.; Sano, T.; Ito, M.; Igarashi, Y., Mechanisms of sphingosine and sphingosine 1-phosphate generation in human platelets. *J Lipid Res* **2005,** 46, (11), 2458-67.

54. Theilmeier, G.; Schmidt, C.; Herrmann, J.; Keul, P.; Schafers, M.; Herrgott, I.; Mersmann, J.; Larmann, J.; Hermann, S.; Stypmann, J.; Schober, O.; Hildebrand, R.; Schulz, R.; Heusch, G.; Haude, M.; von Wnuck Lipinski, K.; Herzog, C.; Schmitz, M.; Erbel, R.; Chun, J.; Levkau, B., High-density lipoproteins and their constituent, sphingosine-1-phosphate, directly protect the heart against ischemia/reperfusion injury in vivo via the S1P3 lysophospholipid receptor. *Circulation* **2006,** 114, (13), 1403-9.

55. Igarashi, J.; Miyoshi, M.; Hashimoto, T.; Kubota, Y.; Kosaka, H., Statins induce S1P1 receptors and enhance endothelial nitric oxide production in response to high-density lipoproteins. *Br J Pharmacol* **2007,** 150, (4), 470-9.

56. Reiss, U.; Oskouian, B.; Zhou, J.; Gupta, V.; Sooriyakumaran, P.; Kelly, S.; Wang, E.; Merrill, A. H., Jr.; Saba, J. D., Sphingosine-phosphate lyase enhances stress-induced ceramide generation and apoptosis. *J Biol Chem* **2004,** 279, (2), 1281-90.

57. Farwanah, H.; Wohlrab, J.; Neubert, R. H.; Raith, K., Profiling of human stratum corneum ceramides by means of normal phase LC/APCI-MS. *Anal Bioanal Chem* **2005,** 383, (4), 632-7.

58. Riebeling, C.; Allegood, J. C.; Wang, E.; Merrill, A. H., Jr.; Futerman, A. H., Two mammalian longevity assurance gene (LAG1) family members, trh1 and trh4, regulate dihydroceramide synthesis using different fatty acyl-CoA donors. *J Biol Chem* **2003,** 278, (44), 43452-9.

59. Lahiri, S.; Futerman, A. H., LASS5 is a bona fide dihydroceramide synthase that selectively utilizes palmitoyl-CoA as acyl donor. *J Biol Chem* **2005,** 280, (40), 33735-8.

60. Min, J.; Mesika, A.; Sivaguru, M.; Van Veldhoven, P. P.; Alexander, H.; Futerman, A. H.; Alexander, S., (Dihydro)ceramide synthase 1 regulated sensitivity to cisplatin is associated with the activation of p38 mitogen-activated protein kinase and is abrogated by sphingosine kinase 1. *Mol Cancer Res* **2007,** 5, (8), 801-12.

61. Geeraert, L.; Mannaerts, G. P.; van Veldhoven, P. P., Conversion of dihydroceramide into ceramide: involvement of a desaturase. *Biochem J* **1997,** 327 (Pt 1), 125-32.

62. Behne, M.; Uchida, Y.; Seki, T.; de Montellano, P. O.; Elias, P. M.; Holleran, W. M., Omega-hydroxyceramides are required for corneocyte lipid envelope (CLE) formation and normal epidermal permeability barrier function. *J Invest Dermatol* **2000,** 114, (1), 185-92.

63. Pettus, B. J.; Bielawska, A.; Subramanian, P.; Wijesinghe, D. S.; Maceyka, M.; Leslie, C. C.; Evans, J. H.; Freiberg, J.; Roddy, P.; Hannun, Y. A.; Chalfant, C. E., Ceramide 1-phosphate is a direct activator of cytosolic phospholipase A2. *J Biol Chem* **2004,** 279, (12), 11320-6.

64. Abe, A.; Shayman, J. A., Purification and characterization of 1-O-acylceramide synthase, a novel phospholipase A2 with transacylase activity. *J Biol Chem* **1998,** 273, (14), 8467-74.

65. Ito, M.; Kita, K.; Kurita, T.; Sueyoshi, N.; Izu, H., Enzymatic N-deacylation of sphingolipids. *Methods Enzymol* **2000,** 311, 297-303.

66. Van den Boom, M. A.; Groot Wassink, M.; Roelofsen, B.; Tijburg, L. B.; Op den Kamp, J. A., In vivo turnover of 1,2-dipalmitoylphosphatidylcholine and sphingomyelin in rabbit erythrocytes. *Biochim Biophys Acta* **1995,** 1258, (3), 265-71.

67. Kondoh, H.; Kanoh, H.; Ono, T., Deacylation of ceramide, triacylglycerol and phospholipids in guinea pig epidermal cells. *Biochim Biophys Acta* **1983,** 753, (1), 97-106.

68. Svennerholm, L., The Gangliosides. *J Lipid Res* **1964,** 5, 145-55.

69. Bunemann, M.; Liliom, K.; Brandts, B. K.; Pott, L.; Tseng, J. L.; Desiderio, D. M.; Sun, G.; Miller, D.; Tigyi, G., A novel membrane receptor with high affinity for lysosphingomyelin and sphingosine 1-phosphate in atrial myocytes. *Embo J* **1996,** 15, (20), 5527-34.

70. Morales, P. R.; Dillehay, D. L.; Moody, S. J.; Pallas, D. C.; Pruett, S.; Allgood, J. C.; Symolon, H.; Merrill, A. H., Safingol Toxicology After Oral Administration to TRAMP Mice: Demonstration of Safingol Uptake and Metabolism by N-Acylation and N-Methylation. *Drug and Chemical Toxicology* **2007,** 30, (3), 197 - 216.

71. Spiegel, S.; Milstien, S., Sphingosine-1-phosphate: an enigmatic signalling lipid. *Nat Rev Mol Cell Biol* **2003,** 4, (5), 397-407.

72. Hannun, Y. A.; Obeid, L. M., Principles of bioactive lipid signalling: lessons from sphingolipids. *Nat Rev Mol Cell Biol* **2008,** 9, (2), 139-50.

73. Hakomori, S., Structure, organization, and function of glycosphingolipids in membrane. *Curr Opin Hematol* **2003,** 10, (1), 16-24.

74. Bielawska, A.; Crane, H. M.; Liotta, D.; Obeid, L. M.; Hannun, Y. A., Selectivity of ceramide-mediated biology. Lack of activity of erythro-dihydroceramide. *J Biol Chem* **1993,** 268, (35), 26226-32.

75. Matsunaga, I.; Yokotani, N.; Gotoh, O.; Kusunose, E.; Yamada, M.; Ichihara, K., Molecular cloning and expression of fatty acid alpha-hydroxylase from Sphingomonas paucimobilis. *J Biol Chem* **1997,** 272, (38), 23592-6.

76. Sastry, P. S.; Kates, M., Lipid Components of Leaves. Iv. Occurence of Phytosphingosine and Dehydrophytosphingosine-Containing Glucocerebrosides. *Biochim Biophys Acta* **1964,** 84, 231-3.

77. Horning, M. G.; Murakami, S.; Horning, E. C., Analyses of phospholipids, ceramides, and cerebrosides by gas chromatography and gas chromatography-mass spectrometry. *Am J Clin Nutr* **1971,** 24, (9), 1086-96.

78. Sullards, M. C.; Lynch, D. V.; Merrill, A. H., Jr.; Adams, J., Structure determination of soybean and wheat glucosylceramides by tandem mass spectrometry. *J Mass Spectrom* **2000,** 35, (3), 347-53.

79. Rattray, J. B.; Schibeci, A.; Kidby, D. K., Lipids of yeasts. *Bacteriol Rev* **1975,** 39, (3), 197-231.

80. Acharya, U.; Acharya, J. K., Enzymes of sphingolipid metabolism in Drosophila melanogaster. *Cell Mol Life Sci* **2005,** 62, (2), 128-42.

81. Helling, F.; Dennis, R. D.; Weske, B.; Nores, G.; Peter-Katalinic, J.; Dabrowski, U.; Egge, H.; Wiegandt, H., Glycosphingolipids in insects. The amphoteric moiety, N-acetylglucosamine-linked phosphoethanolamine, distinguishes a group of ceramide oligosaccharides from the pupae of Calliphora vicina (Insecta: Diptera). *Eur J Biochem* **1991,** 200, (2), 409-21.

82. Nilsson, O.; Grabowski, G. A.; Ludman, M. D.; Desnick, R. J.; Svennerholm, L., Glycosphingolipid studies of visceral tissues and brain from type 1 Gaucher disease variants. *Clin Genet* **1985,** 27, (5), 443-50.

83. Taketomi, T.; Hara, A.; Uemura, K.; Sugiyama, E., Matrix-assisted laser desorption ionization time-of-flight mass spectrometric analysis of glycosphingolipids including gangliosides. *Acta Biochim Pol* **1998,** 45, (4), 987-99.

84. Colsch, B.; Afonso, C.; Popa, I.; Portoukalian, J.; Fournier, F.; Tabet, J. C.; Baumann, N., Characterization of the ceramide moieties of sphingoglycolipids from mouse brain by ESI-MS/MS: identification of ceramides containing sphingadienine. *J Lipid Res* **2004,** 45, (2), 281-6.

85. Hanada, K.; Kumagai, K.; Yasuda, S.; Miura, Y.; Kawano, M.; Fukasawa, M.; Nishijima, M., Molecular machinery for non-vesicular trafficking of ceramide. *Nature* **2003,** 426, (6968), 803-9.

86. Funato, K.; Riezman, H., Vesicular and nonvesicular transport of ceramide from ER to the Golgi apparatus in yeast. *J Cell Biol* **2001,** 155, (6), 949-59.

87. Kudo, N.; Kumagai, K.; Tomishige, N.; Yamaji, T.; Wakatsuki, S.; Nishijima, M.; Hanada, K.; Kato, R., Structural basis for specific lipid recognition by CERT responsible for nonvesicular trafficking of ceramide. *Proc Natl Acad Sci U S A* **2008,** 105, (2), 488-93.

88. Kolter, T.; Sandhoff, K., Principles of lysosomal membrane digestion: stimulation of sphingolipid degradation by sphingolipid activator proteins and anionic lysosomal lipids. *Annu Rev Cell Dev Biol* **2005,** 21, 81-103.

89. Tani, M.; Ito, M.; Igarashi, Y., Ceramide/sphingosine/sphingosine 1-phosphate metabolism on the cell surface and in the extracellular space. *Cell Signal* **2007,** 19, (2), 229-37.

90. Benaud, C.; Oberst, M.; Hobson, J. P.; Spiegel, S.; Dickson, R. B.; Lin, C. Y., Sphingosine 1-phosphate, present in serum-derived lipoproteins, activates matriptase. *J Biol Chem* **2002,** 277, (12), 10539-46.

91. Pollack, J. D.; Clark, D. S.; Somerson, N. L., Four-directional-development thin-layer chromatography of lipids using trimethyl borate. *J Lipid Res* **1971,** 12, (5), 563-9.

92. Coch, E. H.; Kessler, G., Rapid TLC separation and detection of lecithin and sphingomyelin in amniotic fluid. *Clin Chem* **1972,** 18, (5), 490-2.

93. Schneck, L.; Pourfar, M.; Benjamin, A., Automated tank for one- or two-dimensional thin-layer chromatography. *J Lipid Res* **1970,** 11, (1), 66-7.

94. Pollet, S.; Ermidou, S.; Le Saux, F.; Monge, M.; Baumann, N., Microanalysis of brain lipids: multiple two-dimensional thin-layer chromatography. *J Lipid Res* **1978,** 19, (7), 916-21.

95. Urban, P. F.; Harth, S.; Freysz, L.; Dreyfus, H., Brain and retinal ganglioside composition from different species determined by TLC and HPTLC. *Adv Exp Med Biol* **1980,** 125, 149-57.

96. Jungalwala, F. B.; Evans, J. E.; Bremer, E.; McCluer, R. H., Analysis of sphingoid bases by reversed-phase high performance liquid chromatography. *J Lipid Res* **1983,** 24, (10), 1380-8.

97. Nishimura, K.; Nakamura, A., High performance liquid chromatographic analysis of long chain bases in intestinal glycolipids of adult and embryonic Japanese quails. *J Biochem (Tokyo)* **1985,** 98, (5), 1247-54.

98. Shephard, G. S.; van der Westhuizen, L., Liquid chromatographic determination of the sphinganine/sphingosine ratio in serum. *J Chromatogr B Biomed Sci Appl* **1998,** 710, (1-2), 219-22.

99. Lester, R. L.; Dickson, R. C., High-performance liquid chromatography analysis of molecular species of sphingolipid-related long chain bases and long chain base phosphates in Saccharomyces cerevisiae after derivatization with 6-aminoquinolyl-N-hydroxysuccinimidyl carbamate. *Anal Biochem* **2001,** 298, (2), 283-92.

100. Smith, M.; Monchamp, P.; Jungalwala, F. B., Separation of molecular species of sphingomyelin and ceramide by argentation and reversed-phase HPLC. *J Lipid Res* **1981,** 22, (4), 714-9.

101. Suzuki, A.; Handa, S.; Yamakawa, T., Separation of molecular species of glucosylceramide by high performance liquid chromatography of their benzoyl derivatives. *J Biochem (Tokyo)* **1976,** 80, (5), 1181-3.

102. Caligan, T. B.; Peters, K.; Ou, J.; Wang, E.; Saba, J.; Merrill, A. H., Jr., A high-performance liquid chromatographic method to measure sphingosine 1-phosphate and related compounds from sphingosine kinase assays and other biological samples. *Anal Biochem* **2000,** 281, (1), 36-44.

103. McNabb, T. J.; Cremesti, A. E.; Brown, P. R.; Fischl, A. S., The separation and direct detection of ceramides and sphingoid bases by normal-phase high-performance

liquid chromatography and evaporative light-scattering detection. *Anal Biochem* **1999,** 276, (2), 242-50.

104. Yamazaki, T.; Suzuki, A.; Handa, S.; Yamakawa, T., Consecutive analysis of sphingoglycolipids on the basis of sugar and ceramide moieties by high performance liquid chromatography. *J Biochem (Tokyo)* **1979,** 86, (3), 803-9.

105. McCluer, E. H.; Evans, J. E., Quantitative analysis of brain galactosylceramides by high performance liquid chromatography of their perbenzoyl derivatives. *J Lipid Res* **1976,** 17, (4), 412-8.

106. McCluer, R. H.; Evans, J. E., Preparation and analysis of benzoylated cerebrosides. *J Lipid Res* **1973,** 14, (6), 611-7.

107. Lipsky, N. G.; Pagano, R. E., Sphingolipid metabolism in cultured fibroblasts: microscopic and biochemical studies employing a fluorescent ceramide analogue. *Proc Natl Acad Sci U S A* **1983,** 80, (9), 2608-12.

108. Martin, O. C.; Pagano, R. E., Normal- and reverse-phase HPLC separations of fluorescent (NBD) lipids. *Anal Biochem* **1986,** 159, (1), 101-8.

109. Prinetti, A.; Prioni, S.; Chigorno, V.; Karagogeos, D.; Tettamanti, G.; Sonnino, S., Immunoseparation of sphingolipid-enriched membrane domains enriched in Src family protein tyrosine kinases and in the neuronal adhesion molecule TAG-1 by anti-GD3 ganglioside monoclonal antibody. *J Neurochem* **2001,** 78, (5), 1162-7.

110. Cowart, L. A.; Szulc, Z.; Bielawska, A.; Hannun, Y. A., Structural determinants of sphingolipid recognition by commercially available anti-ceramide antibodies. *J Lipid Res* **2002,** 43, (12), 2042-8.

111. Samuelsson, B.; Samuelsson, K., Gas-liquid chromatographic separation of ceramides as di-O-trimethylsilyl ether derivatives. *Biochim Biophys Acta* **1968,** 164, (2), 421-3.

112. Samuelsson, B.; Samuelsson, L., Separation and identification of ceramides derived from human plasma sphingomyelins. *J Lipid Res* **1969,** 10, (1), 47-55.

113. Samuelsson, K.; Samuelsson, B., Gas-liquid chromatography-mass spectrometry of cerebrosides as trimethylsilyl ether derivatives. *Biochem Biophys Res Commun* **1969,** 37, (1), 15-21.

114. Sweeley, C. C.; Dawson, G., Determination of glycosphingolipid structures by mass spectrometry. *Biochem Biophys Res Commun* **1969,** 37, (1), 6-14.

115. Hammarstrom, S.; Samuelsson, B., On the biosynthesis of cerebrosides from 2-hydroxy acid ceramides: use of deuterium labeled substrate and multiple ion detector. *Biochem Biophys Res Commun* **1970,** 41, (4), 1027-35.

116. Samuelsson, K.; Sameulsson, B., Gas chromatographic and mass spectrometric studies of synthetic and naturally occurring ceramides. *Chem Phys Lipids* **1970,** 5, (1), 44-79.

117. Matsubara, T.; Hayashi, A., Fragmentation pathways of O-trimethylsilyl ethers of dihydroxy long-chain bases analysed by linked-scan mass spectrometry. *J Chromatogr* **1991,** 562, (1-2), 119-24.

118. Iwamori, M.; Kiguchi, K.; Kanno, J.; Kitagawa, M.; Nagai, Y., Gangliosides as markers of cortisone-sensitive and cortisone-resistant rabbit thymocytes: characterization of thymus-specific gangliosides and preferential changes of particular gangliosides in the thymus of cortisone-treated rabbits. *Biochemistry* **1986,** 25, (4), 889-96.

119. Tadano-Aritomi, K.; Kasama, T.; Handa, S.; Ishizuka, I., Isolation and structural characterization of a mono-sulfated isoglobotetraosylceramide, the first sulfoglycosphingolipid of the isoglobo-series, from rat kidney. *Eur J Biochem* **1992,** 209, (1), 305-13.

120. Childs, R. A.; Wright, J. R.; Ross, G. F.; Yuen, C. T.; Lawson, A. M.; Chai, W.; Drickamer, K.; Feizi, T., Specificity of lung surfactant protein SP-A for both the carbohydrate and the lipid moieties of certain neutral glycolipids. *J Biol Chem* **1992,** 267, (14), 9972-9.

121. Hamanaka, S.; Asagami, C.; Suzuki, M.; Inagaki, F.; Suzuki, A., Structure determination of glucosyl beta 1-N-(omega-O-linoleoyl)-acylsphingosines of human epidermis. *J Biochem (Tokyo)* **1989,** 105, (5), 684-90.

122. Hara, A.; Taketomi, T., Detection of D-erythro and L-threo sphingosine bases in preparative sphingosylphosphorylcholine and its N-acylated derivatives and some evidence of their different chemical configurations. *J Biochem (Tokyo)* **1983,** 94, (5), 1715-8.

123. Hayashi, A.; Matsubara, T.; Morita, M.; Kinoshita, T.; Nakamura, T., Structural analysis of choline phospholipids by fast atom bombardment mass spectrometry and tandem mass spectrometry. *J Biochem (Tokyo)* **1989,** 106, (2), 264-9.

124. Jeanette Adams, Q. A., Structure determination of sphingolipids by mass spectrometry. *Mass Spectrometry Reviews* **1993,** 12, (1), 51-85.

125. Qinghong Ann, J. A., Structure-specific collision-induced fragmentations of ceramides cationized with alkali-metal ions *Analytical Chemistry* **1992,** 65, (1), 7-13.

126. Suzuki, M.; Yamakawa, T.; Suzuki, A., High-performance liquid chromatography-mass spectrometry of glycosphingolipids: II. Application to neutral glycolipids and monosialogangliosides. *J Biochem (Tokyo)* **1990,** 108, (1), 92-8.

127. Suzuki, M.; Sekine, M.; Yamakawa, T.; Suzuki, A., High-performance liquid chromatography-mass spectrometry of glycosphingolipids: I. Structural characterization of molecular species of GlcCer and IV3 beta Gal-Gb4Cer. *J Biochem (Tokyo)* **1989,** 105, (5), 829-33.

128. Liebisch, G.; Drobnik, W.; Reil, M.; Trumbach, B.; Arnecke, R.; Olgemoller, B.; Roscher, A.; Schmitz, G., Quantitative measurement of different ceramide species from crude cellular extracts by electrospray ionization tandem mass spectrometry (ESI-MS/MS). *J Lipid Res* **1999,** 40, (8), 1539-46.

129. Levery, S. B.; Toledo, M. S.; Doong, R. L.; Straus, A. H.; Takahashi, H. K., Comparative analysis of ceramide structural modification found in fungal cerebrosides by electrospray tandem mass spectrometry with low energy collision-induced dissociation of Li+ adduct ions. *Rapid Commun Mass Spectrom* **2000,** 14, (7), 551-63.

130. Sullards, M. C.; Merrill, A. H., Jr., Analysis of sphingosine 1-phosphate, ceramides, and other bioactive sphingolipids by high-performance liquid chromatography-tandem mass spectrometry. *Sci STKE* **2001,** 2001, (67), PL1.

131. Sullards, M. C., Analysis of sphingomyelin, glucosylceramide, ceramide, sphingosine, and sphingosine 1-phosphate by tandem mass spectrometry. *Methods Enzymol* **2000,** 312, 32-45.

132. Maceyka, M.; Milstien, S.; Spiegel, S., Sphingosine kinases, sphingosine-1-phosphate and sphingolipidomics. *Prostaglandins Other Lipid Mediat* **2005,** 77, (1-4), 15-22.

133. Petrache, I.; Natarajan, V.; Zhen, L.; Medler, T. R.; Richter, A.; Berdyshev, E. V.; Tuder, R. M., Ceramide causes pulmonary cell apoptosis and emphysema: a role for sphingolipid homeostasis in the maintenance of alveolar cells. *Proc Am Thorac Soc* **2006,** 3, (6), 510.

134. Sullards, M. C.; Merrill, A. H., Jr., Analysis of Sphingosine 1-Phosphate, Ceramides, and Other Bioactive Sphingolipids by High-Performance Liquid Chromatography-Tandem Mass Spectrometry. *Sci. STKE* **2001,** 2001, (67), pl1-.

135. Pettus, B. J.; Bielawska, A.; Kroesen, B. J.; Moeller, P. D.; Szulc, Z. M.; Hannun, Y. A.; Busman, M., Observation of different ceramide species from crude cellular extracts by normal-phase high-performance liquid chromatography coupled to atmospheric pressure chemical ionization mass spectrometry. *Rapid Commun Mass Spectrom* **2003,** 17, (11), 1203-11.

136. Kushi, Y.; Rokukawa, C.; Numajir, Y.; Kato, Y.; Handa, S., Analysis of underivatized glycosphingolipids by high-performance liquid chromatography/atmospheric pressure ionization mass spectrometry. *Anal Biochem* **1989,** 182, (2), 405-10.

137. Suzuki, M.; Yamakawa, T.; Suzuki, A., A micro method involving micro high-performance liquid chromatography-mass spectrometry for the structural characterization of neutral glycosphingolipids and monosialogangliosides. *J Biochem (Tokyo)* **1991,** 109, (4), 503-6.

138. Merrill, A. H., Jr.; Sullards, M. C.; Allegood, J. C.; Kelly, S.; Wang, E., Sphingolipidomics: high-throughput, structure-specific, and quantitative analysis of sphingolipids by liquid chromatography tandem mass spectrometry. *Methods* **2005,** 36, (2), 207-24.

139. Lee, M. H.; Lee, G. H.; Yoo, J. S., Analysis of ceramides in cosmetics by reversed-phase liquid chromatography/electrospray ionization mass spectrometry with collision-induced dissociation. *Rapid Commun Mass Spectrom* **2003,** 17, (1), 64-75.

140. Pacetti, D.; Boselli, E.; Hulan, H. W.; Frega, N. G., High performance liquid chromatography-tandem mass spectrometry of phospholipid molecular species in eggs from hens fed diets enriched in seal blubber oil. *J Chromatogr A* **2005,** 1097, (1-2), 66-73.

141. Fujiwaki, T.; Yamaguchi, S.; Sukegawa, K.; Taketomi, T., Application of delayed extraction matrix-assisted laser desorption ionization time-of-flight mass spectrometry for analysis of sphingolipids in tissues from sphingolipidosis patients. *J Chromatogr B Biomed Sci Appl* **1999,** 731, (1), 45-52.

142. Suzuki, Y.; Suzuki, M.; Ito, E.; Goto-Inoue, N.; Miseki, K.; Iida, J.; Yamazaki, Y.; Yamada, M.; Suzuki, A., Convenient structural analysis of glycosphingolipids using MALDI-QIT-TOF mass spectrometry with increased laser power and cooling gas flow. *J Biochem (Tokyo)* **2006,** 139, (4), 771-7.

143. Siuzdak, G., The emergence of mass spectrometry in biochemical research. *Proc Natl Acad Sci U S A* **1994,** 91, (24), 11290-7.

144. David, J. H., Analysis of carbohydrates and glycoconjugates by matrix-assisted laser desorption/ionization mass spectrometry: An update covering the period 1999-2000. *Mass Spectrometry Reviews* **2006,** 25, (4), 595-662.

145. Kaufmann, R., Matrix-assisted laser desorption ionization (MALDI) mass spectrometry: a novel analytical tool in molecular biology and biotechnology. *J Biotechnol* **1995,** 41, (2-3), 155-75.

146. Karlsson, H.; Johansson, L.; Miller-Podraza, H.; Karlsson, K. A., Fingerprinting of large oligosaccharides linked to ceramide by matrix-assisted laser desorption/ionization time-of-flight mass spectrometry: highly heterogeneous polyglycosylceramides of human erythrocytes with receptor activity for Helicobacter pylori. *Glycobiology* **1999,** 9, (8), 765-78.

147. O'Connor, P. B.; Mirgorodskaya, E.; Costello, C. E., High pressure matrix-assisted laser desorption/ionization Fourier transform mass spectrometry for minimization of ganglioside fragmentation. *J Am Soc Mass Spectrom* **2002,** 13, (4), 402-7.

148. Sugiyama, E.; Hara, A.; Uemura, K.; Taketomi, T., Application of matrix-assisted laser desorption ionization time-of-flight mass spectrometry with delayed ion extraction to ganglioside analyses. *Glycobiology* **1997,** 7, (5), 719-24.

149. Sullards, M. C.; Allegood, J. C.; Kelly, S.; Wang, E.; Haynes, C. A.; Park, H.; Chen, Y.; Merrill, A. H., Jr., Structure-specific, quantitative methods for analysis of sphingolipids by liquid chromatography-tandem mass spectrometry: "inside-out" sphingolipidomics. *Methods Enzymol* **2007,** 432, 83-115.

150. van Echten-Deckert, G., Sphingolipid extraction and analysis by thin-layer chromatography. *Methods Enzymol* **2000,** 312, 64-79.

151. Muthing, J., Analyses of glycosphingolipids by high-performance liquid chromatography. *Methods Enzymol* **2000,** 312, 45-64.

152. Mano, N.; Oda, Y.; Yamada, K.; Asakawa, N.; Katayama, K., Simultaneous quantitative determination method for sphingolipid metabolites by liquid chromatography/ionspray ionization tandem mass spectrometry. *Anal Biochem* **1997,** 244, (2), 291-300.

153. Lieser, B.; Liebisch, G.; Drobnik, W.; Schmitz, G., Quantification of sphingosine and sphinganine from crude lipid extracts by HPLC electrospray ionization tandem mass spectrometry. *J Lipid Res* **2003,** 44, (11), 2209-16.

154. Ann, Q.; Adams, J., Structure-specific collision-induced fragmentations of ceramides cationized with alkali-metal ions. *Anal. Chem.* **1993,** 65, (1), 7-13.

155. Han, X., Characterization and direct quantitation of ceramide molecular species from lipid extracts of biological samples by electrospray ionization tandem mass spectrometry. *Anal Biochem* **2002,** 302, (2), 199-212.

156. Fujiwaki, T.; Yamaguchi, S.; Tasaka, M.; Sakura, N.; Taketomi, T., Application of delayed extraction-matrix-assisted laser desorption ionization time-of-flight mass spectrometry for analysis of sphingolipids in pericardial fluid, peritoneal fluid and serum from Gaucher disease patients. *J Chromatogr B Analyt Technol Biomed Life Sci* **2002,** 776, (1), 115-23.

157. Larson, G.; Samuelsson, B. E., Blood group type glycosphingolipids of human cord blood erythrocytes. *J Biochem (Tokyo)* **1980,** 88, (3), 647-57.

158. Karlsson, A. A.; Michelsen, P.; Odham, G., Molecular species of sphingomyelin: determination by high-performance liquid chromatography/mass spectrometry with electrospray and high-performance liquid chromatography/tandem mass spectrometry with atmospheric pressure chemical ionization. *J Mass Spectrom* **1998,** 33, (12), 1192-8.

159. Isaac, G.; Bylund, D.; Mansson, J. E.; Markides, K. E.; Bergquist, J., Analysis of phosphatidylcholine and sphingomyelin molecular species from brain extracts using capillary liquid chromatography electrospray ionization mass spectrometry. *J Neurosci Methods* **2003,** 128, (1-2), 111-9.

160. Shimizu, A.; Ashida, Y.; Fujiwara, F., Measurement of the ratio of lecithin to sphingomyelin in amniotic fluid by fast atom bombardment mass spectrometry. *Clin Chem* **1991,** 37, (8), 1370-4.

161. Brugger, B.; Erben, G.; Sandhoff, R.; Wieland, F. T.; Lehmann, W. D., Quantitative analysis of biological membrane lipids at the low picomole level by nano-electrospray ionization tandem mass spectrometry. *Proc Natl Acad Sci U S A* **1997,** 94, (6), 2339-44.

162. Karlsson, K. A.; Pascher, I.; Samuelsson, B. E., Analysis of intact gangliosides by mass spectrometry. Comparison of different derivatives of a hematoside of a tumour and the major monosialoganglioside of brain. *Chem Phys Lipids* **1974,** 12, (4), 271-86.

163. Arita, M.; Iwamori, M.; Higuchi, T.; Nagai, Y., Negative ion fast atom bombardment mass spectrometry of gangliosides and asialo gangliosides: a useful method for the structural elucidation of gangliosides and related neutral glycosphingolipids. *J Biochem (Tokyo)* **1983,** 94, (1), 249-56.

164. Muthing, J.; Egge, H.; Kniep, B.; Muhlradt, P. F., Structural characterization of gangliosides from murine T lymphocytes. *Eur J Biochem* **1987,** 163, (2), 407-16.

165. Chen, S.; Pieraccini, G.; Moneti, G., Quantitative analysis of the molecular species of monosialogangliosides by continuous-flow fast-atom bombardment mass spectrometry. *Rapid Commun Mass Spectrom* **1991,** 5, (12), 618-21.

166. Ivleva, V. B.; Sapp, L. M.; O'Connor, P. B.; Costello, C. E., Ganglioside analysis by thin-layer chromatography matrix-assisted laser desorption/ionization orthogonal time-of-flight mass spectrometry. *J Am Soc Mass Spectrom* **2005,** 16, (9), 1552-60.

167. Levery, S. B., Glycosphingolipid structural analysis and glycosphingolipidomics. *Methods Enzymol* **2005,** 405, 300-69.

168. Han, X.; Cheng, H., Characterization and direct quantitation of cerebroside molecular species from lipid extracts by shotgun lipidomics. *J Lipid Res* **2005,** 46, (1), 163-75.

169. Bielawski, J.; Szulc, Z. M.; Hannun, Y. A.; Bielawska, A., Simultaneous quantitative analysis of bioactive sphingolipids by high-performance liquid chromatography-tandem mass spectrometry. *Methods* **2006,** 39, (2), 82-91.

170. Sommer, U.; Herscovitz, H.; Welty, F. K.; Costello, C. E., LC-MS-based method for the qualitative and quantitative analysis of complex lipid mixtures. *J Lipid Res* **2006,** 47, (4), 804-14.

171. Olling, A.; Breimer, M. E.; Peltomaa, E.; Samuelsson, B. E.; Ghardashkhani, S., Electrospray ionization and collision-induced dissociation time-of-flight mass spectrometry of neutral glycosphingolipids. *Rapid Commun Mass Spectrom* **1998,** 12, (10), 637-45.

172. Yoo, H. H.; Son, J.; Kim, D. H., Liquid chromatography-tandem mass spectrometric determination of ceramides and related lipid species in cellular extracts. *J Chromatogr B Analyt Technol Biomed Life Sci* **2006,** 843, (2), 327-33.

173. Hsu, F. F.; Turk, J., Studies on sulfatides by quadrupole ion-trap mass spectrometry with electrospray ionization: structural characterization and the fragmentation processes that include an unusual internal galactose residue loss and the classical charge-remote fragmentation. *J Am Soc Mass Spectrom* **2004,** 15, (4), 536-46.

174. Hsu, F. F.; Bohrer, A.; Turk, J., Electrospray ionization tandem mass spectrometric analysis of sulfatide. Determination of fragmentation patterns and characterization of molecular species expressed in brain and in pancreatic islets. *Biochim Biophys Acta* **1998,** 1392, (2-3), 202-16.

175. Bielawski, J.; Szulc, Z. M.; Hannun, Y. A.; Bielawska, A., Simultaneous quantitative analysis of bioactive sphingolipids by high-performance liquid chromatography-tandem mass spectrometry. *Methods* **2006**.

176. Fujiwaki, T.; Tasaka, M.; Takahashi, N.; Kobayashi, H.; Murakami, Y.; Shimada, T.; Yamaguchi, S., Quantitative evaluation of sphingolipids using delayed extraction matrix-assisted laser desorption ionization time-of-flight mass spectrometry with sphingosylphosphorylcholine as an internal standard. Practical application to cardiac valves from a patient with Fabry disease. *J Chromatogr B Analyt Technol Biomed Life Sci* **2006,** 832, (1), 97-102.

177. Haruo Iwabuchi, E. K. N. K. H. W. M. K. K.-I. N., Studies on drug metabolism using liquid chromatography/mass spectrometry: Comparison of three liquid chromatographic/mass spectrometric interfaces. *Biological Mass Spectrometry* **1994,** 23, (9), 540-546.

178. Ramstedt, B.; Slotte, J. P., Separation and purification of sphingomyelin diastereomers by high-performance liquid chromatography. *Anal Biochem* **2000,** 282, (2), 245-9.

179. Muthing, J.; Unland, F., Improved separation of isomeric gangliosides by anion-exchange high-performance liquid chromatography. *J Chromatogr B Biomed Appl* **1994,** 658, (1), 39-45.

180. Tsui, Z. C.; Chen, Q. R.; Thomas, M. J.; Samuel, M.; Cui, Z., A method for profiling gangliosides in animal tissues using electrospray ionization-tandem mass spectrometry. *Anal Biochem* **2005,** 341, (2), 251-8.

181. Pettus, B. J.; Kroesen, B. J.; Szulc, Z. M.; Bielawska, A.; Bielawski, J.; Hannun, Y. A.; Busman, M., Quantitative measurement of different ceramide species from crude cellular extracts by normal-phase high-performance liquid chromatography coupled to atmospheric pressure ionization mass spectrometry. *Rapid Commun Mass Spectrom* **2004,** 18, (5), 577-83.

182. Masukawa, Y.; Tsujimura, H.; Narita, H., Liquid chromatography-mass spectrometry for comprehensive profiling of ceramide molecules in human hair. *J Lipid Res* **2006,** 47, (7), 1559-71.

183. Jiang, X.; Han, X., Characterization and direct quantitation of sphingoid base-1-phosphates from lipid extracts: a shotgun lipidomics approach. *J Lipid Res* **2006,** 47, (8), 1865-73.

184. Tettamanti, G.; Bassi, R.; Viani, P.; Riboni, L., Salvage pathways in glycosphingolipid metabolism. *Biochimie* **2003,** 85, (3-4), 423-37.

185. Merrill, A. H., Jr.; Sullards, M. C.; Wang, E.; Voss, K. A.; Riley, R. T., Sphingolipid metabolism: roles in signal transduction and disruption by fumonisins. *Environ Health Perspect* **2001,** 109 Suppl 2, 283-9.

186. Suzuki, K., Formation and turnover of myelin ganglioside. *J Neurochem* **1970,** 17, (2), 209-13.

187. Hannun, Y. A.; Obeid, L. M., The Ceramide-centric universe of lipid-mediated cell regulation: stress encounters of the lipid kind. *J Biol Chem* **2002,** 277, (29), 25847-50.

188. Tserng, K. Y.; Griffin, R., Studies of lipid turnover in cells with stable isotope and gas chromatograph-mass spectrometry. *Anal Biochem* **2004,** 325, (2), 344-53.

189. Tserng, K. Y.; Griffin, R., Quantitation and molecular species determination of diacylglycerols, phosphatidylcholines, ceramides, and sphingomyelins with gas chromatography. *Anal Biochem* **2003,** 323, (1), 84-93.

190. Berdyshev, E. V.; Gorshkova, I. A.; Usatyuk, P.; Zhao, Y.; Saatian, B.; Hubbard, W.; Natarajan, V., De novo biosynthesis of dihydrosphingosine-1-phosphate by sphingosine kinase 1 in mammalian cells. *Cell Signal* **2006**.

191. Hanada, K., Serine palmitoyltransferase, a key enzyme of sphingolipid metabolism. *Biochim Biophys Acta* **2003,** 1632, (1-3), 16-30.

192. Wang, H.; Giuliano, A. E.; Cabot, M. C., Enhanced de novo ceramide generation through activation of serine palmitoyltransferase by the P-glycoprotein antagonist SDZ PSC 833 in breast cancer cells. *Mol Cancer Ther* **2002,** 1, (9), 719-26.

193. Mikami, T.; Kashiwagi, M.; Tsuchihashi, K.; Akino, T.; Gasa, S., Substrate specificity and some other enzymatic properties of dihydroceramide desaturase (ceramide synthase) in fetal rat skin. *J Biochem (Tokyo)* **1998,** 123, (5), 906-11.

194. Norred, W. P.; Wang, E.; Yoo, H.; Riley, R. T.; Merrill, A. H., Jr., In vitro toxicology of fumonisins and the mechanistic implications. *Mycopathologia* **1992,** 117, (1-2), 73-8.

195. Haschek, W. M.; Motelin, G.; Ness, D. K.; Harlin, K. S.; Hall, W. F.; Vesonder, R. F.; Peterson, R. E.; Beasley, V. R., Characterization of fumonisin toxicity in orally and intravenously dosed swine. *Mycopathologia* **1992,** 117, (1-2), 83-96.

196. Weibking, T. S.; Ledoux, D. R.; Bermudez, A. J.; Turk, J. R.; Rottinghaus, G. E.; Wang, E.; Merrill, A. H., Jr., Effects of feeding Fusarium moniliforme culture material, containing known levels of fumonisin B1, on the young broiler chick. *Poult Sci* **1993,** 72, (3), 456-66.

197. van der Westhuizen, L.; Shephard, G. S.; Snyman, S. D.; Abel, S.; Swanevelder, S.; Gelderblom, W. C., Inhibition of sphingolipid biosynthesis in rat primary hepatocyte cultures by fumonisin B1 and other structurally related compounds. *Food Chem Toxicol* **1998,** 36, (6), 497-503.

198. Rittershaus, P. C.; Kechichian, T. B.; Allegood, J. C.; Merrill, A. H., Jr.; Hennig, M.; Luberto, C.; Del Poeta, M., Glucosylceramide synthase is an essential regulator of pathogenicity of Cryptococcus neoformans. *J Clin Invest* **2006,** 116, (6), 1651-9.

199. Venkataraman, K.; Riebeling, C.; Bodennec, J.; Riezman, H.; Allegood, J. C.; Sullards, M. C.; Merrill, A. H., Jr.; Futerman, A. H., Upstream of growth and differentiation factor 1 (uog1), a mammalian homolog of the yeast longevity assurance gene 1 (LAG1), regulates N-stearoyl-sphinganine (C18-(dihydro)ceramide) synthesis in a fumonisin B1-independent manner in mammalian cells. *J Biol Chem* **2002,** 277, (38), 35642-9.

200. Mizutani, Y.; Kihara, A.; Igarashi, Y., Mammalian Lass6 and its related family members regulate synthesis of specific ceramides. *Biochem J* **2005,** 390, (Pt 1), 263-71.

201. Hata, K.; Wada, T.; Hasegawa, A.; Kiso, M.; Miyagi, T., Purification and characterization of a membrane-associated ganglioside sialidase from bovine brain. *J Biochem* **1998,** 123, (5), 899-905.

202. Melendez, A. J., Sphingosine kinase signalling in immune cells: Potential as novel therapeutic targets. *Biochim Biophys Acta* **2008,** 1784, (1), 66-75.

203. Limatola, C.; Massa, V.; Lauro, C.; Catalano, M.; Giovanetti, A.; Nuccitelli, S.; Spinedi, A., Evidence for a role of glycosphingolipids in CXCR4-dependent cell migration. *FEBS Lett* **2007,** 581, (14), 2641-6.

204. Nuzzi, P. A.; Senetar, M. A.; Huttenlocher, A., Asymmetric localization of calpain 2 during neutrophil chemotaxis. *Mol Biol Cell* **2007,** 18, (3), 795-805.

205. Alvarez-Vasquez, F.; Sims, K. J.; Cowart, L. A.; Okamoto, Y.; Voit, E. O.; Hannun, Y. A., Simulation and validation of modelled sphingolipid metabolism in Saccharomyces cerevisiae. *Nature* **2005,** 433, (7024), 425-30.

206. Hoetzl, S.; Sprong, H.; van Meer, G., The way we view cellular (glyco)sphingolipids. *J Neurochem* **2007,** 103 Suppl 1, 3-13.